SYNTHESIS AND CHARACTERIZATION OF FORSTERITES FOR POTENTIAL USE AS CATHODE MATERIALS IN MAGNESIUM BATTERY

SITI HAFIZHA BINTI TAMIN

INSTITUTE OF GRADUATE STUDIES
UNIVERSITY OF MALAYA
KUALA LUMPUR

2018

SYNTHESIS AND CHARACTERIZATION OF FORSTERITES FOR POTENTIAL USE AS CATHODE MATERIALS IN MAGNESIUM BATTERY

SITI HAFIZHA BINTI TAMIN

DISSERTATION SUBMITTED IN FULFILMENT OF
THE REQUIREMENTS FOR THE DEGREE OF MASTER
OF PHYLOSOPHY

INSTITUTE OF GRADUATE STUDIES
UNIVERSITY OF MALAYA
KUALA LUMPUR

2018

UNIVERSITY OF MALAYA
ORIGINAL LITERARY WORK DECLARATION

Name of Candidate: **SITI HAFIZHA BINTI TAMIN**

Matric No: **HGA140021**

Name of Degree: **MASTER OF PHILOSOPHY**

Title of Project Paper/Research Report/Dissertation/Thesis ("this Work"):

SYNTHESIS AND CHARACTERIZATION OF FORSTE

RITES FOR POTENTIAL USE AS CATHODE MATERIALS IN MAGNESIUM BATTERY

Field of Study: **APPLIED SCIENCE**

I do solemnly and sincerely declare that:

(1) I am the sole author/writer of this Work;
(2) This Work is original;
(3) Any use of any work in which copyright exists was done by way of fair dealing and for permitted purposes and any excerpt or extract from, or reference to or reproduction of any copyright work has been disclosed expressly and sufficiently and the title of the Work and its authorship have been acknowledged in this Work;
(4) I do not have any actual knowledge nor do I ought reasonably to know that the making of this work constitutes an infringement of any copyright work;
(5) I hereby assign all and every rights in the copyright to this Work to the University of Malaya ("UM"), who henceforth shall be owner of the copyright in this Work and that any reproduction or use in any form or by any means whatsoever is prohibited without the written consent of UM having been first had and obtained;
(6) I am fully aware that if in the course of making this Work I have infringed any copyright whether intentionally or otherwise, I may be subject to legal action or any other action as may be determined by UM.

Candidate's Signature Date:

Subscribed and solemnly declared before,

Witness's Signature Date:

Name:

Designation:

SYNTHESIS AND CHARACTERIZATION OF FORSTERITES FOR POTENTIAL USE AS CATHODE MATERIALS IN MAGNESIUM BATTERY

ABSTRACT

Following the achievements in the field of lithium battery, there have been more and more attempts over the years to develop magnesium rechargeable batteries. However, the development of magnesium rechargeable batteries was hindered because of the difficulty to realize fast Mg^{2+} transport in the host cathode material. Recently, orthosilicate cathode materials have gained considerable attention because of their structural stability and high reversible capacity. This type of materials have been widely investigated and successfully applied in lithium rechargeable batteries. Herein, orthosilicate Mg_2SiO_4 have been proposed as potential cathode material in rechargeable magnesium batteries. Doping approach has been employed in this work to improve the structural and morphological properties of Mg_2SiO_4 materials hence enhancing the performance of cathode materials. Sol-gel method has been employed to synthesize Mg_2SiO_4 and Mg_2SiO_4 doped materials. Mg_2SiO_4 compound was chosen as the parent compound in this work and was addressed as System I. The X-ray diffraction result shows the formation of pure orthorhombic Mg_2SiO_4 crystal structure with a = 10.1693 Å, b = 5.9685 Å and c = 4.6886 Å. Sample sintered at 1100 °C has the largest unit cell volume V = 284.5759 Å^3 which provide more space for magnesium ion transfer and owned the smallest $R_{ct} = 7.01 \times 10^8\ \Omega$. CV results show that the electrochemical process consists of two pairs of redox peaks.. System II has been prepared based on stoichiometric $Mg_{2-x}Mn_xSiO_4$. Effect of Mn doping on the structural, morphological and electrochemical properties were investigated. X-ray diffraction results show that Mn doping does not destruct the lattice structure of the compound for $x \leq 0.6$. The introduction of Mn^{2+} considerably improves the structural and morphological properties of the parent compound hence enhancing the electrochemical properties of the compound. Sample with $x = 0.6$ has the largest unit cell volume $V = 296.0189$ Å^3 and smallest $R_{ct} = 2.15 \times 10^8\ \Omega$. CV result show that $Mg_{2-x}Mn_xSiO_4$ could be a good host for Mg^{2+} intercalation, and a potential cathode material for magnesium batteries. Zr^{4+} doped $Mg_{1.8}Mn_{0.2}SiO_4$ ($Mg_{1.8}Mn_{0.2}Si_{1-y}O_4Zr_y$, $0.0 \leq y \leq 0.4$) samples were prepared and assigned as System III. X-ray diffraction patterns of the materials exhibited no extra peak for $y \leq 0.3$ indicated that Zr entered the structure rather than forming impurities. Zr doping contributed to the enhancement of the electrochemical performance of $Mg_{1.8}Mn_{0.2}SiO_4$. For this work, $Mg_{1.8}Mn_{0.2}Si_{0.7}O_4Zr_{0.3}$ which possessed the largest unit cell volume, $V = 297.5823$ Å^3 have the smallest R_{ct}, suggesting that the electrode possesses an easier charge transfer process than the other. A pair of anodic and cathodic peak can be distinguished from voltammogram of $Mg_{1.8}Mn_{0.2}Si_{0.7}O_4Zr_{0.3}$ indicates that intercalation and deintercalation process proceed *via* one stage. Results show that Zr doping improved the electrochemical performance of $Mg_{1.8}Mn_{0.2}SiO_4$ and this material can be used as cathode in magnesium batteries. Results show that Mg_2SiO_4 and Mg_2SiO_4 doped materials could be a potential cathode material for magnesium batteries and this works could be extended to obtain promising cathode materials.

Keywords: forsterite, cathode, magnesium battery, cyclic voltammetry

SINTESIS DAN PENCIRIAN FORSTERITE YANG BERPOTENSI UNTUK DIGUNAKAN DALAM BATERI MAGNESIUM

ABSTRAK

Pencapaian yang memberangsangkan dalam bidang bateri litium telah menjadi pemangkin untuk membangunkan bateri magnesium boleh cas. Walau bagaimanapun, perkembangan bateri magnesium boleh cas terhalang kerana kesukaran untuk menghasilkan hos bahan katod yang mempunyai kadar mobiliti Mg^{2+} ion yang tinggi. Baru-baru ini, bahan katod ortosilikat telah mendapat perhatian kerana kestabilan struktur dan keupayaan berbalik yang tinggi. Jenis bahan ini telah banyak digunakan dalam bateri litium boleh cas. Orthosilicate Mg_2SiO_4 telah dicadangkan sebagai bahan katod yang berpotensi untuk digunakan dalam bateri magnesium boleh cas. Pendekatan pendopan telah digunakan dalam kerja ini untuk memperbaiki sifat-sifat struktur dan morfologi bahan Mg_2SiO_4 seterusnya dapat meningkatkan prestasi bahan katod. Kaedah sol-gel telah digunakan untuk mensintesis bahan Mg_2SiO_4 dan Mg_2SiO_4 yang didop. Bahan Mg_2SiO_4 telah dipilih sebagai sebatian induk dalam kerja ini dan dinamakan sebagai Sistem I. Keputusan belauan sinar-X menunjukkan pembentukan struktur kristal Mg_2SiO_4 ortorombik dengan a = 10.1693 Å, b = 5.9685 Å dan c = 4.6886 Å. Sampel yang disinter pada 1100 ° C mempunyai isipadu unit sel yang paling besar, V = 284.5759 $Å^3$ memberikan lebih banyak ruang untuk pemindahan ion magnesium dan memiliki $R_{ct} = 7.01 \times 10^8\ \Omega$ yang paling kecil. Hasil keputusan CV menunjukkan bahawa proses elektrokimia terdiri daripada dua pasang puncak redoks. Sistem II telah disediakan berdasarkan stoikiometri $Mg_{2-x}Mn_xSiO_4$. Kesan penambahan Mn terhadap struktur, morfologi dan elektrokimia disiasat. Keputusan difraksi sinar-X menunjukkan bahawa pendopan terhadap Mn tidak merosakkan struktur asal untuk $x \leq 0.6$. Penambahan Mn^{2+} kepada struktur asal telah meningkatkan struktur dan morfologi induknya dengan itu meningkatkan sifat elektrokimia dari sebatian tersebut. Sampel dengan $x = 0.6$ mempunyai isipadu unit sel yang terbesar, $V = 296.0189$ Å^3 dan nilai $R_{ct} = 2.15 \times 10^8\ \Omega$ yang paling kecil. Keputusan CV menunjukkan bahawa $Mg_{2-x}Mn_xSiO_4$ berpotensi untuk menjadi perumah untuk interaksi Mg^{2+} , dan bahan katod untuk bateri magnesium. Zr^{4+} telah di tambah kedalam $Mg_{1.8}Mn_{0.2}SiO_4$ dengan stoikiometri $Mg_{2-x}Mn_xSi_{1-y}O_4Zr_y$ untuk $0.0 \leq y \leq 0.4$). Sampel yang disediakan telah dikelaskan sebagai Sistem III dalam kerja ini. Corak difraksi sinar-X yang diperolehi tidak menunjukkan puncak tambahan untuk bendasing bagi nilai $y \leq 0.3$. Ini membuktikan bahawa Zr memasuki struktur dan bukannya membentuk bendasing dalam struktur. Penambahan Zr menyumbang kepada peningkatan prestasi elektrokimia $Mg_{1.8}Mn_{0.2}SiO_4$. Dalam kerja ini, $Mg_{1.8}Mn_{0.2}Si_{0.7}O_4Zr_{0.3}$ yang mempunyai isipadu unit sel yang paling besar, $V = 297.5823$ Å^3 mempunyai R_{ct} yang paling kecil, menunjukkan bahawa elektrod daripada bahan ini mempunyai proses pemindahan caj yang lebih mudah daripada yang lain. Sepasang puncak anodik dan katodik dengan arus puncak anodik dan katod boleh dilihat dari voltammetrik lengkung $Mg_{1.8}Mn_{0.2}Si_{0.7}O_4Zr_{0.3}$ dan ini menunjukkan bahawa proses interkalasi dan deinterkondisi diteruskan melalui satu peringkat. Keputusan menunjukkan bahawa penambahan Zr telah meningkatkan prestasi elektrokimia $Mg_{1.8}Mn_{0.2}SiO_4$ dan bahan ini boleh digunakan sebagai bahan katod untuk bateri magnesium. Keseluruhannya, keputusan menunjukkan bahan Mg_2SiO_4 dan bahan Mg_2SiO_4 yang telah didop berpotensi untuk menjadi bahan katod untuk bateri magnesium dan kerja ini berpotensi untuk diteruskan bagi menghasilkan bahan katod yang bagus.

Kata kunci: forsterite, katok, bateri magnesium, kitaran voltametri

ACKNOWLEDGEMENTS

In the name of ALLAH S.W.T., the Most Gracious and the Most Merciful. First and foremost, I would like to extend my praise to Allah s.w.t. for giving me the strength, determination, patience and courage to finish this thesis.

I would like to express my special gratitude to Dr. Syed Bahari Ramadzan Syed Adnan, Professor Dr. Nor Sabirin Mohamed and Mr. Hilmi Jaafar from Centre of Foundation Studies in Science, University of Malaya for all they have done for me as research supervisors and advisors. Without their assistance, guidance, ideas, supervision and encouragement, I would not be able to complete my graduate studies at University of Malaya.

I would like to express my appreciation to all research members including lecturers and postgraduate students of Electrochemical Materials and Devices (EMD) group for their assistance and valuable experience during the course of this work. Research facilities and the financial aids provided by University Malaya are greatly acknowledged.

Lastly, to my beloved husband, Muhamad Hifzhudin Noor Aziz, thank you for being such a supportive, understanding and helpful husband. I'm also grateful to both my parents Tamin Ibrahim and Ruziah Rahmad for their prayers, patience and moral support. Not to be forgotten, my siblings for their endless support for all these years.

TABLE OF CONTENTS

LIST OF FIGURES

LIST OF TABLES

LIST OF SYMBOLS AND ABBREVIATIONS

(CH3.COO)2 Mg : Magnesium acetate

(CH3.COO)2 Mn : Manganese acetate

(CH3.COO)2 Zr : Zirconium acetate

°C : Degree celcius

Å : Armstrong

A : Crossectional area

a, b, c : Lattice parameters

AgCl : Silver chloride

$AlCl_2Et$: Ethylaluminum Dichloride

$AlCl_3$: Aluminum trichloride

ATR : Attenuated total reflection

$C_6H_8O_7$: Citric acid

Cd^{2+} : Cadmium ion

CE : Counter electrode

Co^{2+} : Cobalt ion

CP : Chevral Phase

Cu^+ : Copper ion

Cu_2I_2 : Copper Iodide

CuCl : Copper Chloride

Cu-Kα : Copper K-alpha emission

CV : Cyclic voltammetry

D : Distance of crystal plane

DEC : Diethyl carbonate

DMC : Dimethyl carbonate

DSC : Scanning Calorimetry

EC : Ethylene carbonate

EDX : Energy Dispersive X-ray

EIS : Electrochemical impedance spectrscopy

E_{pa} : Anodic Peak potential

E_{pc} : Cathodic peak potential

EtMgCl : Ethyl magnesium chloride

Fe^{2+} : Ferum ion

FTIR : Fourier Transform Infrared Spectroscopy

GPE : Gel/plasticizer based polymer electrolyte,

H_2O : Water

HMDSMgCl : Hexamethyldisilazide magnesium chloride

ICSD : Inorganic Crystal Structure Database

I_{pa} : Anodic peak current

I_{pc} : Cathodic peak current

K : Kelvin

$KN(SiMe_3)_2$: Potassium hexamethyldisilazide

L : Crystallite size

LDM : Laser diffraction method

Li : Lithium

Li^+ : Lithium ion

LIB : Lithium ion battery

Mg : Magnesium

Mg^{2+} : Magnesium ion

Mg_2SiO_4 : Forsterite

$MgBu_2$: Dibuthylmagnesium

MgO : Periclase

$MgSiO_3$: Enstatine

$MgTf_2$: Magnesium trifluoromethane sulfonate

Mn : Manganese

Mn^{2+} : Manganese ion

$MnCO_3$: Manganese (II) carbonate

MnO_2 : Manganese Oxide

MSS : Molten salt synthesis

NASICON : Sodium Super Ionic Conductor

Ni : Nickel

Ni^+ : Nickel ion

P : Phosphorus

PAN : Poly-acrylonitrile

PC : Propylene carbonate

PEC : Polyethylene carbonate

PEO : Poly-ethylene oxide

PMMA : Polymethylmethacrylate

PVDF : Poly-vinylidenefluoride

R_{ct} : Resistance

RE : Reference electrode

S : Sulphur

Se : Sellenium

SEM : Scanning Electron Microscopy

SHE : Standard hydrogen electrode

SiO_4 : Orthosilicate

SPE : Solid state polymer electrolyte

T_c	:	Crystallization temperature
Te	:	Tellurium ion
TEOS	:	Tetraethyl orthosilicate
T_g	:	Glass transition temperature
TGA	:	Thermogravimetric analysis
THF	:	Tetrahydrofuran
T_m	:	Melting temperature
TMO	:	Transition metal oxide
TN	:	Transference number
V	:	Unit cell volume
V_2O_5	:	Vanadium oxide
V^{5+}	:	Vanadium ion
WE	:	Working electrode
XRD	:	X-Ray Diffraction
Zn^{2+}	:	Zinc ion
Zr^{4+}	:	Zirconium ion
θ	:	Bragg angle
λ	:	Wavelength of the X-ray
ρ	:	Density

CHAPTER 1: INTRODUCTION

1.1 Research Background

Energy can be considered as an essential need in the history of mankind and the energy needs of mankind are forever growing. The search for energy sources has been an important activity throughout the ages. Environmental concerns have created enormous interest in the development of clean energy sources. Electrochemical power sources are attractive in this regard as they provide clean energy. Over centuries, different types of energy sources: (i) batteries, (ii) fuel cell (Dyer, 2002; Kim et al., 2007; Paladini et al., 2007; Ross, 2006) and (iii) supercapacitors (Barak, 1980; Frackowiak, 2007; Simon et al., 2008) have been developed to power the machines that men have invented. For small, portable and electrical machines, the most common energy sources in use today are known as batteries (Van Mierlo et al., 2006). Batteries are devices that convert electrical energy from chemical energy via electrochemical reduction and oxidation (redox) reaction of their active materials (Huggins, 2008; Linden, 1984).

Basically, chemical batteries storage can be divided into two main categories which are primary and secondary battery (Barak, 1980). These two types of batteries owned similar properties in term of discharging energy or storing electricity. The only difference is whether the chemical process inside the battery involved single or multiple charging/discharging process (Winter et al., 2004). A primary battery is the one that cannot be recharged for reuse. It is also called single-use, or “throw-away” since the original idea of this battery was it will be disposed once used. Portable devices with small current drain such as communication circuit and alarm commonly used this type of battery. This kind of devices is not fully dependent on a single power supply. Battery inside the devices is only used intermittently when the devices are away from electrical power source. On the other hand, the second type of battery is the rechargeable (secondary) battery. The two electrodes inside the battery made up of active materials that can be reconstituted structurally and chemically by applying electrical potential between them. The electrochemical reaction inside this battery is reversible when reverse current is applied. These secondary batteries can be discharged and recharged repeatedly (Edison, 1907).

The development of batteries started 25 years before century. The Baghdad Battery, developed by Wilhelm Konig in 1938, is believed to have belonged to the Parthian Empire and was used for electroplating (Palacin, 2009). After Luigi Galvani's discovery that frog legs would twitch when connected by two different metals, Alessandro Volta developed the first modern battery known as "voltaic pile" by stacking zinc and copper disks (Dibner, 1964).The first rechargeable battery, lead acid battery was invented by Gaston Plante and the Lechlanche cell was modified by Carl Gassner to develop the first dry cell (Alvarez et al., 1981). Next, alkaline manganese and nickel-cadmium batteries were invented by Lewis Urry and Waldemar Jungner respectively. Wilson Greatbatch implanted the first totally implantable cardiac pacemaker and later improved the battery with lithium-iodine technology. In 1979, making used of lithium cobalt oxide, John Goodenough assembled the first working rechargeable lithium-ion battery (Goodenough et al., 2009).

In 1859, the first secondary battery, lead/acid battery was invented (Colin et al., 1984; Linden et al., 2001). An active material of the electrodes was obtained by passing a current between soft lead plates in the original version of Plante cell. It was then improved by Faure in 1881 (Dell, 2000). The contribution of this type of battery to the society is undeniable. This lead/acid battery has been around for almost 100 years and it is still in use today but with better design and much improved technology. Popular at the end of the 19th century, rechargeable alkaline battery was introduced by Edison in the USA and Junger in Sweden (Dell, 2000). Commonly known as ‘nickel/cadmium, and ‘nickel/iron’ batteries since this battery are based on either cadmium or iron for the negative electrode and nickel oxide as it positive electrode.

Lithium ion batteries (LIB) presently stand as a market leader and forerunner in the portable secondary battery market. The technology offered by LIB was pioneered by Sony as early as 1991 (Nishi, 2001). The motivation for using Li based relied initially on the fact that Li is the lightest metal with equivalent weight, $M = 6.94$ gmol^{-1} (J. S. Lee et al., 2011) and $\rho = 0.53$ gcm^{-3} in such a way ease the design of storage with high energy density (Tarascon et al., 2001). These rocking chair batteries provide two way movements of lithium ions during charge and discharge processes between electrodes through the electrolyte (Scrosati, 1992). Figure 1.1 shows the summary of battery technology development. Nowadays, the LIB has been acclaimed as advanced power sources, slowly replacing several versions of conventional system such as nickel cadmium and lead acid batteries. However, cost, safety and environmental concerns have become trust areas for the 21st century. In this regard, the magnesium based battery offer to provide environmental and safety solutions.

The majority of relevant research interest focuses on the development of insertion reaction of lithium batteries. However, very limited attention has been paid to the divalent magnesium. Realizing the great potential of metallic magnesium, especially in term of safety and cost, research into the technology has accelerated in recent years. Magnesium based technology is promising for several reasons. First, magnesium can be obtain easily as it is abundant in nature (13.9 % in earth’s crust as compared to 10^{-4} % for Li) (Levi et al., 2009), its incorporation into electrode materials is inexpensive. Due to the fact that magnesium has higher melting point compared to lithium, therefore magnesium is the best choice in term of safety and higher stability at ambient temperature makes the handling and electrode preparation easier for magnesium. In addition, the divalent nature of magnesium ions also offers higher volumetric capacity (3833 mAhcm^{-1}), higher than that for lithium (2046 mAhcm^{-1}). The comparison of the natural magnesium and lithium is simplified in Table 1.1.

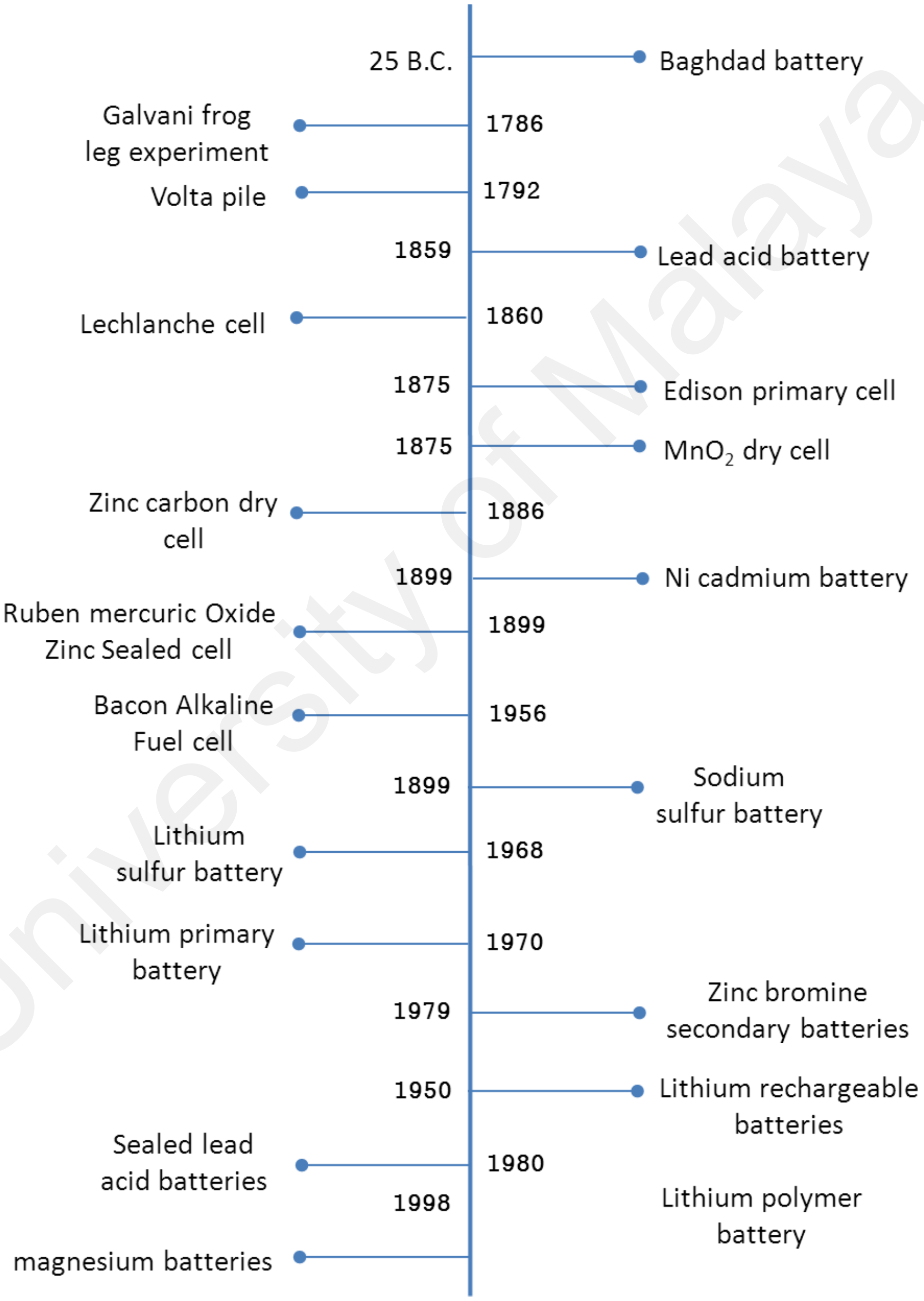

Figure 1.1: Chart shows development of battery technology

Table 1.1: Comparison of lithium and magnesium characteristics

Characteristics	Lithium (Li)	Magnesium (Mg)	References
Elemental abundance (ppm in earth's crust)	0.20×10^2	0.23×10^5	Haynes, 2014
Price (US$/ton)	21000	3000	Fritts et al., 1993
Volumetric capacity (mA h cm^{-3})	2046	3833	Saha et al., 2014
Gravimetric capacity (mA h g^{-1})	3862	2205	Yoo et al., 2013
Voltage vs S.H.E	-3.04	-2.07	Press, 2003
Pauling ionic radius	60	65	Huheey et al., 2006
Melting point (K)	453	923	Yoo et al., 2013

1.2 Problem statement

In the field of electrochemical application, magnesium has the potential to replace lithium ion battery especially when it comes to the inherent safety aspect and cost barrier. Lithium ion batteries are relatively expensive and lacks safety limitations which hinders it to be applied widely in the industry (Aurbach et al., 2001). Magnesium based batteries should be explored as an interesting alternative to the lithium ion batteries because of its advantages such as low price, large theoretical specific capacity, very low potential vs normal hydrogen electrode (NHE) and high safety (Novák et al., 1999). New rechargeable battery systems which are made of cheap environmental friendly materials and suitable for upscaling to large size are urgently needed. Synthesis route plays a vital role in determining chemical and physical properties of materials. Normally, the most common method used to prepare Mg_2SiO_4 is the conventional method of solid state method. However, materials prepared by solid state method have certain drawbacks such as the use of high heating temperature, long heating time, volatilization, lack of control of microstructure and contamination. In addition, the synthesis of orthosilicate compound of a pure phase without any impurities is very difficult, especially when performed by solid state reaction method. Adnan et al. (2011) has succeeded in obtaining orthosilicate containing compound $LiSiO_4$ via citric acid assisted sol-gel method. This method is suitable for small and large scale application and can produce high purity materials. Therefore, in this study, this method is considered in order to synthesis high purity and homogenous Mg_2SiO_4 materials.

Another problem regarding the rechargability of Mg batteries is the difficulty for the divalent Mg-ion to diffuse in solid-state electrode compared to the monovalent Li-ion. The choice of cathode materials has been limited because of the difficulty of intercalating Mg ion in many hosts (Levi et al., 2009). The slow Mg diffusion was generally assigned to strong Mg interactions with anions and the cations of the host (Amatucci et al., 2001) or to the polarized effect on Mg^{2+} cation with a high charge/radius ratio (Novák et al., 1999). Therefore, in order to overcome this problem, partial substitution of ions may be done which is expected to enlarge the migration channel of the Mg-ion (Fergus, 2010). Besides, the reduction of the particle size can also be done in order to shorten the diffusion path for the Mg-ion (NuLi et al., 2010).

There are number of studies conducted on forsterite Mg_2SiO_4 (Nuli et al., 2011; Kharaziha et al., 2009; Morin et al., 1977). However, the study is only focus on structural characterization and applied in different field. Very few work reported on the electrochemical studies of Mg_2SiO_4. Realize the potential of this forsterite material, therefore in this work forsterite based materials have been synthesized and the materials were tested electrochemically.

1.3 Objectives of study

The main purpose of the proposed research work is to develop new electrode Mg-based material with properties suitable for application in solid state electrochemical devices using cheap, easy and low temperature method. Studies were carried out with the objectives as follows:

i. To obtain pure magnesium based compound (Mg_2SiO_4) as a potential parent electrode material for rechargeable magnesium batteries using sol gel method.

ii. To produce Mg_2SiO_4 based compounds with improved properties by doping with divalent cation Mn^{2+} and Zr^{4+}

iii. To identify the electrochemical performance of the obtained materials

1.4 Thesis organization

This thesis is divided into 7 chapters. Chapter 2 of this thesis provides literature review related to magnesium rechargeable battery and cathode materials of magnesium battery. Chapter 3 reveals the details of the experimental techniques used for synthesizing and characterizations of the materials. The materials were subjected to various characterizations to study thermal, structural, morphological, elemental as well as it electrochemical properties. Techniques involved include Scanning Calorimetry (DSC), thermogravimetric analysis (TGA), X-Ray Diffraction (XRD), Fourier Transform Infrared Spectroscopy (FTIR), particle size analysis, Scanning Electron Microscopy (SEM), Energy Dispersive X-ray (EDX), Electrochemical Impedance Spectroscopy, transference number and cyclic voltammetry (CV). Each technique is briefly reviewed and the significant of each analysis is explained technically. In addition, the method used to prepare the electrolyte and cathode preparation for CV cell fabrication is also disclosed in this chapter. Results obtained were discussed in detail in chapter 4, 5 and 6. Chapter 4 focuses on the analysis of the first system, Mg_2SiO_4 while results and analysis of the second system, $Mg_{2-x}Mn_xSiO_4$ are elaborated in chapter 5 followed by results and discussion of the third system, $Mg_{2-x}Mn_xZr_ySi_{1-y}O_4$ in chapter 6. The conclusions of the whole works are reported in the last chapter, which is chapter 7. Suggestions for future work are also included in chapter 7.

CHAPTER 2: LITERATURE REVIEW

2.1 Rechargeable Battery

An electrochemical cell is a device, which is capable of converting chemical reaction into electrical energy. Generally, an electrochemical cell build up from two electrodes separated by at least one electrolyte phase (Bard, 1980). The three major components of the electrochemical cells (Figure 2.1) are described as follows:

1. The positive electrode (cathode), which responsible to accepts electrons from the external circuit and experienced reduction during the intercalation/deintercalation process.
2. The negative electrode (anode), which responsible to gives up electrons to the external circuit and experienced oxidation during the intercalation/deintercalation process.
3. The ionic conductor (electrolyte), which provides the medium for electronic charge transfer out of cell, as ions, inside the cell between the anode and cathode (Linden, 1984). Commonly, the electrolyte used is in liquid forms, which are made up of a mixture of solvent and salts, alkalis or acids.

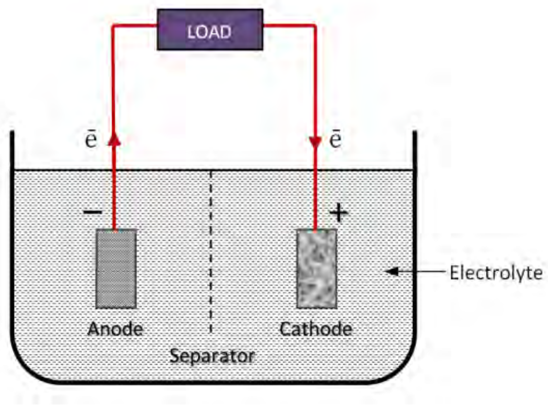

Figure 2.1: Schematic representation of electrochemical cell

There are many types of practical devices based on electrochemical cells. Batteries, fuel cells, electrochemical capacitors, electrochemical devices, and electrochemical sensors are some examples of practical electrochemical devices. Battery is a device that consists of few electrochemical cells assembled in parallel or series depending on the chosen output capacity and output voltage for specific applications. The electrochemical cells in the battery convert the electrical energy from chemical energy in the active materials through the electrochemical (oxidation–reduction) process.

Generally, batteries can be divided into two main categories depending on the reversibility of the redox reactions involved in the energy conversion (Linden, 1984) If the electrochemical redox reactions cannot be reversed, then such a battery is called a primary battery. On the other hand, if the reactions can be reversed, then the battery is called a secondary (rechargeable) battery. There are several terms that are commonly used to define the characteristics of various types of batteries. However, cell potential of battery depending on the combination of electrode materials and the type of chemical reactions involved. An ideal battery has a specific cell potential, but a practical battery may show lower and varying potentials depending upon the service conditions. The difference between the ideal cell potential and actual potential is called polarization. The battery operation may involve several types of polarizations, which may lower the observed or operating potential. Polarizations can be divided into three large categories as illustrated in Figure 2.2 (Hossain et al., 1995).

a) Ohmic polarization (IR drop), which arises from the combined sum of the electronic resistances of the active mass, the contact resistance between the current collector and active mass, ionic resistance of the electrolyte, the current collectors and electrical tabs of both electrodes.

b) Activation polarization, which arises from the resistance to transport the working ions across the electrolyte – electrode interfaces.

c) Concentration polarization, which arises from the concentration differences of the bulk as a result of mass transfer and in the products and reactants at the electrode surface.

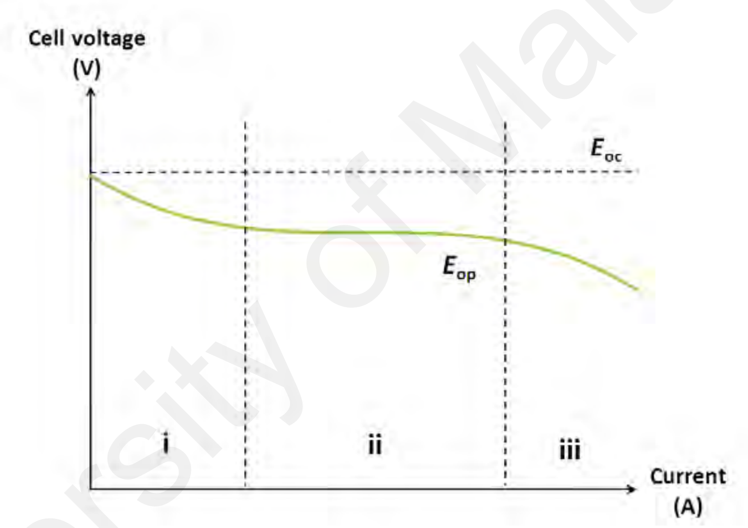

Figure 2.2: Cell polarization associated with a typical discharge curve. (a) Ohmic polarization (IR drop), (b) activation polarization, and (c) concentration polarization

Generally, the system of magnesium battery is also identical to any other standard electrochemical energy storage. Magnesium batteries made up of magnesium at the anode as the active element in an electrochemical cell. Rechargeable batteries are those, which can be reused by reversing (charging) the electrochemical reaction through the application of reverse current. Rechargeable batteries are in demand with the rapid development of electronic devices and automobiles, which needs reliable power sources. Rechargeable magnesium batteries are poised to be capable candidates for large scale application in energy storage devices for smart grid communication and electric vehicle. However, due to the limitation that arises especially due to the cathode materials, magnesium batteries currently proposed offer low energy density. Therefore, there is an urgent need in finding promising cathode materials.

2.2 Cathode materials for Mg batteries

For the past few years, many efforts have been dedicated to the progress of cathodes for Mg batteries. Some cathode materials such as AgCl, CuCl, Cu_2I_2, $PdCl_2$, MnO_2 and CuSCN have been extensively explored for reverse type Mg battery system which normally requires high power output and energy density, very low temperature and long lifetime performance. All mentioned cathodes so far could be used in primary batteries, however recharging and operating them as secondary batteries is impossible due to the passivation layer formation on the anode surface. Due to the present of high resistive blocking layer, it is a must to apply a large potential to recharge the battery. Besides that, realization of practical rechargeable Mg batteries was hampered by the sluggish reaction kinetics, the absence of practical cathode and appropriate electrolytes (Levi et al., 2009). Realization of rechargeable magnesium system still far to be done. Further enhancement of the cathode performance and a proper understanding of the cathode reaction are needed to produce working rechargeable system. In order to develop the next generation of Mg battery cathode, the most important issues are monitoring Mg^{2+} ion's mobility in the diffusion pathway and overcoming the negative impact arising from divalent Mg^{2+} ions. Most of inorganic hosts thus far explored proved to be good in Li cathodes but showed deficient electrochemical response when studied as potential intercalation cathodes, instable crystal structure and kinetically slow Mg^{2+} ion remain key obstacles in development of working cathodes with high voltage.

There have been few representative strategies for the realization of good Mg cathode. The first one is to shield the divalent Mg^{2+} ion with strong dipoles such as H_2O in the solution or in layer (Novak et al., 1993). The second one is reducing the particle size of materials, which will reduce the transport distance for the ions and electrons. Enhanched Mg^{2+} ions during intercalation/deintercalation process is expected to improve the capacity retention and increase the reaction kinetics (Shao et al., 2014). This particle size reduction method has been tested in a number of Li rechargeable battery studies as an effective method to enhance cycling stability and rate capacity (Fey et al., 2009; Sides et al., 2005). Fast and efficient Mg^{2+} ions intercalation/deintercalation was reported for nano-sized crystallite materials (Amatucci et al., 2001), nano tubes (Tao et al., 2004) or thin films (Sian et al., 2004). In such system, sample in micron-sized would have better ion diffusion.

Another aspect that influences the electrochemical performance of a material is through structural modification by doping. The promoting effect of doping process on the cycling stability and rate capacity has been demonstrated in Li rechargeable battery (Roberts et al., 2008; Wen et al., 2006; Ying et al., 2006; Zhang et al., 2006). The positive effect of doping was used to the improved ion diffusion coefficient and the increase intrinsic electronic conductivity in doped materials (Liao et al., 2007; Shin et al., 2008; Sun et al., 2009; Zhang et al., 2006). On the other hand, researchers made efforts to boost the electronic contact between the electronic conductor and active powders by adding conductive carbon. Mixing procedure used and the amount of conductive carbon loaded in the prepared cell notably contribute in the electrochemical performance. However, it is reported that loading large amount of conductive carbon effectively improves the cell's rate capacity but poor energy density (Chen et al., 2002; Dominko et al., 2003; Zhang, 2010).

Good cathode materials for rechargeable battery should satisfy several criteria as listed below:

1. Large work function compared to that for anode to maximize the cell voltage
2. Large degree of magnesium insertion /extraction to maximize the cell capacity
3. Good structural stability after continuous intercalation/deintercalation process (magnesium ion intercalation)
4. Good chemical stability in electrolyte that is based on organic solvents.
5. Ease of synthesis
6. High density to provide high volumetric capacity
7. Light weight to provide higher gravimetric energy density.
8. Easy diffusivity pathways for magnesium ions in the crystal to provide high rate capability.
9. Good electrical conductivity to provide high rate capability
10. Low cost
11. Environmentally benign

2.3 Types of cathode materials

2.3.1 Chevral Phase

In the last few decades, Chevrel phases (CPs) have been extensively explored as cathode in Li batteries. CPs are considered a unique class of host materials that have the ability to exchange ions during redox process. Besides their ability to transport monovalent (Cu^+, Li^+, Na^+), CPs allows fast insertion of divalent cations, such as Zn^{2+}, Fe^{2+}, Co^{2+} Ni^{2+}, Mn^{2+}, and Cd^{2+} (Takeda et al., 1985; Wakihara et al., 1989). The crystal structure of Mo_6T_8 (T = S, Se and Te) consists stacking of Mo_6T_8 blocks composed of the octahedral molybdenum atoms cluster inside the anion cube of selenium /sulphur /tellurium atoms. Figure 2.3 shows a basic CPs crystal structure. There are three cavities formed between Mo_6T_8 blocks but only two of them are available for cation insertion (cavity 1 and cavity 2). Occupation of cavity 3 is prohibited because of the strong repulsion between inserting cation and Mo atoms (Levi et al., 2006).

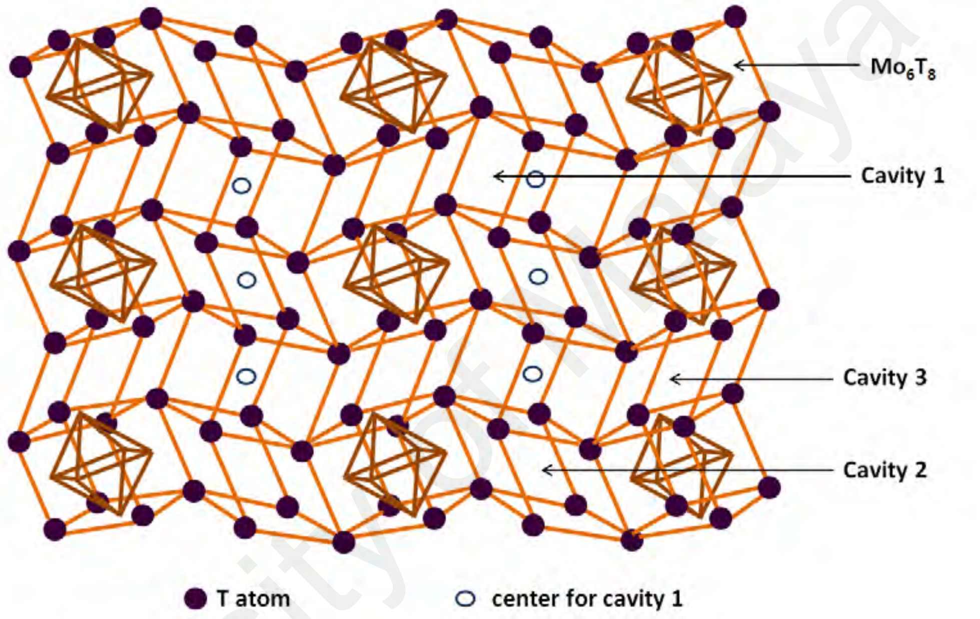

Figure 2.3: Basic CPs crystal structure with Mo_6 clusters

In 2000, Aurbach et al discovered that this CP Mo_6S_8 can be an excellent cathode material in magnesium rechargeable batteries using magnesium organo-haloaluminate complex electrolyte solutions. It was reported that the performance of this cathode over > 1800 cycles was very stable with small percent of capacity fade (Aurbach et al., 2000). However, Mg^{2+} ions only were fully extracted at elevated temperature, unless about 20 - 25 % of them were trapped in CP lattice in early electrochemical process. Introduced Se to the CP crystal structure was reported resulting in higher capacity at higher rate and at lower temperature (Levi et al., 2006). Se-substituted CP cathode point out an outstanding accessibility of Mg^{2+} ions even at lower temperature. The only disadvantage of CPs is the low voltage for Mg intercalation/deintercalation, ~1.0 V vs. Mg^{2+}/Mg at relatively small capacities which invariably yields Mg battery system with very small energy density (Levi et al., 2009).

2.3.2 NASICON Type Materials as Cathode

NASICON type materials with a general formula of $A_nM_2(XO_4)_3$ where (A= Na or Li; M = transition metal; X = P, As, or S) have been extensively explored mainly in Li batteries. This type of well-known NASICON compounds (Wang et al., 1995) have high structural stability and large enough interstitial vacancies to uptake guest species based on three-dimensional frame-work. Figure 2.4 show basic NASICON structure. Both sodium ions and lithium ions can be extracted/inserted reversibly from/into a series of NASICON compounds.

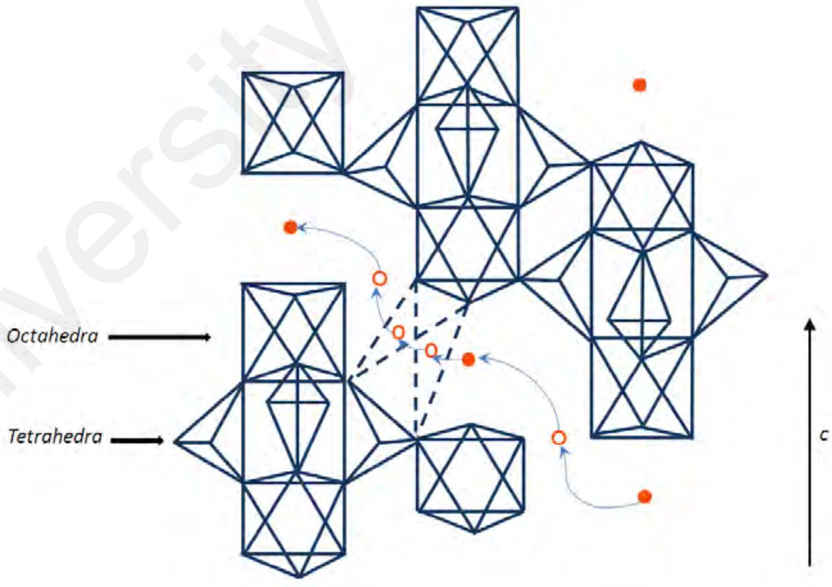

Figure 2.4: Basic NASICON structure

Likewise, this NASICON structure seems to have a great potential as a promising host for Mg^{2+}. Mg^{2+} ion is expected to transport in such lattice structure. Makino et.al (Makino et al., 2001) reported that in $Mg(ClO_4)_2$/propylene carbonate (PC) electrolyte solution, Mg^{2+} ion can be electrochemically inserted into $Mg_{0.5}$ $Ti_2(PO_4)_3$ NASICON structure. Nevertheless, the diffusion rate of Mg-ion was indeed slow and kinetically limited. Later, modifications have been done on the structure by adding transition metal Fe. $Mg_{0.5+y}(Fe_yTi_{1-y})_2(PO_4)_3$ (MCTP), ($0 \leq y \leq 0.5$) have been synthesized by employing sol-gel method. However, the cycling behavior of the system is still not much improve (Makino et al., 2001).

2.3.3 Mg-ion Insertion Type Cathode V_2O_5

In addition to NASICON type cathode materials for Mg battery, V_2O_5 was also reported as one of the possible host for chemical insertion of magnesium ions. Crystalline Vanadium oxide, V_2O_5 consists of layers of a weak O-V interaction with the 6th oxygen and square-pyramidal V^{5+} co-ordinated to 5-oxygen which provide pathways for ion insertion and removal.

However, (Shklover et al., 1996) suggested that the electrochemical insertion of Mg^{2+} into bulk V_2O_5 at room temperature is very slow and most of Mg^{2+} are absorbed on the surface electrode material. Reversible electrochemical reduction of Mg^{2+} into V_2O_5 is only practical in the $Mg(CF_3SO_3)_2$ sulfolane and $Mg(ClO_4)_2$/molten dlmethylsulfone and based electrolytes at elevated temperature (T = 150 ºC) (Pereira-Ramos et al., 1987). According to Novak and Desilvestro (Novak et al., 1993) reversible magnesium insertion is only possible with the present of water molecules in the electrolytes. The best discharge capacity reported was ~170 mA h g^{-1} in acetonitrile solution containing H_2O. The presence of bonded lattice water in the crystal structure of the $Mg_xV_2O_5$ also enhanced the insertion reaction of the Mg^{2+}. However, it is noted that the presence of traces of water will affect the performance of non-aqueous Mg battery and should be completely avoided for any non-aqueous Mg battery system as it will extremely compromise the battery performance. In conclusion, for this time being, Mg-ion insertion into a V_2O_5 lattice was found to be very slow. The Mg ions only get solvated and can only be inserted easily into the host structure that consists of water molecules.

2.3.4 Magnesium-sulphur Conversion Cathode

Magnesium–sulfur (Mg-S) is a potential system with the present of Sulphur element that undergoes conversion reaction with metallic Mg cathode (the potential of electrochemical reaction, E = 1.70 V). In addition, Mg-S cathode offer reasonable theoretical capacity around ~1670 mA h g^{-1}, magnesium-sulfur is considered as a promising system. The combination of a magnesium anode and sulfur cathode can in turn deliver higher theoretical energy density which is way higher than the current used Li-ion system of ~4000Wh l^{-1}. However, the development of Mg-S cell was hindered by main challenge which is limited number of compatible electrolyte for the system. Kim et al. (2011) exploring rignard based organochloro electrolytes but they found no way to continue of using this electrolyte in Mg based battery system. These electrolytes are nucleophilic in nature and readily react with electrophilic sulfur to form polysulfide compounds. This reaction will end up causing sulfur dissolution due to the loss of Sulphur which is similar to the Li–S system.

Charge-discharge curve for the 1st two cycles of Mg-S cell is displayed in Figure 2.5. The 1st discharge capacity was observed around ~1000 mA h g^{-1} due to breaking of the resistive surface layer on metallic magnesium followed by a small increase in the voltage plateau from ~0.50 V to 0.90 V. The next cycle discharge capacity was dramatically decreased to ~390 mA h g^{-1} (Kim et al., 2011). It was reported that the separator used in the cell changes in color due to the formation of Sulphur dissolution or polysulphide anions. The capacity of the cell reduced due to the present od the dissolution & anions. Nonetheless, Toyota was the first to assemble Mg-S battery with a promising energy density. Toyota come out with one working Mg-S battery which consist of a non-nucleophilic base namely hexamethyldisilazide magnesium chloride (HMDSMgCl) salt in tetrahydrofuran as electrolyte, elemental sulfur as conversion cathode and magnesium anode. The choice of this electrolyte was reported to overcome sulfur dissolution in the system. Reaction of non-nucleophilic potassium hexamethyldisilazide $KN(SiMe_3)_2$ salt and ethyl magnesium chloride (EtMgCl) was done in the present of tetrahydrofuran (as the solvent) to obtained desired non-nucleophilic magnesium electrolyte of HMDSMgCl. This finding gives a huge contribution toward the development of Mg-S technology which the put Mg-S battery in the same vein as lithium ion battery and Li-S battery. Effort have been dedicated to mitigate the capacity fade including replacing tetrahydrofuran solvent with ionic liquid, glymes and block copolymer gel electrolyte (Muldoon et al., 2012). There are also a number of researchers used Sulphur composite instead of mesophorous carbon to enhance the cell capacity.

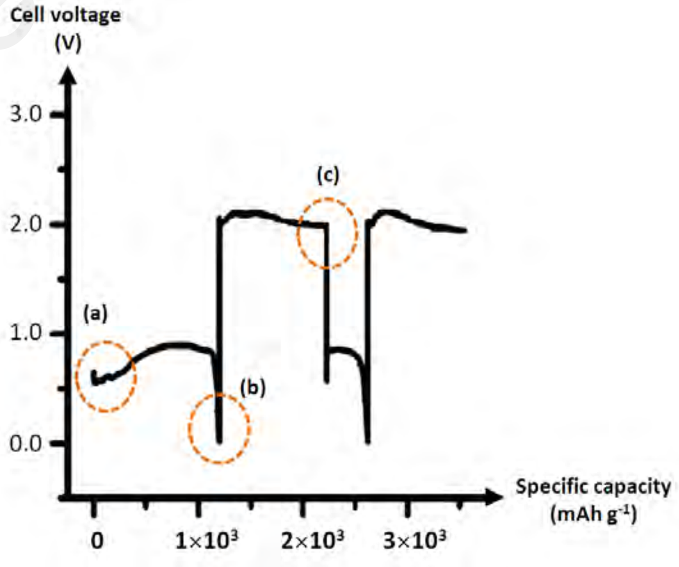

Figure 2.5: Charge and discharge of a Mg-S coin cell

2.3.5 Transition Metal Dichalcogenides Intercalation Cathode

Another type of cathode which was widely investigated in rechargeable battery especially Li is Transition metal dichalcogenides (XY_2, X = transition metal and Y = S, Te and Se) such as VS_2 and TiS_2. This type of cathodes was among the earliest cathode in Li rechargeable battery dated back to late 1971s. There are a number of researchers works on rechargeable Mg based battery were electrochemically investigated the capability of this type of compound in different forms including the fullerene-like hollow-cage nanoparticles, spherical nano vesicles and fibrous flocculated structures.

The performance of graphene-like MoS_2 composed of single and several layers of highly exfoliated MoS_2 was studied using CR2032 coin-type cell (Liang et al., 2011). It was reported that the electrochemical performance of the cell with $Mg(AlCl_3Bu)_2$ in THF as the electrolyte exhibited average operating voltage around 1.8 V. From a first principles density function theory (DFT) study conducted by (Chen et al.,2011) they found out that MoS_2 can be treated as zigzag nanocarbons. In zigzag MoS_2 nanoribbon, Mg was identified interested on the top sites of Mo at the edge of nanoribbons surface (T-sites). These sites offer up to ~ 223 mA h g^{-1} theoretical capacity. Besides that, as observed in Figure 2.6, Mg atom also tends to occupy in between two adjacent T-sites centred by nearest neighboring H-site (hollow at the center of the hexagon).

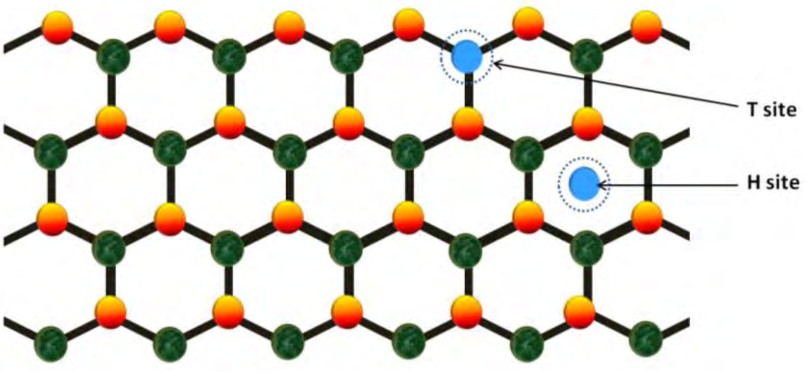

Figure 2.6: Structure of MoS_2

Another type of transition metal dichalcogenides for Mg cell which are famous among researchers is WSe_2 and the electrochemical performance was documented (Liu et al., 2013). Coin cells were used to test the electrochemical performances of ~100 nm WSe_2 nanowires. Results obtained supported that this WSe_2 nanowire electrodes have a promising structural stability. The discharge capacity was about 1.6 V accompanied by a very small decay meanwhile the reversible specific capacity was around 203 mA h g^{-1}.

2.3.6 Transition Metal Oxide Type Intercalation Cathode

Transition metal oxide (TMO) systems demonstrating ability to intercalate Mg^{2+} has been reported (Liebenow, 1997). In this regard, Gummow et al. (2010) employed co-precipitation route to synthesize $Mg_{0.67}Ni_{1.33}O_2$. This material owned reasonable electrical conductivity with an open circuit voltage ~3.5 V vs. Mg^{2+}/Mg at ambient temperature. However, due to the limited number of stable electrolytes beyond ~3.5 V, the actual potential of these cathode materials is yet remain uncertain. We also synthesized similar transition metal containing oxides. Inadequate crystal structural stability as well as the electrolyte voltage stability combined with the electronic conductivity of the material hindered the Mg^{2+} response, hence failed to demonstrate any distinct reversible cycling of Mg^{2+}. Additionally, a report of Mg^{2+} ions insertion of a strained Mg_xMnO_4 cathode in a 0.1 mol $Mg(ClO_4)_2$ – 0.5 mol H_2O tetrahydrofuran electrolyte was also documented (Brenner, 1971). They claimed that Mg^{2+} ions can be chemically inserted in this materials at voltage potential of ~0.7 V vs. Mg/Mg^{2+}. an aspect that needs further investigation.

2.3.7 Olivine Compound $MgMSiO_4$ (M = Co, Mn, Fe) Cathode

Another type of cathode materials that catch the attention of researchers is olivine compound, which is very well-known cathode compound in Li-ion battery. This type of compound has been extensively explored in Li ion battery and said offer some good properties, which is suitable for cathode materials. $LiFePO_4$ was reported to be the most encouraging olivine compound which owned very stable due to the present of polyanion in the structure (Padhi et al., 1997). Huge success of olivine compound in Li-ion batteries was a great motivation to explore olivine type compound for Mg based batteries. The potential of olivine compound $MgMSiO_4$ which belong to orthorhombic crystal structure was reported in a number of studies (Nuli et al, 2008; Zheng et al, 2012; Sun et al, 2013). Lattice parameter of $MgMSiO_4$ compound is $a = 4.79$, $b = 10.49$ and $c = 6.12$ Å with a space group of *Pbnm* (62). The crystal structure of olivine reveals the typical tetrahedral and octahedral coordinations for the different metal cations wherein the alternate sites of Mg1Mn1 and Mg2Mn2 are within the octahedral and Si occupies the tetrahedral sites, while oxygen atoms are located in the corners as shown in Figure 2.7.

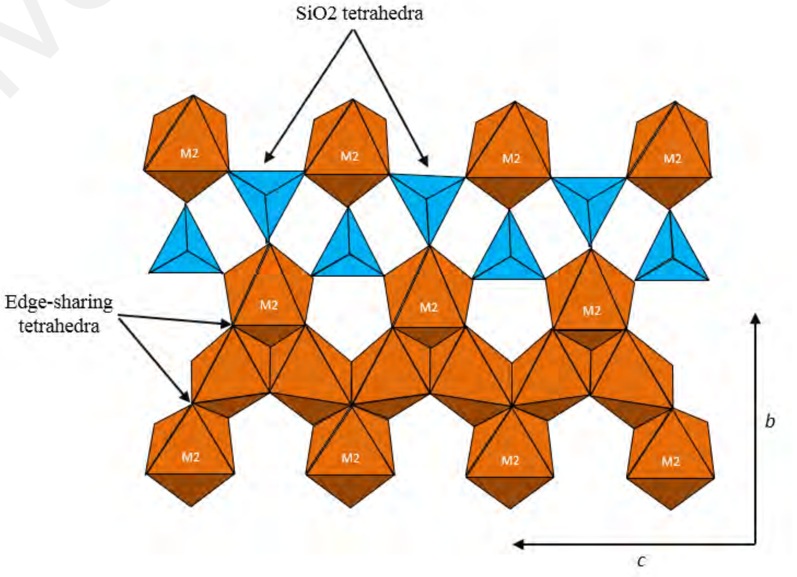

Figure 2.7: Olivine crystal structure

Table 2.1 summarized olivine $MgXSiO_4$ (X = Fe, Co, Ni, Mn) structure cathode materials that has been explored. Li et. al (2011) synthesized micro sized $MgFeSiO_4$ cathode material by using molten salt route. This type of cathode materials has been proposed as an intercalation cathode for Mg batteries which exhibit discharge capacity of ~121 mA h g^{-1}. $MgCoSiO_4$ has been explored by (Zheng et al, 2012). Electrochemical testing was done and it's demonstrated of ~121 mA h g^{-1} discharge capacity. In addition to that, Ni also has been used by (Sun et. al (2013) to improve the performance of olivine structured cathode material. $MgNiSiO_4$ has been synthesized by using sol-gel method and molten salt method.

Table 2.1: Olivine structure cathode materials for magnesium battery

Compound	**Method used (Starting materials)**	**Final firing temperature, time**	**References**
$Mg_{2-x}Mn_xSiO_4$	Sol Gel (Mg Acetate tetrahydrate, Manganese acetate tetrahydrate and tetraethylorthosilicate)	700°C, 24 hours	NuLi et al., 2008
	Modified Sol Gel method (Mg acetate tetrahydrate, Mn acetate tetrahydrate and nanoscale silicon dioxide)	900°C, 24 hours	NuLi et al., 2010
	High Temp Solid State reaction (Mg oxide, manganese (II) carbonate, silicon dioxide)	1250°C, 10 hours	Feng et al., 2008
	Molten Salt Synthesis (Magnesium oxide (MgO), manganese(II) carbonate ($MnCO_3$) and SiO_2)	1000°C, 10 hours	NuLi et al., 2009
$Mg_{2-x}Fe_xSiO_4$	Molten Salt KCl, MgO, Iron Oxalate dehydrate and SiO_2	800°C, 900°C, 1000°C	Ni et al., 2007
$Mg_{2-x}Co_xSiO_4$	Solid state reaction (MgO, Co_3O_4 and SiO_2)	1200°C, 32hours 1300°C, 16 hours	Zheng, 2012
	Molten salt method (KCl, MgO and $CoCO_3$)	1000°C, 6 hours	
	Mixed solvothermal method (Mg acetate, cobalt acetate and urea)	500°C, 4 hours 900°C, 6 hours	
$Mg_{2-x}Ni_xSiO_4$	Sol-gel (Magnesium acetate and Nickel Acetate)	800°C, 24 hours	Sun et al, 2013
	Molten salt method (KCl, MgO, $NiCO_3$ and SiO_2)	1000°C, 6 hours	

2.4 Preparation method of cathode materials

Cathode materials can be prepared by using various methods. Methods commonly used can be divided into two main categories which are solution chemistry method (method that use solution as the starting materials) and solid-state chemistry method (method that use solid phase as the starting materials). Example of solid state chemistry method is mechanochemical activation, microwave processing, carbothermal reduction and solid-state reaction meanwhile precipitation method, sol-gel processing, spray pyrolysis, emulsion-drying method and hydrothermal processing can be categorized under solution chemistry method. However, solution chemistry method is more popular among these two types of methods due to its ability of achieving better mixing and homogeneity of the starting materials on molecular level. Throughout the year, different types of method have been explored to synthesize Magnesium Silicate compound (which are reported in this study) such as solid-state reaction, sol-gel method and molten salt method. In the following subsections, method that are commonly used to synthesis Magnesium Silicate will be further explained.

2.4.1 Solid State Reaction Method

Solid-state method is considered as a familiar method used by researchers in synthesizing electrode materials. This method is also known as solventless reaction or dry media reaction. A solid state is a chemical reaction in which solvents are not used. In a normal reaction, the reacting agents, also called the reactants, are placed in a solvent before the reaction can take place. These reactants react to form a new substance. Figure 2.8 illustrates the general steps involved in material processing using solid state reaction. This method is very practical for preparing huge number of compounds. This method is suitable for a large-scale production such as for industrial purpose. However, high temperature is needed for this method because sometimes the desired compound may decompose at high temperatures. The reaction may proceed very slowly at low temperature, but increasing the temperature can speed up the reaction. The diffusion rate can be enhancing at high temperature environment. In this reaction, large amount of energy to overcome the lattice energy. Therefore over 500 °C generally required to perform this method so that cation or anion can diffuse into different site. Besides that, this technique also needs long reaction time and produced a large synthesized powder, which is not suitable for electrochemical devices application. Forsterite is widely synthesized via a solid-state reaction. However, the downsides mentioned above make the solution based techniques more advantageous for forsterite synthesis.

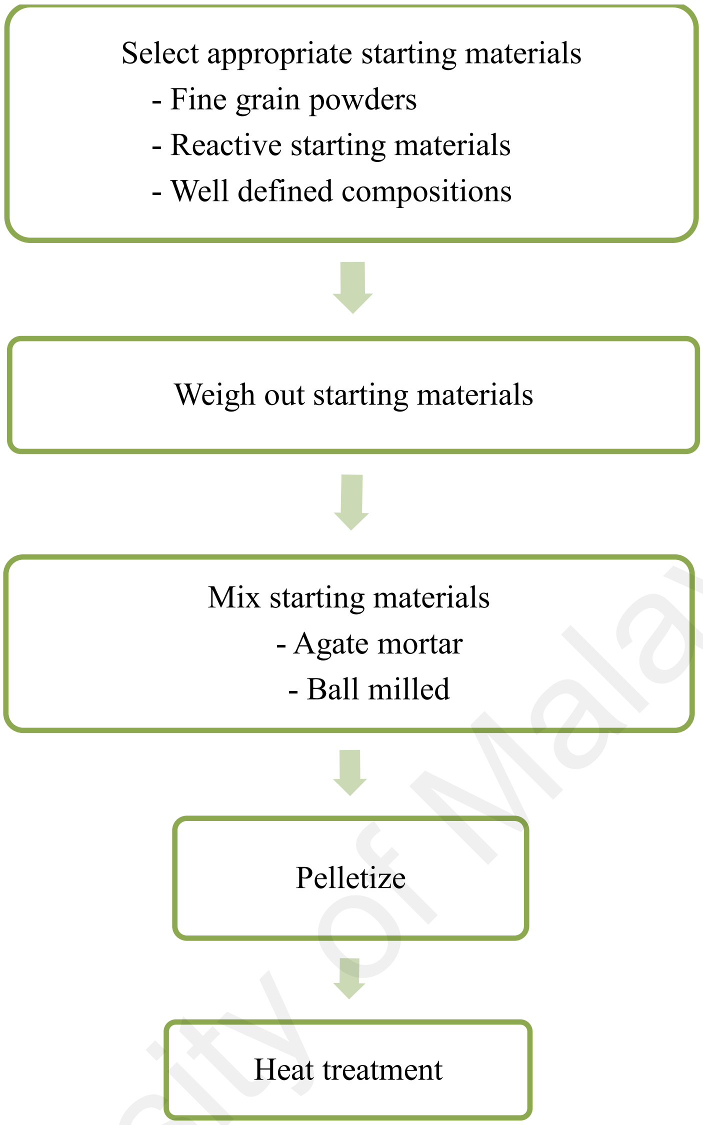

Figure 2.8: Steps involved in solid state reaction

For example, Lee et al. (2011) used this method to synthesize bioceramics material with the starting precursor consists of talc ($Mg_3Si_4O_{10}(OH)_2$) and magnesium oxide, MgO. Mixture of MgO and talc powder in the weight ratio of 1: 1.88 was first prepared. The powders were subjected to high frequency vibrations to ensure homogeneous mixing for 2 minutes. The powders were milled for 10 hours using ball milling to further refine the powder particles. The powder was heated for 2 hours at 1200 ºC with ramp rate of > 9 ºC min^{-1}. They reported that, forsterite materials were successfully synthesized by using solid state reaction method.

2.4.2 Molten Salt

Molten salt synthesis (MSS) is a new class of synthesis method for preparing inorganic materials. Molten salt with low melting point was used as reaction aid or reaction media in this method. The reaction take place when selected molten salt were dissolved in any suitable solvents, then only the desired product would be successfully synthesized (Ni et al., 2007). MSS requires short time and low reaction temperature compared to other methods. It was mentioned in (Zhang et al., 2014) that the materials prepared via this molten-salt method showed faster kinetics which then led to better electrochemical performance and cycling stability.

Stoichiometric amounts of manganese (II) carbonate ($MnCO_3$), magnesium oxide (MgO) and silicon dioxide were used by Nuli et al. as the starting materials to prepare $Mg_{1.03}\,Mn_{0.97}\,SiO_4$ by this method (NuLi et al., 2011). In addition, Zhang et al also used molten salt method to synthesize magnesium silicate to study the influence of material's particle size on the on properties of obtained materials. Starting materials used were natural forsterite and $NaSo_4$ molten salt (Zhang et al., 2014).

2.4.3 Sol-gel Method

Sol-gel is one of solution chemical process method mention earlier. This method commonly used to prepare glass and ceramic materials in the form of powders, fibers and even thin films. This method has been established. The sol-gel is a very long known since the late 1800s. The word sol itself means a stable suspension of colloidal solid particles or polymer in a liquid while the word gel can be explained as porous, three-dimensional and continuous network surrounding a continuous liquid phase. Sol-gel method is used for producing solid materials from small molecules. The processes involved are hydrolysis, condensation, gelation, ageing, drying and densification. Figure 2.9 presents basic steps in a sol-gel technique.

Several chelating agents, which are commonly used in sol-gel method, include citric acid, polyacrylic acid and polyethylene glycol. The sol-gel method has some potential advantages over other method. By employing sol-gel method, the end product can be either in the form of powder, film and fiber. Besides that, it also allows homogenous mixing of the components at the atomic scale (Chen et al., 2002). In addition, sol gel method is considered as a practical and useful method as it presents various superiorities such as obtaining good particle size distribution, low sintering temperature, short calcination period and allowing a good stoichiometric control (Kakihana, 1996).

Sol-gel was adopted as the reliable synthesis route in the current investigation. Sol-gel method have been used by Ni et al. (2007) to prepare forsterite powder. Taking reagent-grade magnesium nitrate hexahydrate ($Mg(NO_3)_2.6H_2O$) a colloidal SiO_2 as the starting materials with initial molar ratio of 2. Forsterite powder about 5–50 µm were successfully obtained after calcination process for 3 hours.

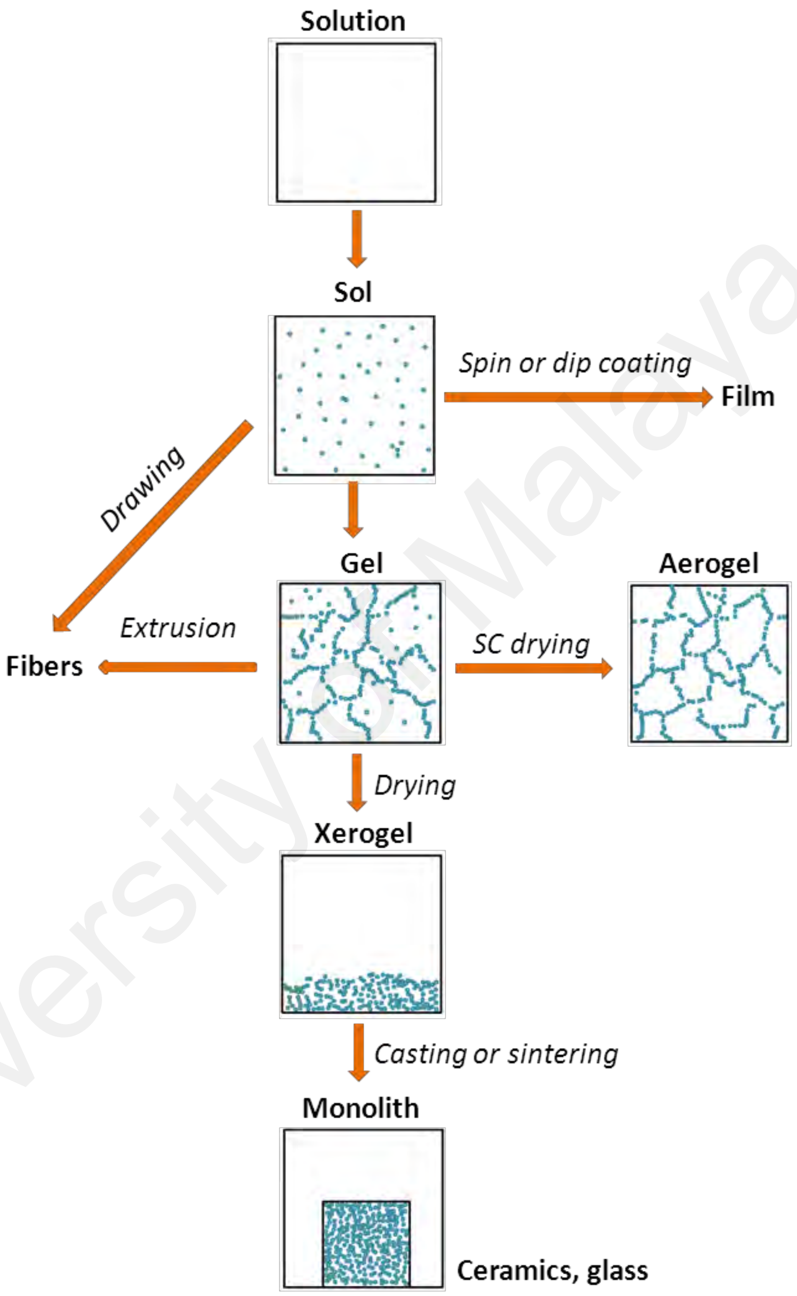

Figure 2.9: Steps involved in sol gel method

2.5 Electrolyte in Mg Batteries

Development of Mg based batteries also was hampered by limited suitable electrolyte with high ionic conductivity. Early works proved that simple Mg salts solution such as $Mg(Cl_4)_2$ in typical organic solvent (*N,N*-dimethylformamide, acetonitrile and propylene) formed a dense passivation layer on the electrode surface when used as electrolyte in Mg based rechargeable batteries (Brown et al., 1985; Lu et al., 1999; Peled et al., 1977). Mg could not be reversible in such electrolyte, but formed insoluble halides/salts instead when reacts with anion such as BF_4^- and ClO_4^-. The insoluble layer completely blocks the magnesium electrodes. As a result, Mg^{2+} ions mobility through the electrode is extremely poor due to the present of that insoluble layer. In addition, the capacity of the cell composes of electrolyte from simple Mg salts and typical organic solvent fades after some time of operation.

Early works demonstrated that deposited of Mg using ethereal solvents and Grignard reagents gives a positive respond (Brenner, 1971; Genders et al., 1986). Hence the finding was extended by Liebenow et al.(Liebenow, 1997) found out that solution of tetrahydrofuron (THF) using amidomagnesium halide and Grignard's reagent (MgX-R, where X = Cl, Br and R = alkyl) can be used to fabricate working Mg based electrochemical cell as Mg can be deposited reversibly. Nevertheless, it was considered incompatible for insertion cathode due to the limited oxidative stability (BuMgCl, EtMgBr) and strong reducing character of Grignard reagents.

Motivated from above finding, a huge attention has been paid to the non-aqueous electrochemistry of magnesium. Only solutions containing amidomagnesium halides, and magnesium organoborates in ether (Brenner, 1971; Liebenow, 1997; Liebenow et al., 2000) and Grignard reagents (Gregory et al., 1990) solution give out a reversible electrochemical Mg deposition, which do not react with Mg. It was Gregory et al.

(1990) who initially demonstrated that the application of electrolytes consist of magnesium tetrabutyl borate, $Mg(BBu_4)_2$ in primary amines (*N*-methylaniline) of tetrahydrofuron (THF) at appropriate values of over-potentials. Gregory developed non-aqueous electrolyte by reacting tri-n-butyl borane/THF (Lewis acid) with dibutylmagnesium/heptane (Lewis base) (Gregory et al., 1990). The electrolyte proposed showed a higher anodic stability compared to Grignard reagent but a bit low in coulombic efficiency. Gregory's work was very useful and contributed to the knowledge of the vital of Lewis acid for deposition and dissolution in mg based electrochemical cell.

Based on the finding reported by Gregory, in 2000 Aurbach et. al presented electrolytes solution of organohalualuminate salts in polyethers of the glyme family or THF (Aurbach et al., 2002). The proposed electrolytes were obtained when Lewis acid $EtAlCl_2Mg$ reacted with Lewis base Bu_2Mg. Mg can be deposited reversibly in electrochemically stable etheral solution containing magnesium organoalumintae compounds, $Mg(AlCl_{4-n} R_n)_2$, where R = Bu (C_4H_9) and Et (C_2H_5); n = 1,2 and dissolved in THF at room temperature (Aurbach et al., 2000; Huggins, 2008).

It has been reported that the electrochemical window depends on the Lewis acidity of the aluminum compounds involved, and some complex species formed in the electrolyte have been suggested based on the analysis of nuclear magnetic resonances and Raman spectroscopy (Nakayama et al., 2008). It is also revealed that the stability of the complex salt solution toward oxidation is higher for electrolyte with stronger Lewis acidity of the acid (organochloro aluminum anion). Besides that, it was reported that the R group involve in the reaction ruled the electrolytes anodic stability in the reaction. The variation of the anodic stability is change as follows: $-C_4H_9 < -C_2H_5 < -CH_3$

Electrolyte with complex crystal structure of $Mg(AlCl2BuEt)_2$/THF was proposed by (Nakayama et al., 2009). From X-ray absorption fine structure (XAFS) measurement, they found that four different kinds of aluminium complexes were present in the electrolyte which remains in equilibrium during deposition and dissolution. Further analysis was conducted and they proposed that the electrochemical characteristic of the electrolyte solution was mainly due to the equilibrium species. Besides that, it was a known fact that in the process of establishing an electrolyte solution with a reasonable ionic conductivity for mg batteries, the solvent used also plays a vital role as a polar medium. The electrolyte mentioned above demonstrated an ionic conductivity of few 10^{-3} S cm^{-1} with an electrochemical window of ~2.2 V. The ionic conductivity of this electrolyte can be further enhanced by adding simple chloride based salt such as lithium chloride or tetrabutyl ammonium chloride (Gofer et al., 2006). However, due to the limited electrochemical anodic stability of this electrolyte, realization of working cell with high energy density is still far.

Table 2.2 presents some electrolytes that have been used by previous reported works on rechargeable magnesium batteries. Endless efforts need to be put towards achieving compatible (allow Mg^{2+} intercalation and deintercalation) and high ionic conductivity for rechargeable magnesium battery. In this work, $Mg(AlCl2EtBu)_2$/THF have been chosen as the electrolyte to be used for electrochemical analysis.

Table 2.2: Summary of promising electrolyte for Mg batteries in two and three-electrode cell configuration

Cathode/ working electrode	Anode/ counter electrode	Electrolyte	Voltage (V)	Initial capacity (mAh/g)	References
V_2O_5 thin film	Activated carbon	0.1 M MgTFSI/acetonitrile	2.3	180	Gershinsky et al., 2013
V_2O_5 gel/carbon	Mg	0.5 M $Mg(ClO_4)_2$ in acetonitrile	1.5	450	Jiao et al., 2005
Layered MnO_2	Mg	1.0 M $Mg(ClO_4)_2$ in acetonitrile	1.5	109	Rasul et al., 2012
α-MnO_2	Mg	PhMgCl-$AlCl_3$/THF	1.5	208	Zhang et al., 2012
α-MnO_2/Carbon black	Mg	1.5 M $Mg(ClO_4)_2$-propylene carbonate	1.5	310	Rasul et al., 2012
λMnO_2	Mg	0.5 M $Mg(ClO_4)_2$ in acetonitrile	1.5	330	Kim et al., 2015
Spinel MnO_2	Pt	1.0 M $Mg(NO_3)_2$	~ 2.6	190	Kim et al., 2015
RuO_2	Graphite	1.0 M Mg/MMOITFSI	3.5	100	Sutto et al., 2012
O_2 (Mg-air cell)	Mg	0.5 M $Mg(ClO_4)_2$/DMSO with I_2	1.2	2200	Shiga et al., 2013
NiHCF (aqueous)	Pt	1 M $Mg(NO_2)_2/H_2O$	2.9	~ 50	Wang et al., 2013
MgFeSiO4	Mg	0.5 M TFSI in AN	2.2	55	Li et al., 2011
$Mg_{1.03}Mn_{0.97}SiO_4$	Mg	0.25 M $Mg(AlCl_2EtBu)_2$/THF	1.6	300	Feng et al., 2008
Graphene-like MoS_2	Nano-sized Mg metal	$Mg(AlCl_2EtBu)_2$	1.7	170	Liang et al., 2011
$MgCoSiO_4$	Mg	0.25 M $Mg(AlCl_2EtBu)_2$/THF	1.6	300	NuLi et al., 2011

CHAPTER 3: RESEARCH METHODOLOGY

In this work, the experimental part was divided into three main parts. The first part is the sample preparation, the second part is the materials characterization that includes thermal, morphological and structural characterizations and the last part is the test on electrochemical behavior. The preparation method employed for the samples plays an important role since the final materials are highly dependence on the preparation route which in turn affects the electrochemical performance. Therefore, the sol-gel method was chosen for this work since it is one of the promising techniques for preparation of forsterite and forsterite-doped samples. Compared to other methods, sol-gel method has its own advantage in terms of cost, simplicity, particle size distribution and high purity of the final product. The experimental methods used in this work are explained in detail in the following sections.

3.1 Materials

Listed below are the details of the starting materials used in this research work. Without further refinement, the entire chemicals were directly used as received.

i. Magnesium acetate $(CH_3.COO)_2$ Mg

   Molecular weight: 214.45 g mol^{-1}

ii. Manganese acetate $(CH_3.COO)$ Mn

   Molecular weight: 245.09 g mol^{-1}

iii. Zirconium acetate $(CH_3.COO)$ Zr

   Molecular weight: 285.362 g mol^{-1}

iv. Tetraethyl orthosilicate (TEOS)

Molecular weight: 208.33 g mol^{-1}

Density: 0.934 g mL^{-1}

v. Citric acid ($C_6H_8O_7$)

Molecular weight: 192.124 g mol^{-1}

Density: 1.67 g cm^{-3}

3.2 Preparation of Samples

Three systems of forsterite (Mg_2SiO_4) and modified forsterite were synthesized by using water based citrate sol-gel method. System I was with stoichiometric formula of Mg_2SiO_4 meanwhile system II and system III were based on ($Mg_{2-x}Mn_xSiO_4$) and ($Mg_{2-x}Mn_xZr_ySi_{1-y}O_4$) stoichiometric formula respectively.

For the preparation of system I (Mg_2SiO_4), starting materials used were $(CH_3COO)_2Mg$ and $SiC_8H_{20}O_4$. Citric acid was used as a chelating agent. The synthesis of the samples started with the dispersion of the starting materials in deionized water. 100 mL of deionized water was used to dissolve each starting materials separately. All solutions of starting materials were mixed together. Citric acid was then mixed together with the previously prepared solution and transferred to reflux system. Under magnetic stirring, the reflux process was performed at 70 °C throughout 24 hours. The solution was then evaporated for at least 4 hours at 75 °C. In order to eliminate unwanted elements such as resistance organic group, solvent and water particles, the resulting viscous gel was dried in a vacuum oven at 150 °C for 24 hours. The heating process led to the formation of metal-citrate complex due to the binding of metal ions to the citrate acid and chelating agent. Formation of citrate-metal complexes occurred when the citric acid and chelating agent with metal ions upon heating. Most of the unwanted elements were removed and polymerization occur by further heating (Behera et al., 2004). The gel formed was heated at 400 °C in a furnace. The obtained precursor was then pulverized into powder by using a mortar. The sample was the ball milled using Fristsch Pulverisettle-7 planetary ball mill for 4 hours operated at 350 rpm to obtain a very fine powder. Balance chemical reactions of the precursor for system I can be described as below:

$$Mg(CH_3CO_2)_2 + 2H_2O \rightarrow Mg(OH)_2 + 2CH_3COOH$$

$$Si(C_2H_5O)_4 + 2H_2O \rightarrow SiO_2 + 4C_2H_5OH$$

In order to obtain a single-phase structure, sintering process was applied. The powder precursor was then heat treated with different sintering temperatures 400 °C, 600 °C, 800 °C, 900 °C, 950 °C, 1000 °C, 1050 °C and 1100 °C for 4 hours so that the particle could bind without melting (Kolar, 2000). During sintering process, suggested chemical reaction for system I is:

$$2Mg(OH)_2 + SiO_2 \rightarrow Mg_2SiO_4 + 2H_2O$$

System II and system III were also obtained by employing the same route that was used to obtain system I. However, magnesium acetate ($(CH_3COO)_2Mg$), manganese acetate tetrahydrate ($(CH_3COO)_2Mn$) and ethyl orthosilicate ($SiC_8H_{20}O_4$) were used as the starting materials for the system II. Meanwhile $Mg_{2-x}Mn_xZr_ySi_{1-y}O_4$ magnesium acetate ($(CH_3COO)_2Mg$), manganese acetate ($(CH_3COO)_2Mn.4H_2O$), zirconium acetate ($(CH_3COO)_2Zr$) and ethyl orthosilicat ($SiC_8H_{20}O_4$) were used as the starting materials. Chelating agent used remain the same as for system II and system III that was citric acid ($C_6H_8O_7$). System II and system III have been sintered at 1100 °C for 4 hours. Suggested chemical reactions during the preparation of system II and system III precursor is as below:

System II

$Mg(CH_3CO_2)_2 + 2H_2O \rightarrow Mg(OH)_2 + 2CH_3COOH$

$Mn(CH_3CO_2)_2 + 2H_2O \rightarrow Mn(OH)_2 + 2CH_3COOH$

$Si(C_2H_5O)_4 + 2H_2O \rightarrow SiO_2 + 4C_2H_5OH$

During sintering process

$Mg(OH)_2 + Mn(OH)_2 + SiO_2 \rightarrow MgMnSiO_4 + 2H_2O$

System III

$Mg(CH_3CO_2)_2 + 2H_2O \rightarrow Mg(OH)_2 + 2CH_3COOH$

$Mn(CH_3CO_2)_2 + 2H_2O \rightarrow Mn(OH)_2 + 2CH_3COOH$

$Zr(CH_3CO_2)_2 + 4H_2O \rightarrow Zr(OH)_4 + 4CH_3COOH$

$Si(C_2H_5O)_4 + 2H_2O \rightarrow SiO_2 + 4C_2H_5OH$

During sintering process

$2Mg(OH)_2 + 2Mn(OH)_2 + Zr(OH)_4 + SiO_2 \rightarrow 2MgMnZr_{0.5}Si_{0.5}O_4 + 6H_2O$

For system I, sample precursor subjected to thermal analysis TGA and DSC in order to confirm thermal behavior of the sample. Total of 8 samples have been synthesized initially in system I to study the effect of sintering temperature on the sample precursor. XRD analyses have been conducted on all 8 samples. XRD analysis shows that only samples sintered at temperature 900 and above can be indexed to desire stoichiometric. Therefore, sample 900°C, 1000 °C and 1100 °C have been selected for the next characterization including scanning electron microscopy (SEM), energy dispersive X-ray (EDX) analysis, particle size analysis, Fourier transform Infrared (FTIR), electrochemical impedance spectroscopy (EIS), transference number (TN) and cyclic voltammetry (CV).

For system 2 with stoichiometric $Mg_{2-x}Mn_xSiO_4$, 5 different samples with deferent dopand (Mn) ratio have been synthesized initially. x was varied in the range of 0.2 – 1.0 and samples were sintered at temperature 1100 °C for 4 hours. The temperature was selected based on results obtained in system I. XRD analyses have been done on all 5 samples and found out that samples with $x \geq 0.6$ contained impurities and cannot be indexed to desire stoichiometric. Samples with $x = 0.2$, 0.4 and 0.6 was selected for the next characterization such as FTIR, SEM, EDX, particle size analysis, EIS, TN and CV.

For system III, samples synthesized based on stoichiometric $Mg_{2-x}Mn_xSi_{1-y}O_4Zr_y$ for every $x = 0.2$, 0.4 and 0.6 with y varied from 0.1 - 0.3. The range of x were selected based on results obtained in system II and the sintering temperature used for system III is 1100 °C for 4 hours. XRD analyses shows that only 4 samples out of 9 samples can be indexed to the desire stoichiometric. Meanwhile, the other 5 samples contained impurity. Therefore, for the purpose of this study, 3 sample with $x = 0.2$ have been proceed for FTIR, SEM, EDX, particle size analysis, EIS, TN and CV analysis.

Table 3.1 summarized all samples synthesized in system I, system II and system III. Preparation of all 3 systems is illustrated in Figure 3.1. The end products of system I, II and III were in the form of powder.

Table 3.1: List of samples synthesized

System	Sample prepared initially		Sample proceeded for characterization	
	Name of sample	Stoichiometric	Name of sample	Stoichiometric
System I	400 °C	Mg_2SiO_4	-	-
	600 °C	Mg_2SiO_4	-	-
	800 °C	Mg_2SiO_4	-	-
	900 °C	Mg_2SiO_4	900 °C	Mg_2SiO_4
	950 °C	Mg_2SiO_4	-	-
	1000 °C	Mg_2SiO_4	1000 °C	Mg_2SiO_4
	1050 °C	Mg_2SiO_4	-	-
	1100 °C	Mg_2SiO_4	1100 °C	Mg_2SiO_4
System II	$x = 0.2$	$Mg_{1.8}\,Mn_{0.2}\,SiO_4$	$x = 0.2$	$Mg_{1.8}\,Mn_{0.2}\,SiO_4$
	$x = 0.4$	$Mg_{1.6}\,Mn_{0.4}\,SiO_4$	$x = 0.4$	$Mg_{1.6}\,Mn_{0.4}\,SiO_4$
	$x = 0.6$	$Mg_{1.4}Mn_{0.6}\,SiO_4$	$x = 0.6$	$Mg_{1.4}\,Mn_{0.6}\,SiO_4$
	$x = 0.8$	$Mg_{1.4}\,Mn_{0.8}\,SiO_4$	-	-
	$x = 1.0$	$Mg_{1.0}\,Mn_{1.0}\,SiO_4$	-	-
System III	$x = 0.2$ $y = 0.1$	$Mg_{1.8}Mn_{0.2}Zr_{0.1}Si_{0.9}O_{4.0}$	$y = 0.1$	$Mg_{1.8}Mn_{0.2}Zr_{0.1}Si_{0.9}O_{4.0}$
	$x = 0.2$ $y = 0.2$	$Mg_{1.8}Mn_{0.2}Zr_{0.2}Si_{0.8}O_{4.0}$	$y = 0.2$	$Mg_{1.8}Mn_{0.2}Zr_{0.2}Si_{0.8}O_{4.0}$
	$x = 0.2$ $y = 0.3$	$Mg_{1.8}Mn_{0.2}Zr_{0.3}Si_{0.7}O_{4.0}$	$y = 0.3$	$Mg_{1.8}Mn_{0.2}Zr_{0.3}Si_{0.7}O_{4.0}$
	$x = 0.4$ $y = 0.1$	$Mg_{1.6}Mn_{0.4}Zr_{0.1}Si_{0.9}O_{4.0}$	-	-
	$x = 0.4$ $y = 0.2$	$Mg_{1.6}Mn_{0.4}Zr_{0.2}Si_{0.8}O_{4.0}$	-	-
	$x = 0.4$ $y = 0.3$	$Mg_{1.6}Mn_{0.4}Zr_{0.3}Si_{0.7}O_{4.0}$	-	-
	$x = 0.6$ $y = 0.1$	$Mg_{1.4}Mn_{0.6}Zr_{0.1}Si_{0.9}O_{4.0}$	-	-
	$x = 0.6$ $y = 0.2$	$Mg_{1.4}Mn_{0.6}Zr_{0.2}Si_{0.8}O_{4.0}$	-	-
	$x = 0.6$ $y = 0.3$	$Mg_{1.4}Mn_{0.6}Zr_{0.3}Si_{0.7}O_{4.0}$	-	-

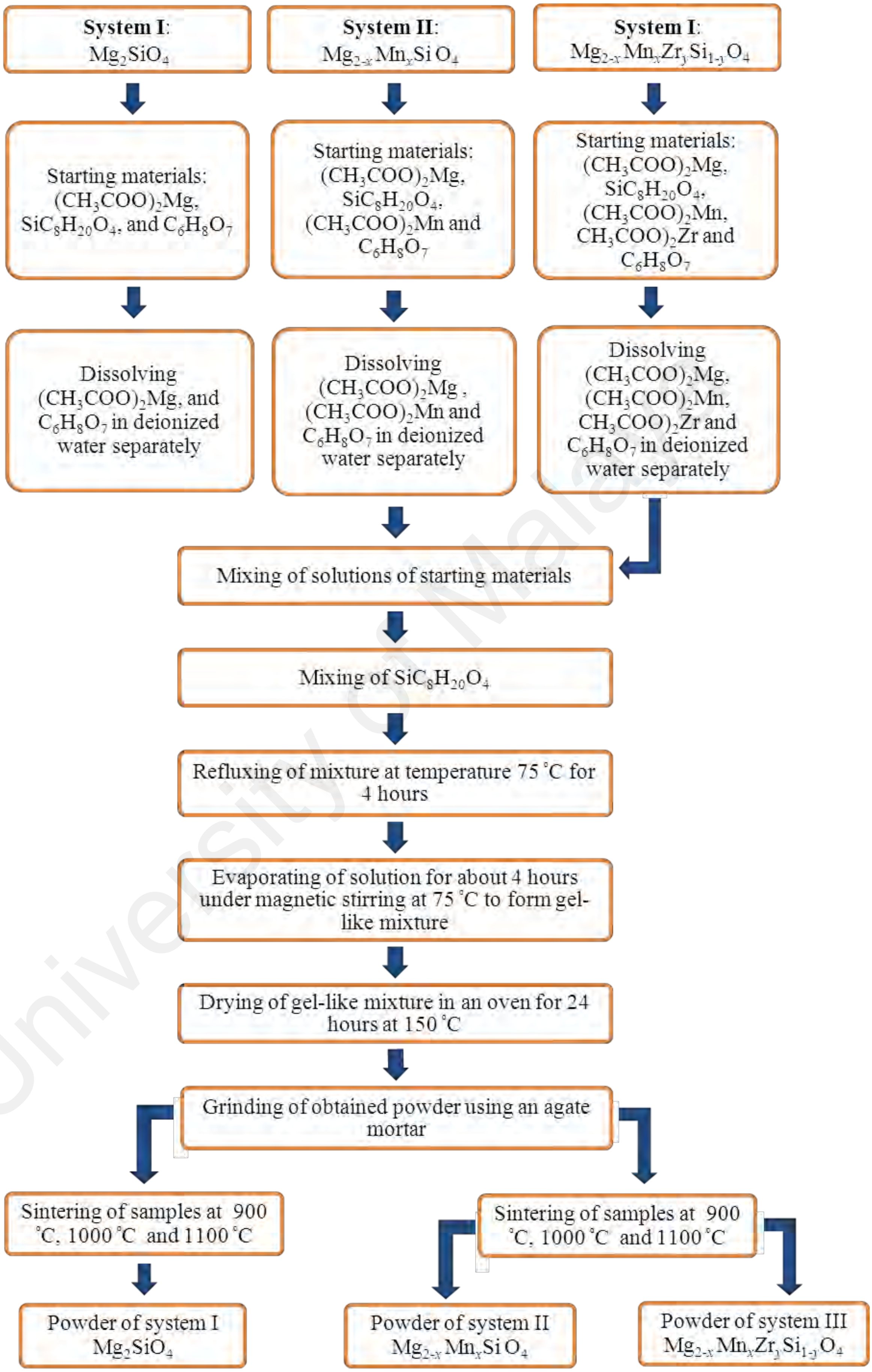

Figure 3.1: Preparation steps for system I, system II and System III

3.3 Material Characterizations

The prepared samples were subjected to various studies including TGA, DSC, XRD, FTIR, laser particle sizer, SEM, EDX, EIS, transference number measurement and CV.

3.3.1 Thermogravimetric Analysis and Differential Scanning Calorimetry

During heating, materials undergo phase transition, structural change or/and decomposition. TGA and DSC analysis are fundamental analyses that can be used to determine suitable sintering temperatures. In TGA analysis, mass loss during constant heating under synthetic air or nitrogen environment is measured. Change in mass indicates that the measured substance undergoes degradation. On the other hand, in DSC analysis, correlation between material's transition with respect to temperature and heat flow in a controlled atmosphere can be obtained. Acquired DSC curve provide qualitative and quantitative information on the chemical and physical changes exit in the sample. Complimentary information acquired allows differentiation between exothermic and endothermic processes while heating the sample. Together with TGA, DSC analysis is very useful to identify transition temperature of a material such as its glass transition temperature T_g, crystallization temperature T_c, melting point T_m. Choosing Setaram Labsys Evo operate at a steady heating rate of 30 K min^{-1} in nitrogen atmosphere over a wide temperature range of 30 $^{\circ}$C to 1100 $^{\circ}$C, TGA and DSC analysis were conducted to examine the thermal behavior of the sample's precursor.

3.3.2 X-Ray Diffraction

X-ray diffraction (XRD) is a rapid and non-destructive analytical technique primarily used to recognize various crystalline forms, known as 'phases' and for identification of the structural aspects, the degree of crystallinity and identification of materials. Since

XRD spectrum for every crystallite substance is different and unique, all the information can be attained by comparing the obtained XRD pattern of the studied sample with the library spectrum in the Inorganic Crystal Structure Database (ICSD). Basic principle used in XRD is diffraction phenomenon which occurs when X-rays hit a crystalline target. Interference pattern of X-rays scattered by crystals was explained by applying Bragg's law. Bragg's law is the result of experiments derived by a physicist, Sir William Lawrence Bragg, in 1912 and first presented in the same year to the Cambridge Philosophical Society (Bragg, 1929). The incident beam of X-rays interferes with one another as they leave the crystals. This is caused by the atomic planes of crystal that are spaced a distance d apart. The phenomenon occurs if conditions stated by Bragg law or Laue equation are fulfilled. The Bragg equation is given by:

$$d_{hkl} = \frac{\lambda}{2 \sin \theta_{\mathrm{hkl}}} \tag{3.1}$$

where λ is the wavelength of the X-ray

d_{hkl} is the crystal plane distance of (*hkl*)

θ_{hkl} is the crystal plane's diffraction angle (*hkl*)

a, *b* and *c* are lattice parameters.

In this experiment, PANanalytical-X'pert^3 X-ray diffractometer with 1.5406 Å wavelength of Cu-K$_\alpha$ radiation was used to analyse the studied samples' structural properties. For XRD analysis, the sample was first prepared by depositing a small amount of powdery materials using a flat spatula on a glass slide. The sample was evenly smeared on the glass slide and then put on a sample holder. The sample was scanned with 0.026° in step size at 2θ range from 10° and 45°. Data obtained from this analysis were used to calculate important parameters such as the lattice parameters, crystallite size and phase composition of the tested sample. The following formula was employed to calculate the samples's lattice parameters lattice parameters:

$$\frac{1}{\ ^{2}} = \frac{^{2}}{^{2}} \quad \frac{^{2}}{^{2}} \quad \frac{^{2}}{^{2}} \tag{3.1}$$

The sample crystallite size was determined by applying Scherer equation:

$$\beta(2\theta) = \frac{k\lambda}{L\ cos\,\theta} \tag{3.2}$$

where θ is the bragg angle

λ is the wavelength

L is the crystallite size

k is a constant (0.9)

3.3.3 Fourier Transform Infrared

Fourier transform infrared (FTIR) spectroscopy can be used for identification of a wide range of compounds. This is because chemical compounds show distinctive absorption of certain infrared spectral line characteristics of the compounds. Infrared spectroscopy can also be used to shed some light on the purity of a compound. In addition, FTIR spectra can also provide information related to the number of components in a mixture and to determine the quality and the consistency of a sample. FTIR relies on the fact that most molecules absorb light in the infra-red region of the electromagnetic spectrum. This absorption corresponds specifically to the bonds present in the molecules (Moore, 2016; Smith, 1995). In this work, samples were characterized using Perkin-Elmer Frontier spectrometer. The sample powder was placed onto an ATR crystal and analyzed in the frequency range of 400 cm^{-1} to 4000 cm^{-1} with a scan resolution of 2 cm^{-1} at room temperature.

3.3.4 Particle Size Analyser

FRITSCH-Analysette 22 NanoTec laser particle sizer was used throughout the experiment to attain the information on the samples' particle size. This laser particle sizer is considered as the first established laser measuring device for the determination of particle size distributions and recognition of the particle shape collectively in a single process. The ANALYSETTE 22 NanoTec plus is widely applicable and excellent laser particle sizer for effective and safe determination of particle size distributions down into the nano range. According to laser diffraction method, particle diameter is identical to that of a sphere giving the same diffraction as the particles. A laser diffraction particle size analyser sees the particle as a two-dimensional object and gives its grain size as a function of the cross-sectional area of the particle (Di Stefano et al., 2010). The following assumptions are considered when using a laser particle analyser (Konert et al., 1997).

i. Based on matrices, diffraction pattern to grain sizes transformation is always assumed and calculated for spheres. Consequently, the diffraction along the particle's cross-sectional area is set to diffraction of sphere.
ii. If the laser measurements are accomplished in the condition where the particles may be oriented with respect to its shape (continuous suspension), the particle orientation is considered to be randomly distributed.

In this experimental work, the particle sizes of samples obtained were examined. This characterization is important because the size of the particles affects the electrical performance of the samples.

3.3.5 Scanning Electron Microscopy

Scanning electron Microscopy (SEM) was used to observe the samples morphology. SEM offers various advantages that make it one of the most beneficial instruments in many research areas. SEM has a large depth of field, which allows a large number of samples to be in focus at one time in high resolution so that even closely spaced samples can be magnified at much higher levels. In this work, ZEISS EVO MA 10 scanning electron microscope with 10 kV incident electron beam was used. Samples first were mounted on the aluminum samples holder and coated with gold using sputter coating machine for 60 s before the analysis is conducted to avoid charging. During SEM analysis, coated surface is useful to discharge excess electrons to ground and thus improves the imaging of samples.

3.3.6 Energy Dispersive X-Ray Analysis

Energy Dispersive X-ray (EDX) analysis is a very powerful technique used in materials science. EDX can be used to check on the present of certain atomic in a material sample. As it is a quantitative method for determining the presence of elements, it can give an idea of the stoichiometry of the material. The method is very useful to confirm and support the results obtained from XRD analysis. In this work, EDX analysis was conducted in order to give the idea of magnesium element stoichiometry of magnesium, silicon and oxygen in the sample as well as that of manganese and zirconium element. The EDX was executed by using Oxford Aztec X-Act EDX spectrometer which is attached to the Ziess-Evo MA10 scanning electron microscope used for SEM analysis.

3.3.7 Transference Number measurement

Transference number (TN) was evaluated using Wagner's polarizing technique in order determine the contribution of the ion and electron to the total conductivity of materials. The curve of polarized current versus time is then plotted and the ionic and electronic transference number can be calculated using the following equation:

$$t_{\mathrm{ion}} = 1 - \frac{I_{\mathrm{f}}}{I_{\mathrm{i}}} \tag{3.3}$$

$$t_{\mathrm{ele}} = \frac{I_{\mathrm{f}}}{I_{\mathrm{i}}} \tag{3.4}$$

where t_{ele} is the electronic transference number

I_{f} is the final current

I_{i} is the initial current

3.3.8 Electrochemical Impedance spectroscopy

Electrochemical impedance spectroscopy (EIS) was used in this work to further analyze the effect of doping on electrode reaction impedance. Solatron 1260 Impedance analyser over frequency range 1 to 10^6 Hz Impedance data obtained fit the equivalent circuit developed by Jamnik shown in Figure 3.2. The equivalent circuit developed was simplified as parallel combination of constant phase element (CPE) and electronic resistance, R_1 which is in serial with the ionic resistance, R. Nyquist plot exhibit semicircle in the high frequency region and a line in low frequency region. According to the equivalent circuit, the diameter of the semicircle describes the value of charge transfer resistance (R_{ct}). The linear plot in the low frequency region indicates to the diffusion of ion in the cathode material.

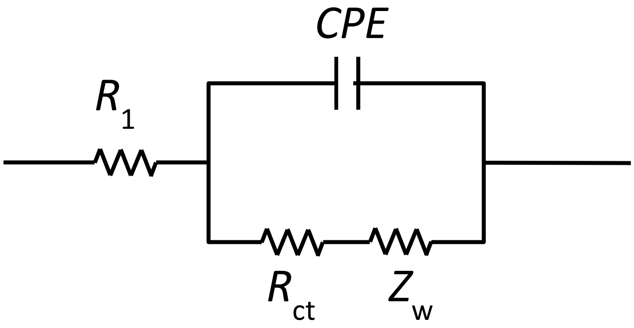

Figure 3.2: Equivalent circuit of the electrode system

3.4 Fabrication of electrochemical cells

The studied cathode materials were then used for fabrication of electrochemical cell for CV analysis. The Mg_2SiO_4 / $Mg_{2-x}Mn_xSiO_4$ / Mg_{2-x} $Mn_xZr_ySi_{1-y}O_4$ was used as the active material, ethanol acted as a binder while acetylene black as the conducting agent. Conducting agent is one of important materials as without it, no magnesium deintercelation can occur. Firstly, the active material was heated at 120 °C for 48 hours in a vacuum oven. Appropriate amounts of the active material and acetylene black were thoroughly ground in a mortar which was subjected to prior degreasing in acetone until homogenous slurry was obtained. Slurry formed then pasted on a current collector by using blade to form a piece of cathode with uniform thickness of composite materials was obtained. This piece of cathode was weighted and then allowed to dry under argon atmosphere at 100 °C for 24 hours. Figure 3.3 shows the procedures of the cathode preparation.

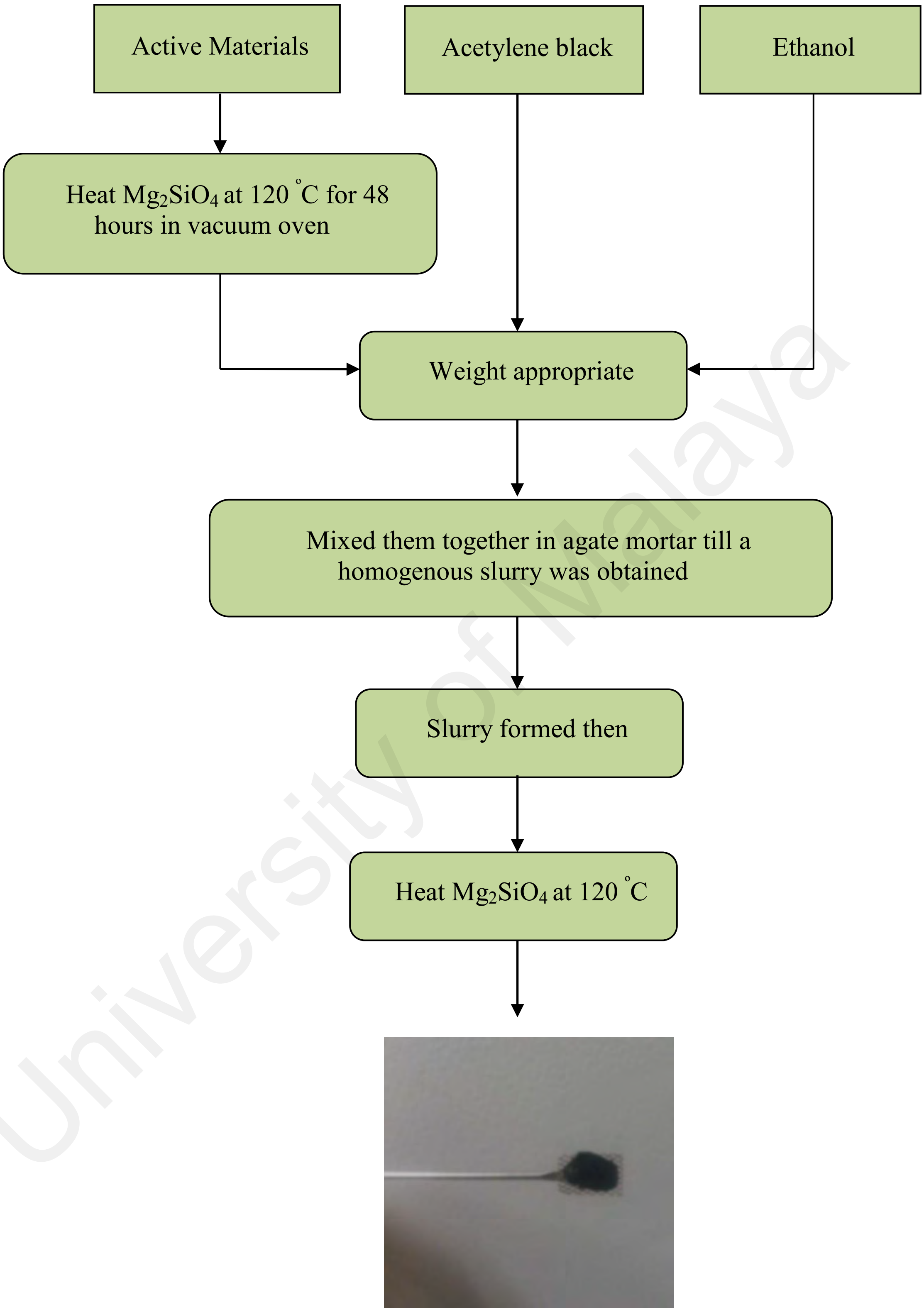

Figure 3.3: Cathode preparation procedures

Electrolyte used in this work is 0.25 mol L^{-1} $Mg(AlCl_2BuEt)_2$/THF which was proposed by Aubach et. al as reported in (Aurbach et al., 2000). The electrolyte solution developed is based on Mg organohaloaluminate salts, Mg(AlCl2RR')2 where R and R' are alkyl groups in tetrahydrofuron (THF). In this solution, magnesium electrochemical deposition-dissolution is reversible at almost 100% efficiency. In addition, this solution exhibits an electrochemical window of more than 2.5 V, much wider than any other electrolyte solution tested previously in Mg batteries (Aurbach et al., 1998; Levi et al., 2009; Liebenow, 1997)

For the purpose of preparing this electrolyte, stoichiometric amounts of dibuthylmagnesium ($MgBu_2$) in heptane and ethylaluminum dichloride ($AlCl_2Et$) in hexane in 1:2 volume ratio were mixed in an argon-filled glove box. The mixture of these two starting materials was stirred continuously for 48 hours until the solvents (hexane and heptane) were completely evaporated. This resulted in the formation of white precipitate. The remaining white precipitate was dissolved in inhibitor-free purified anhydrous THF to form 0.25 mol L^{-1} $Mg(AlCl_2BuEt)_2$/THF. Steps involved in the preparation of electrolyte are illustrated in Figure 3.4.

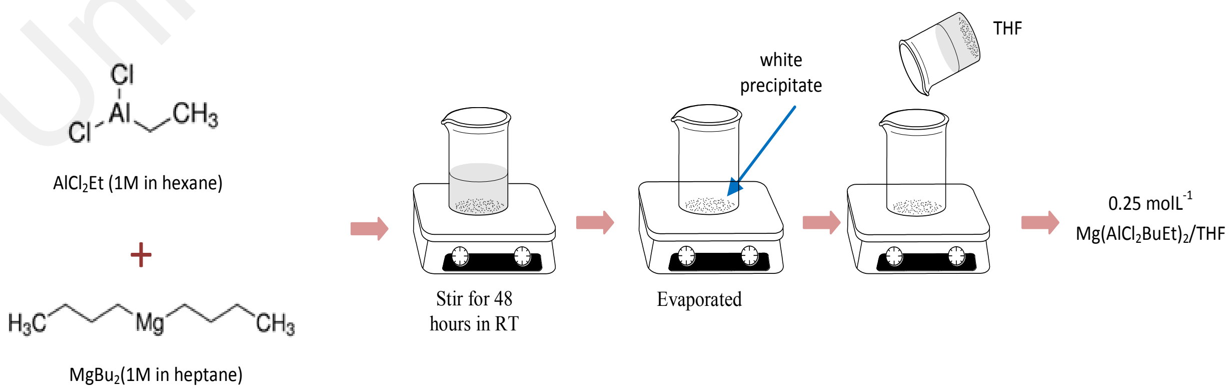

Figure 3.4: Step involve in electrolyte preparation

3.5 Electrochemical testing

Cyclic voltammetry is the most frequently used technique to study electrochemical properties of materials. The information obtained from CV analysis is presented as an *I*-*E* curve, called cyclic voltammogram. The earliest voltammetric technique is polarography which was developed in early 1920s. Jaroslav Heyrovsky was awarded the Nobel Prize in Chemistry in 1959 for this achievement. Figure 3.5 show the example of graph I-V from CV analysis.

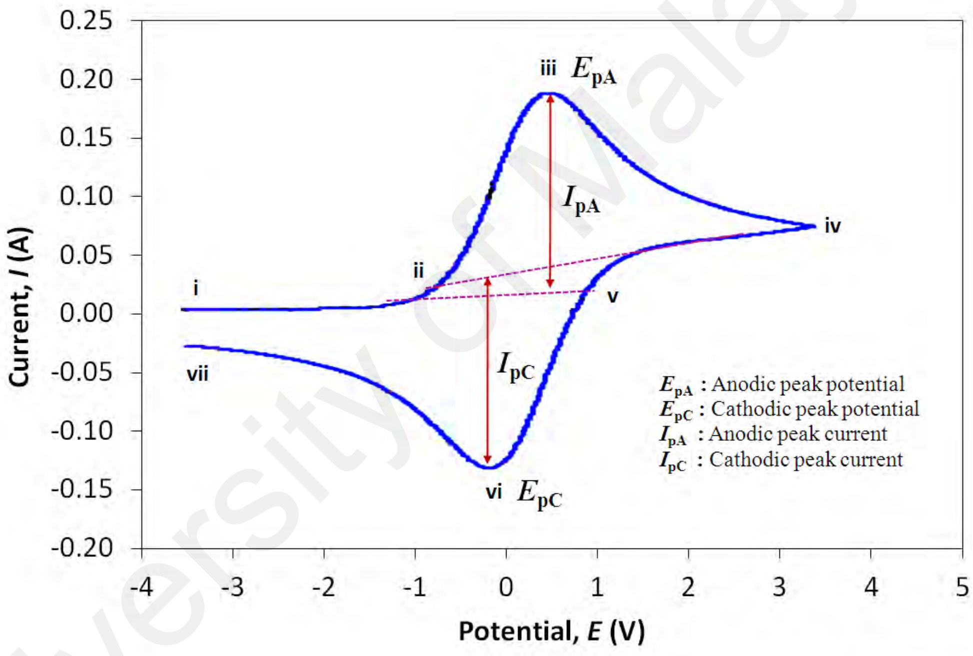

Figure 3.5: Typical cyclic voltammogram of simple reaction

By convention, the positive current reflects oxidation, whereas the negative current represents reduction reaction. In Figure 3.5, the oxidation process occurs from (i) the initial potential to (iv) the switching potential. In this region, the potential scans positively from (i) to (iv). This results in anodic current (I_{pA}) and oxidation to occur. The peak potential at (iii) is called the anodic peak potential (E_{pA}), and is reached when all of the substrate at the surface of the electrode has been oxidized. After the switching potential has been reached (iv), the potential is scanned negatively to cause a reduction. The resulting current is called cathodic current (I_{pC}). The corresponding peak potential occurs at (vi), and is called the cathodic peak potential (E_{pC}). The E_{pC} is reached when all of the substrate at the surface of the electrode has been reduced. Direct and simple method called Cyclic Voltammetry is applied to measure the formal potential of a half reaction when both oxidized and reduction forms are stable during the time required to obtain the voltammogram (current-potential curve). During the potential scan, the current produced at working electrode was measured to acquire a cyclic voltammogram (Kissinger et al., 1983). Without much resource to detailed calculations, cyclic voltametry can be considered as a powerful tool that allows rapid information to be obtained (Pletcher, 1991).

In this work, cyclic voltammetry measurement involves the following set up of CV cell. $Mg_{2-x}Mn_xZr_ySi_{1-y}O$/$Mg_{2-x}Mn_xSiO_4$ /Mg_2SiO_4 were assigned as the working electrode. As mentioned ealier, the electrolyte used was 0.25 mol L^{-1} $MgAlCl_2EtBu_2$/THF. Three-electrode configuration, as shown in Figure 3.6 consisting of the working electrode and magnesium foil as the reference and counter electrode was set up to perform the cyclic voltammetry. The cyclic voltammetry was performed using a Wonatech ZIVE MP2 multichannel electrochemical workstation with scan rate 0.5 mV s^{-1} between -1.0 V and 3.0 V.

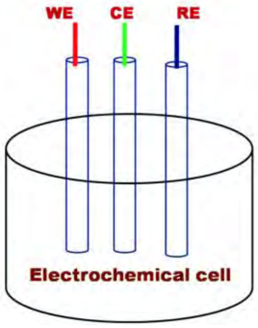

Figure 3.6: Three electrode CV cell set up

CHAPTER 4: Mg_2SiO_4

4.1 Introduction

In this work, olivine forsterite, Mg_2SiO_4 was chosen as the parent compound. The forsterite has been obtained by using sol-gel method with firing temperature of at least 850 ºC. This chapter provides the results and discussion of thermal, structural, electrical and electrochemical investigations of the Mg_2SiO_4 material. TGA and DSC analysis of precursor were carried out to determine the suitable sintering temperature of the precursor. XRD was done to obtain the structural information of Mg_2SiO_4 samples and to monitor the growth of precursor. Based on thermal and structural information from XRD, three samples with sintering temperature 900 °C, 1000 °C and 1100 °C were characterized using FTIR, SEM, EDX, EIS, transference number and CV. FTIR study was conducted to confirm the present of the Mg_2SiO_4 characteristic peaks and reveal any transformation that occur in the samples. SEM and EDX were also done to look into the morphological and elemental properties of the samples. Furthermore, the prepared samples were also subjected to other characterizations including conductivity measurement by using EIS, transference number and CV.

4.2 Thermal Gravimetric Analysis and Differential Scanning Calorimetry

Thermal profiles of forsterite powder obtained from TGA and DSC are presented in Figure 4.1. There are three prominent stages of weight losses identified in the TGA trace upon heating treatment up to 1200 °C. The first weight loss observed is in the temperature range from 200 °C to 400 °C that represents the first mass change, Δm_1 = 28.15% of the total starting material's weight. This weight loss accompanied by an exothermic peak observed in DSC trace at the temperature of 234 °C which is due to the dehydration of the sample precursor. DSC trace exhibits a distinguishable exothermic peak at the temperatures of 438 °C and 463 °C accompanied with a weight loss, Δm_2 = 28.93% attributed to the formation of periclase (MgO) peak (Saberi et al., 2009). Further heating of the sample produced a small exothermic peak around 850 °C accounted for a weight loss, Δm_3 = 11.57% from 550 °C to 900 °C. This small exothermic peak indicates the crystallization of forsterite (Mitchell et al., 1999; Saberi et al., 2007; Saberi et al., 2009). The plateau appeared at the temperature of 890 °C and above suggests that all chemical reactions for forsterite prepared by sol-gel method have completed and that the sample needs to be sintered at temperature at least 850 ºC in order to obtain forsterite powder. As such, we have chosen temperatures of 850, 900, 1000 and 1100 ºC for sintering process.

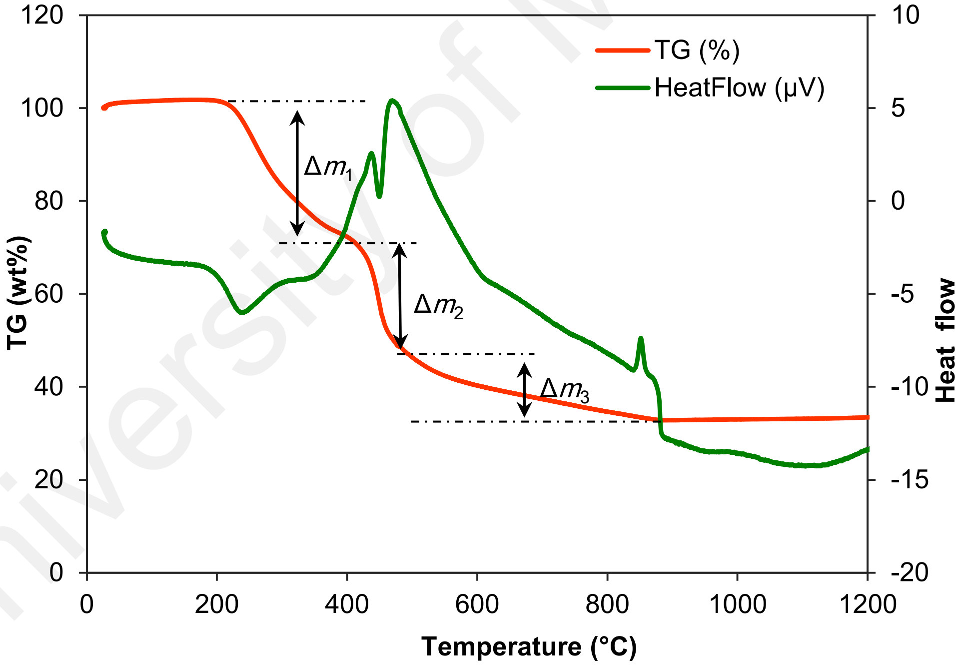

Figure 4.1 : Simultaneous TGA and DSC curves of Mg_2SiO_4 precursor

4.3 X-Ray Diffraction

The structural properties of Mg_2SiO_4 samples sintered at different temperatures were determined from XRD analysis. Figure 4.2 presents the XRD spectra for the Mg_2SiO_4 samples sintered at different temperatures. The XRD spectra obtained from the experiment were indexed based on XRD reference Inorganic Crystal Structure Database ICSD 98-000-9688. Sintering at temperature 400 °C, 600 °C and 800 °C did not successfully form Mg_2SiO_4. Nevertheless, two diffraction peaks observed at 2θ of 42.49° and 61.94° assigned to periclase (MgO)(Saberi et al., 2007). These peaks indicate the presence of impurity in the samples. According to (Kazakos et al., 1990), it is very difficult to avoid the formation of periclase (MgO) and enstatite ($MgSiO_3$) during the synthesis of forsterite. Thermal heat treatment at least 850 °C is necessary to obtain crystalline forsterite. However, as the sintering temperature increased to 900°C, 950°C, 1000°C, 1050°C and 1100°C, it can be observed that the XRD spectra only attributed to forsterite peak. There is no impurity peaks detected when the samples were sintered at the temperature higher than 900 ºC. Besides that, Figure 4.2 shows that the intensity of the XRD spectra also increased as the sintering temperature increased implies that the different in crystal size. The production of forsterite via sol-gel method can provide molecular-level of mixing and high degree of homogeneity, which leads to reduce crystallization temperature and prevent from phase segregation during heating (Saberi et al., 2007). Therefore, in this work, pure forsterite was obtained at lower temperature compared to the forsterite obtained by employing solid state reaction (S. K. Lee et al., 2011). XRD data evidently demonstrate that heat treatment plays a vital role in governing the growth of forsterite peaks. So, to further study the effects of sintering temperature on the forsterite samples, the authors just focus on three sintering temperatures which are 900 °C, 1000 °C and 1100 °C.

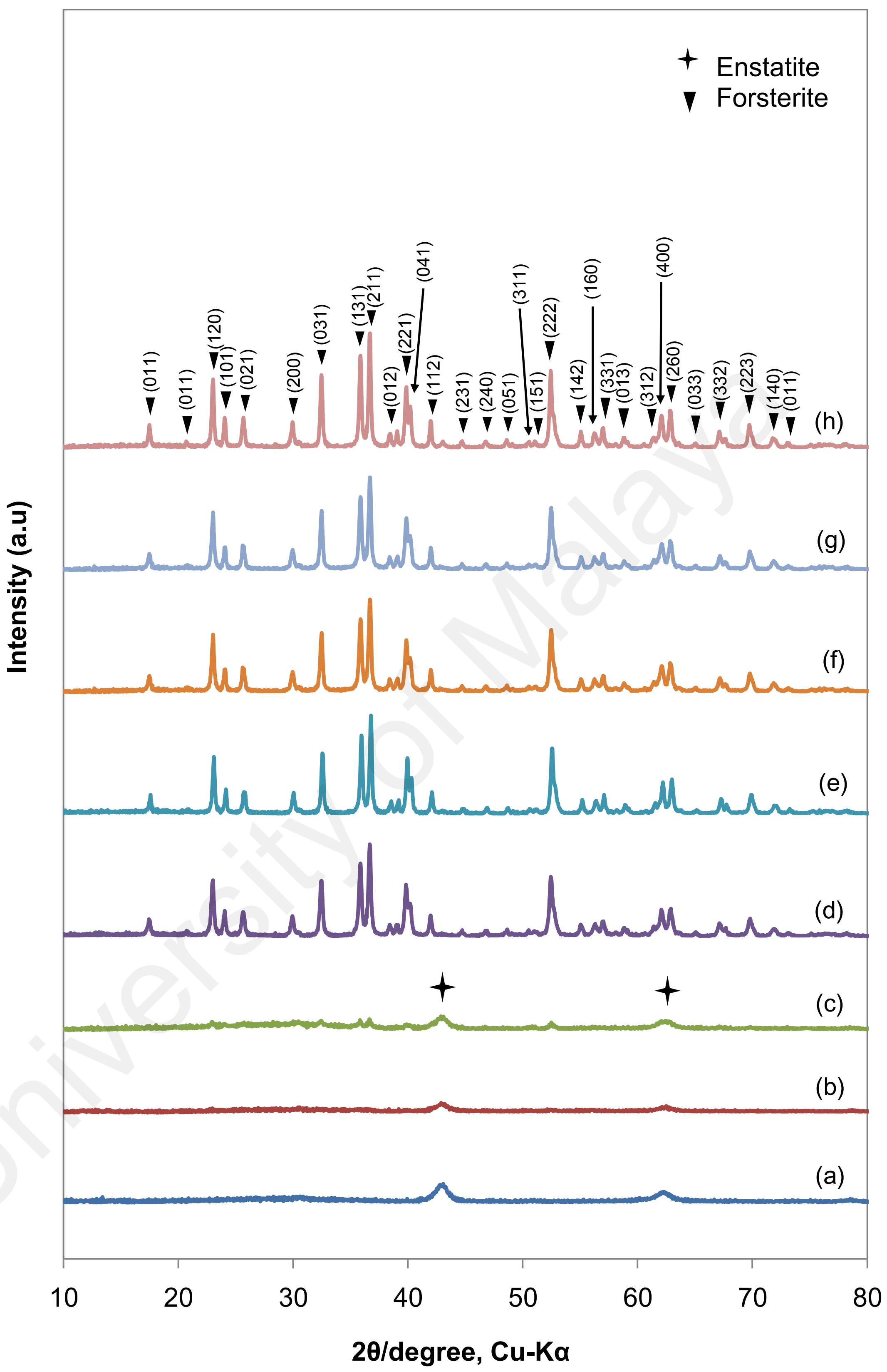

Figure 4.2: XRD spectra of Mg_2SiO_4 sintered at (a) 400 ºC (b) 600 ºC, (c) 800 ºC (d) 900 ºC (e) 950 ºC (f) 1000 ºC (g) 1050 and (h)1100 ºC

Table 4.1: Lattice parameters, unit cell volume and crystallite size of Mg_2SiO_4 sintered at 900 ºC, 1000 ºC and 1100 ºC

Sintering temperature (◦C)	Lattice parameter			Volume of unit cell, V [Å^3]	Crystallite Size [Å]
	a [Å]	b [Å]	c [Å]		
900	10.1293	5.9591	4.6807	282.5324	32.54
1000	10.1342	5.9617	4.6812	282.8226	36.42
1100	10.1693	5.9685	4.6886	284.5759	39.57

The variation of all lattice parameters for the samples sintered at 900 ºC, 1000 ºC and 1100 ºC were calculated by selecting three miller planes (*hkl*), (200), (020), (400), (040) or (004). From Table 4.1, it is clear that values of *a, b, c* and unit cell volume (*V*) are affected by the change in sintering temperature. Unit cell volume decreases as the sintering temperature increases. However, the crystallite size increases as the sintering temperature increases. The remarkable increase in crystallite size is owing to the grain growth by surface diffusion (Rao et al., 2002). Grain growth is the process in which average size of material's crystallite increases continuously during heat treatment without a change in the grain's shape (Lee et al., 1994).

4.4 Fourier Transform Infrared

The formation of Mg_2SiO_4 was also monitored by FTIR spectrometer. Figure 4.3 presents the FTIR spectra of pure Mg_2SiO_4 compound sintered at 900 ºC, 1000 ºC and 1100 ºC in the region from 550 to 1350 cm^{-1}.

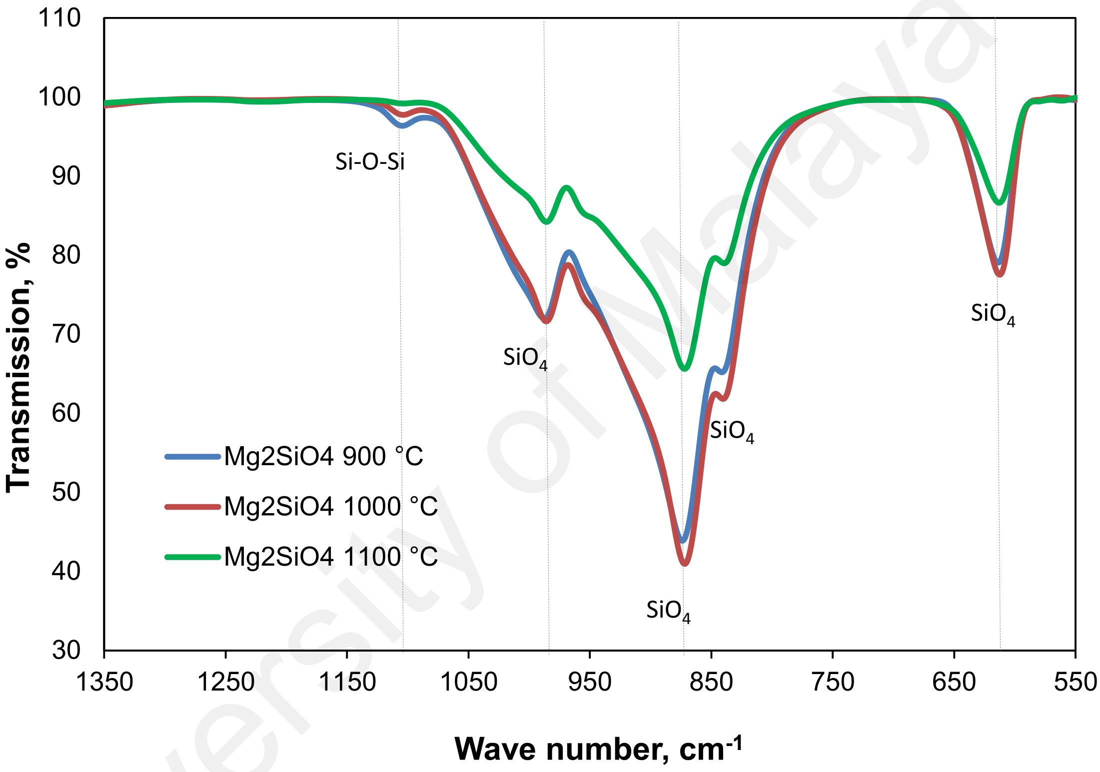

Figure 4.3: FTIR spectra of Mg_2SiO_4 sintered at 900 ºC, 1000 ºC and 1100 ºC

The peaks appeared in the range of 550 - 650 cm^{-1} correspond to SiO_4 bending vibration modes (Kharaziha et al., 2009; Saberi et al., 2007). The peaks centered at 835 cm^{-1} and 874 cm^{-1} are assigned to symmetric stretching vibrations of Si-O-Si (Mazza et al., 1993; Tsai, 2002). Meanwhile, the characteristic peaks associated to SiO_4 stretching vibration modes are located in the range from 950 cm^{-1} to 990 cm^{-1} (Kharaziha et al., 2009; Saberi et al., 2007). Lastly, the peaks appeared at 1105 cm^{-1} are attributed to Si-O-Si asymmetric stretching vibration mode of Mg_2SiO_4 (Mazza et al., 1993; Saberi et al., 2007; Tsai, 2002). The characteristic bands are observed to be at the same wavenumbers in all samples. However, the intensity of the bands decreases with increasing sintering temperature. This effect is due to the coordination of cation Si^{4+} with the oxygen atom, which results in the weakening of the Si-O-Si bond when the sintering temperature increases. This leads to an increase the crystal size as the sintering temperature increase that is consistent with the result of XRD study discussed earlier. The existence of the Mg_2SiO_4 related peaks give an additional proof of the formation of Mg_2SiO_4 compound.

4.5 Scanning Electron Microscopy and Particle Sizer

The SEM micrographs and particle size distribution of Mg_2SiO_4 samples are presented in Figure 4.4 and Figure 4.5 respectively. SEM images for Mg_2SiO_4 sintered at temperatures 900 °C, 1000 and 1100 revealed that the obtained materials consist of agglomeration of fine particles. The result is perceived when the sol-gel method is used for sample preparation and acetate metal as the starting materials (Ni et al., 2007). The size of the powder agglomeration ranges from small to large. The agglomerations of powder were made up from a mixture of loosely packed fine particles.

From the particle size distribution graph presented in Figure 4.5, it is found that the average particle size for the Mg_2SiO_4 sample increases from 21.3 µm to 36.7 µm as the sintering temperature increases from 900 °C to 1100 °C.

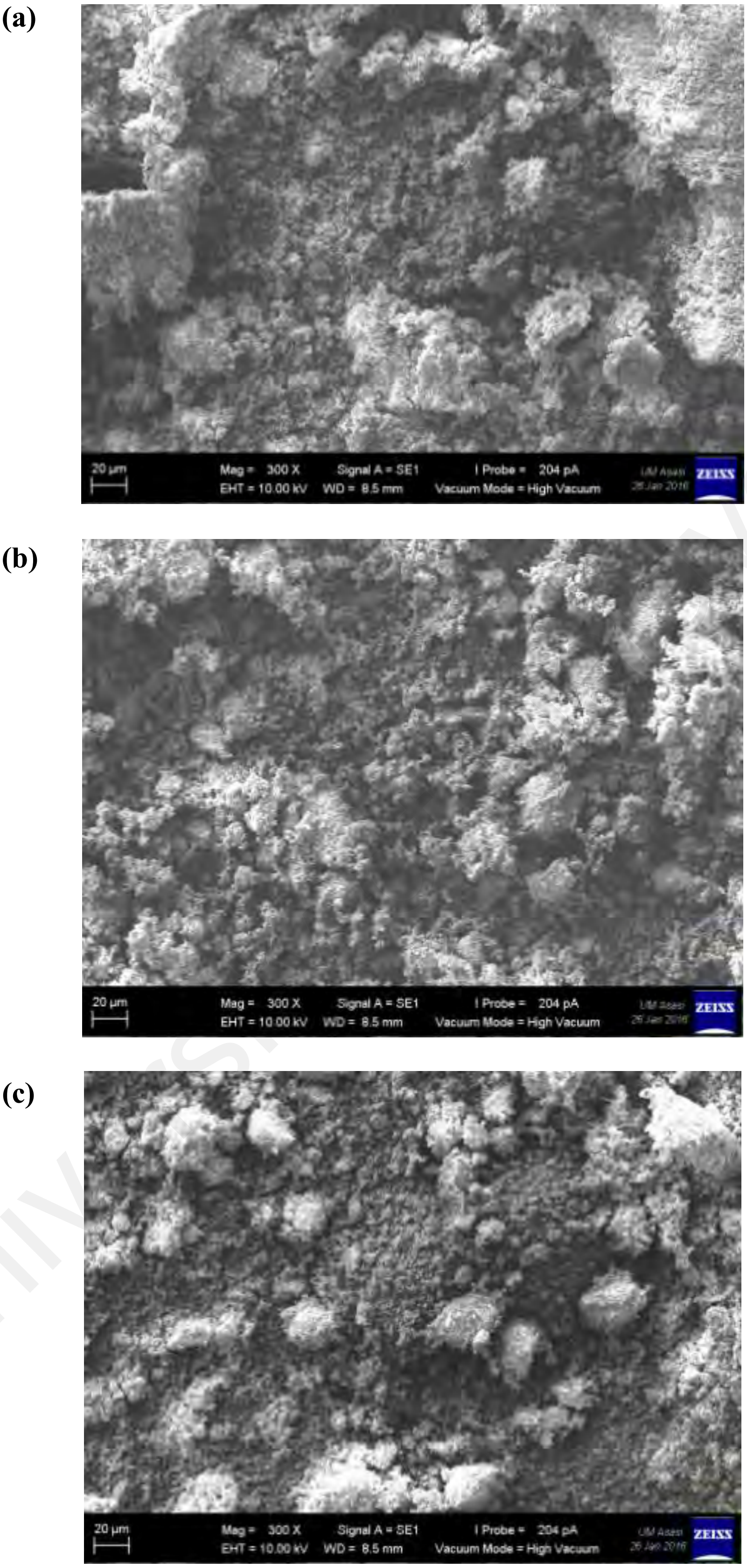

Figure 4.4: SEM micrographs of Mg_2SiO_4 sintered at (a) 900 ºC, (b) 1000 ºC and (c) 1100 ºC

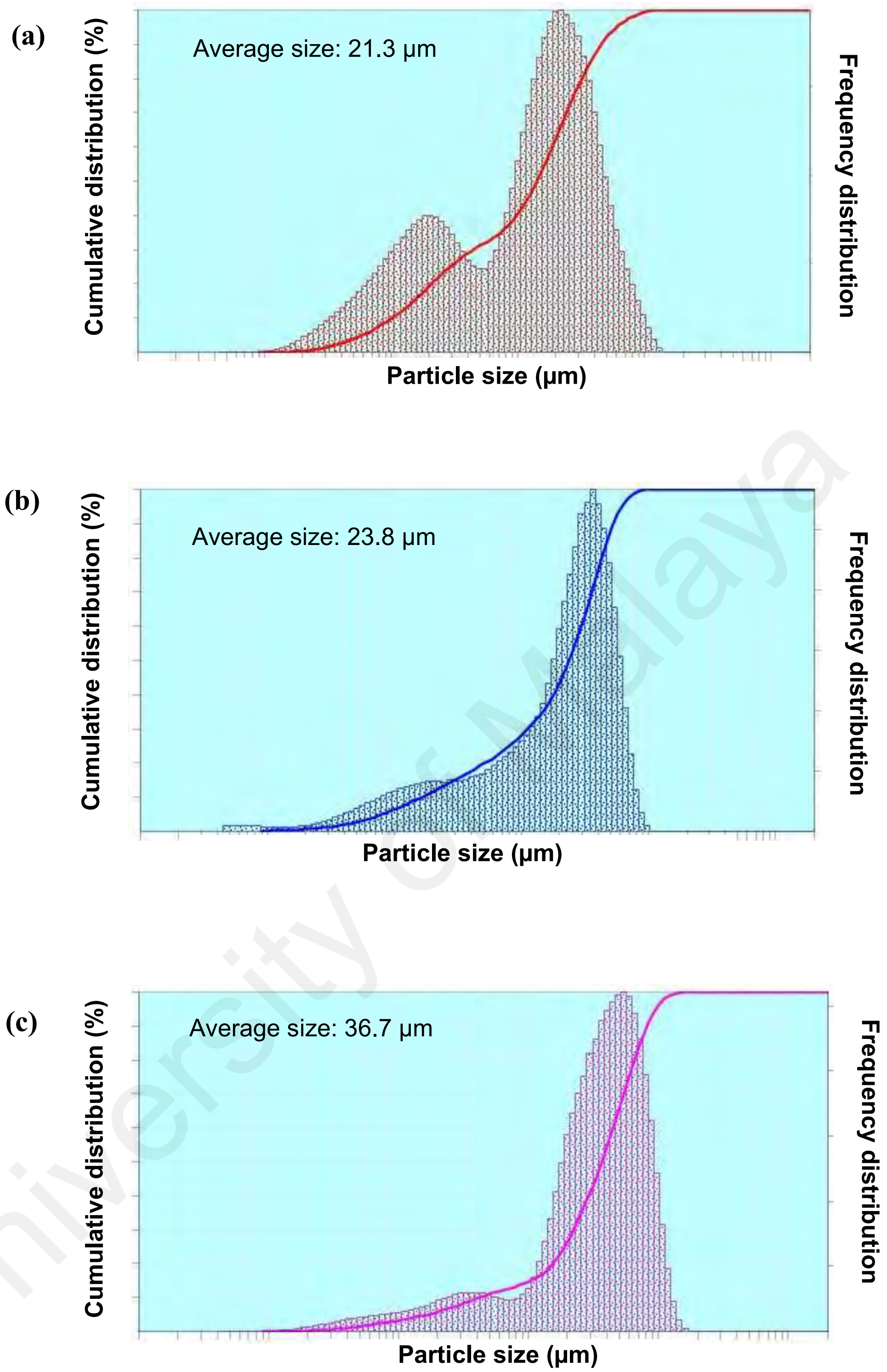

Figure 4.5: Particle size distribution of Mg_2SiO_4 sintered at (a) 900 ºC, (b) 1000 ºC and (c) 1100 º

4.6 Energy Dispersive X-Ray Analysis

In order to confirm the stoichiometric proportions of the prepared Mg_2SiO_4, EDX analysis was done. EDX analysis was conducted on 3 different selected regions and the average stoichiometric weight percentage was calculated based on the three regions for each sample. Figure 4.6(a), Figure 4.6(b) and Figure 4.6(c) illustrate EDX spectra for Mg_2SiO_4 sintered at 900 ^oC, 1000 ^oC and 1100 ^oC respectively. EDX data obtained show that the samples consist of magnesium (Mg), silicon (Si) and oxygen (O) elements. Elemental compositions obtained from EDX were compared with that of the theoretical atomic ratio and data obtained are presented in Table 4.2. It was found that the ratios of the elements in all the samples are in good agreement with the stoichiometric ratio of the starting materials. This confirms that the Mg_2SiO_4 material was successfully synthesized.

Table 4.2: EDX stoichiometric atomic ratios of Mg_2SiO_4 sintered at 900 ^oC, 1000 ^oC and 1100 ^oC

Sample, Sintering temperature (^oC)	Calculated stoichiometric, Atomic ratio	Average stoichiometric, Atomic ratio		
		Mg 2.00	Si 1.00	O 4.00
Mg_2SiO_4 900	EDX atomic percent (%)	2.01	1.00	4.01
Mg_2SiO_4 1000	EDX atomic percent (%)	2.03	1.00	4.09
Mg_2SiO_4 1100	EDX atomic percent (%)	1.99	1.00	4.10

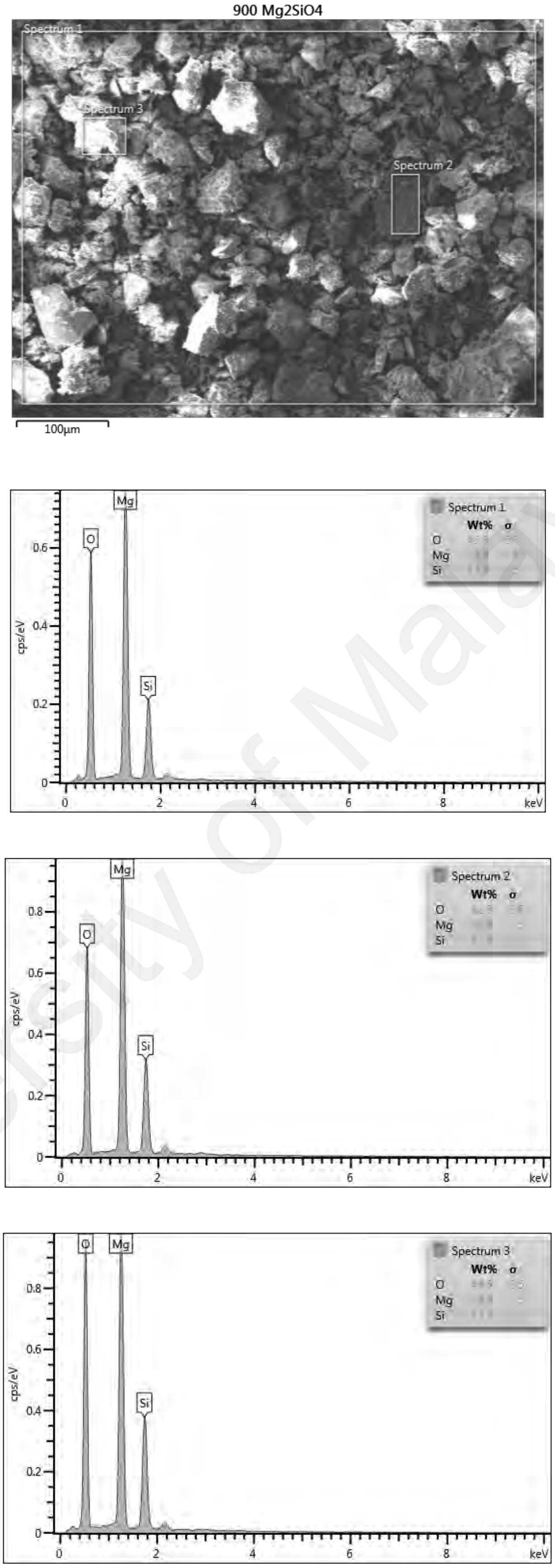

Figure 4.6 (a): EDX spectra for Mg_2SiO_4 sintered at 900 °C

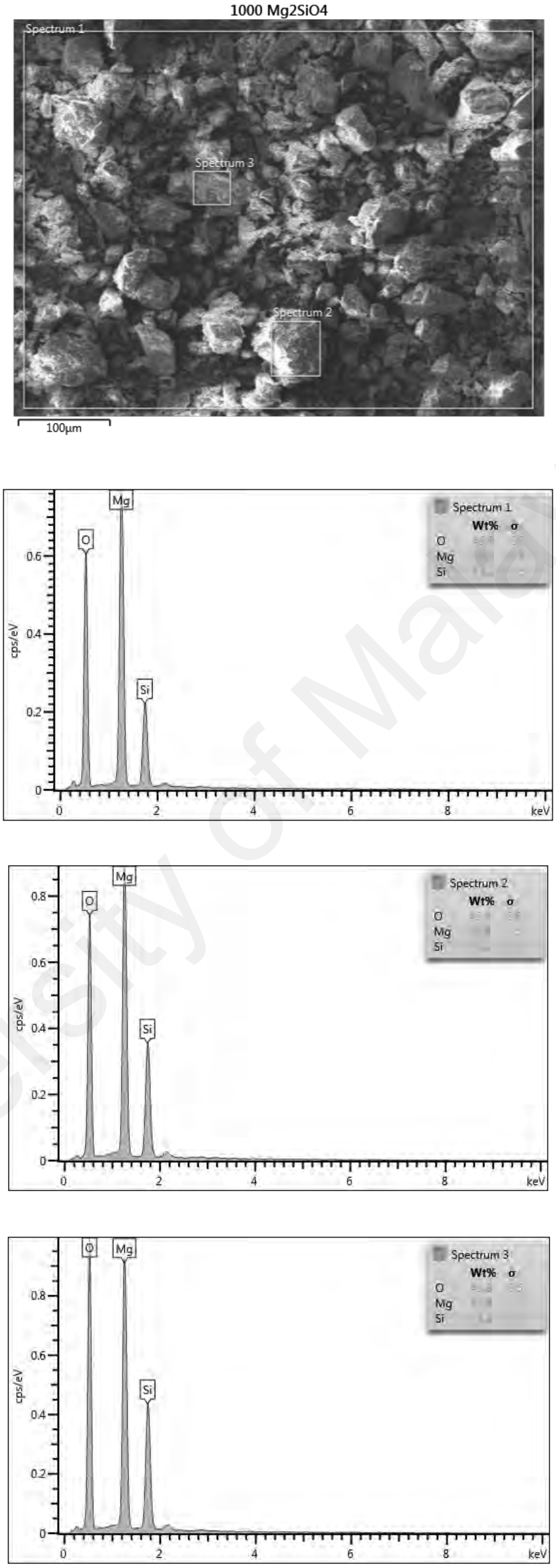

Figure 4.6 (b): EDX spectra for Mg_2SiO_4 sintered at 1000 °C

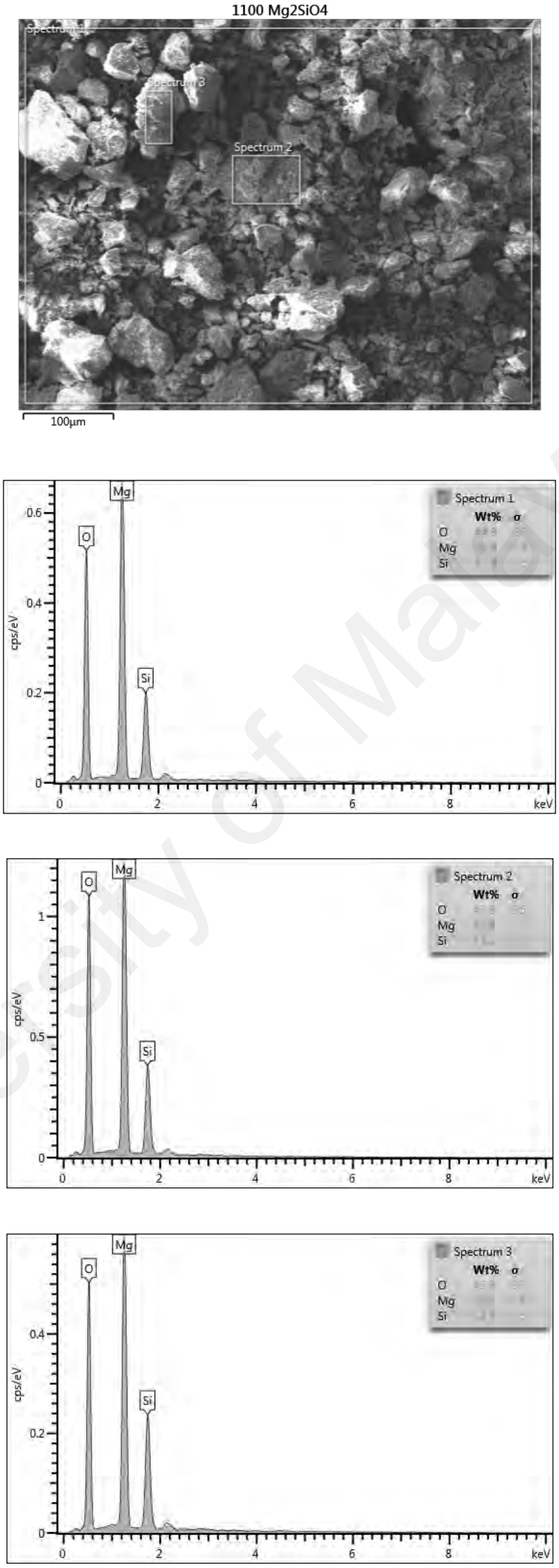

Figure 4.6 (c): EDX spectra for Mg_2SiO_4 sintered at 1100 ^{o}C

4.7 Electrochemical Impedance Spectroscopy

The details of ion migration were investigates by electrochemical impedance spectroscopy measurements that were carried out at room temperature. Typical Nyquist plots obtained are presented in Figure 4.7 (a - c). The high frequency semicircle is related to the charge transfer process and the diameter of the semicircle is approximately equal to the charge transfer resistance (R_{ct}). The sloping line at low frequency is associated with the ion diffusion in the materials (Deng et al., 2010). Presented in Table 4.3 is the variation of R_{ct} with different sintering temperature of Mg_2SiO_4. From Table 4.3, it can be observed that the R_{ct} value decreases with the sintering temperature implying that the charge transfer process in materials depends on the sintering temperature. The semicircle is the smallest for the sample synthesized at 1100 ºC, suggesting that the sample possessed the easiest charge transfer process compared to the other samples. This can be correlated with the unit cell volume of the material. Largest unit cell volume, V owned by the sample sintered at 1100 °C is expected to contribute to easy charge transfer process during intercalation and deintercalation.

Table 4.3: Charge transfer resistance of Mg_2SiO_4 samples sintered at 900 ºC, 1000 ºC and 1100 ºC

Sintering temperature	Charge transfer resistance R_{ct} (Ω)
900 ºC	1.05×10^9
1000 ºC	8.09×10^8
1100 ºC	7.01×10^8

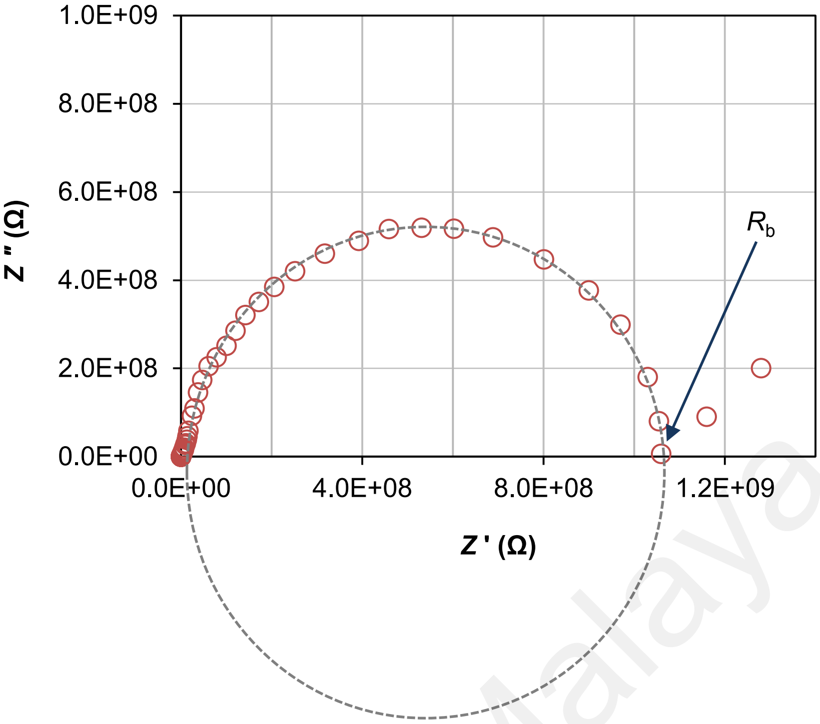

Figure 4.7 (a): Impedance plot of Mg_2SiO_4 sample sintered at 900 ºC

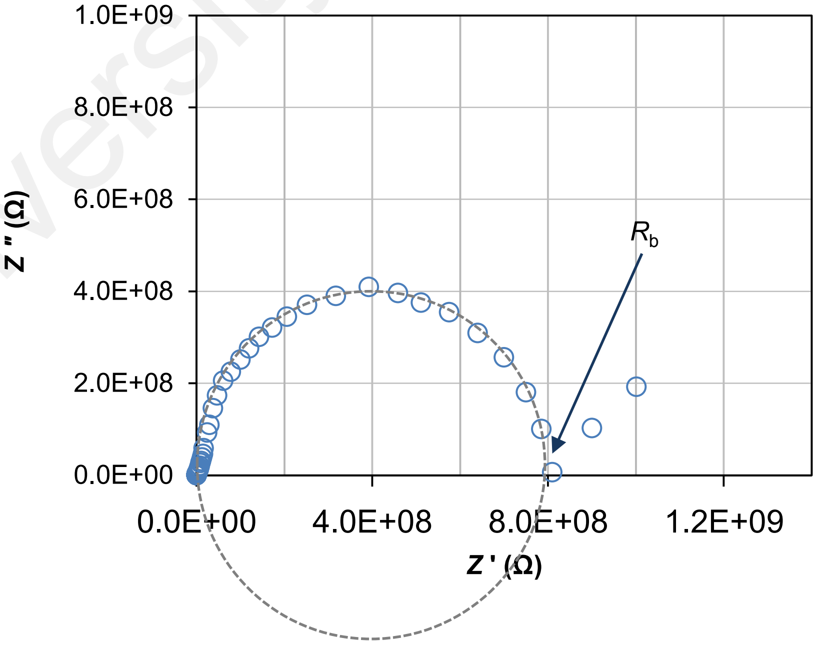

Figure 4.7 (b): Impedance plot of Mg_2SiO_4 sample sintered at 1000 ºC

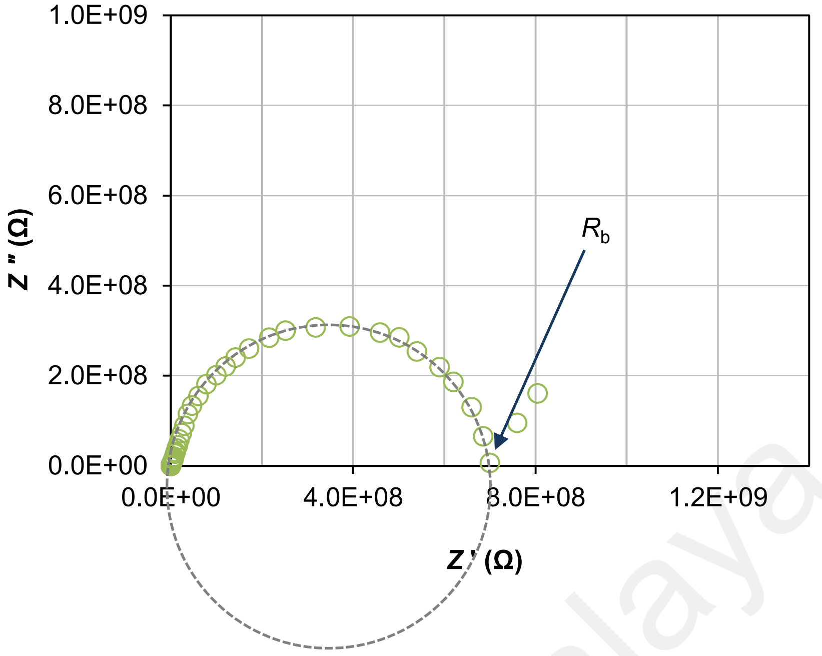

Figure 4.7(c): Impedance plot of Mg_2SiO_4 sample sintered at 1100 ºC

4.8 Transference Number Measurement

Transference number measurement was done on all three sample 900 °C, 1000 °C and 1100 °C. Direct current was recorded as a function of time upon application of constant DC voltage across the sample. The graph of normalized current versus time after polarization with highest transference number was displayed in Figure 4.8. From the graph, it can be seen that the current decreases exponentially with respect to time and saturates after about 5000 s.

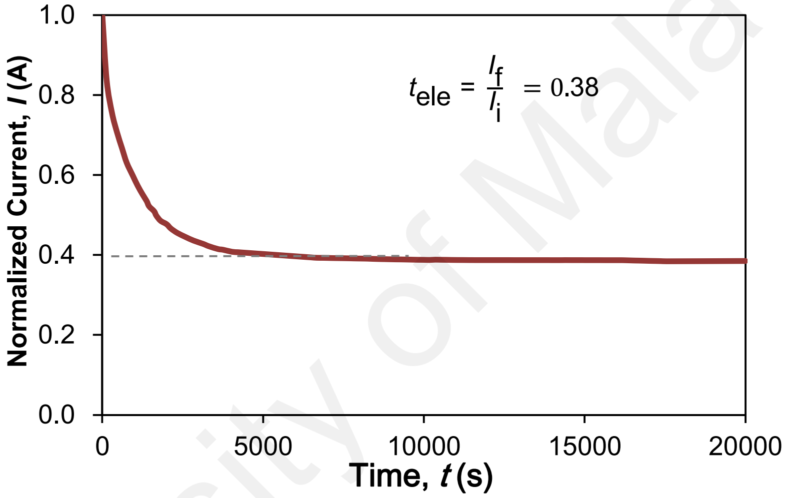

Figure 4.8: *I* - t curve of Mg_2SiO_4 sample sintered at temperature 1100 °C

Table 4.4 summarized the value of transference number for sample 900 °C, 1000 °C and 1100°C. Sample 900 °C with the highest R_{ct} value have the smallest transference number value and sample 1100 °C with the smallest R_{ct} value have the smallest transference number value. The transference, t_{ele} for sample 1100 °C is 0.38. This suggests that this type of materials is a mixed conductor and thus suitable for use as cathode material in electrochemical cells.

Table 4.4: Transference number for samples sintered at 900 ºC, 1000 ºC and 1100 ºC

Sintering temperature	Transference number, t
900 ºC	0.34
1000 ºC	0.35
1100 ºC	0.38

4.9 Cyclic voltammetry

The effect of various sintering temperatures on the electrochemical performance of the samples was investigated by cyclic voltammetry. Figure 4.9 shows cyclic voltammograms of the electrode comprising Mg_2SiO_4 sintered at 900°C, 1000°C and 1100°C at scan rate 0.5 mV s^{-1} between -1.0 V and 3.0 V.

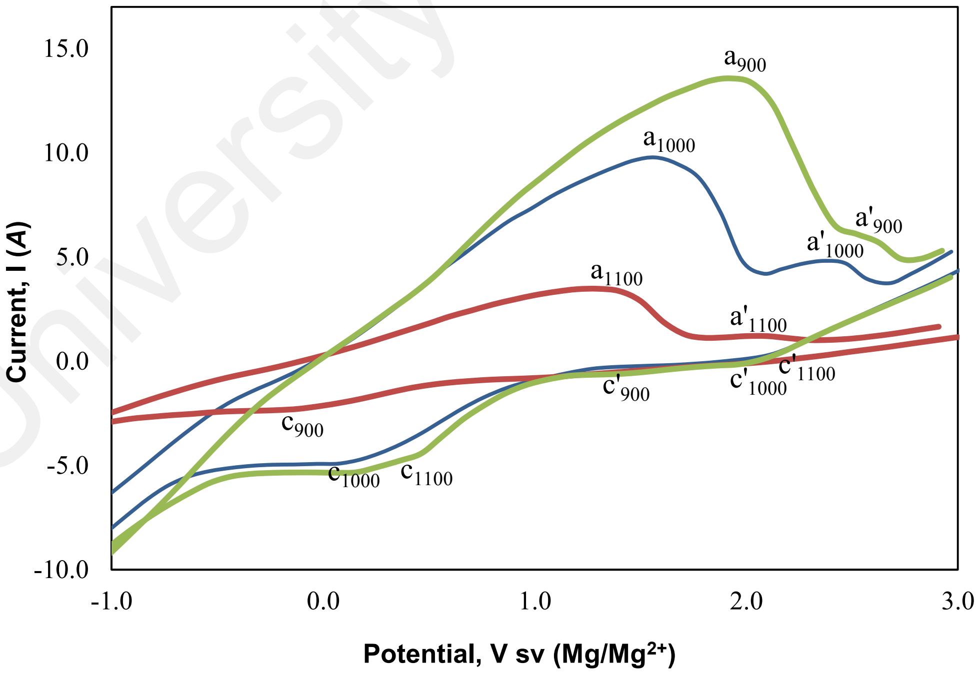

Figure 4.9: Cyclic voltammograms of Mg_2SiO_4 sintered at 900 ºC, 1000 ºC and 1100 ºC

The voltammograms show a typical and expected feature of electrochemical magnesium deintercalation and intercalation reactions. Two steps of Mg^{2+} deintercalation/intercalation can be distinguished, corresponding to two pairs of anodic/cathodic peaks marked as a/c and a'/c'as shown in Figure 4.9. The trend is similar to that reported by cyclic voltammetry (NuLi et al., 2009). In Mg_2SiO_4 structure, there are two kinds of occupation sites for Mg atoms, Mg (1) and Mg (2). Since the Mg(1)-O bonds can be formed more easily, Mg atoms prefer to occupy Mg(1) sites at first in thermodynamics. Peaks a/c and a'/c' can be attributed to the deintercalation/intercalation of Mg^{2+} from Mg(1) and Mg(2) respectively (NuLi et al., 2009). It is well known that the potential separation between anodic and cathodic peaks is an important parameter to evaluate the reversibility of electrochemical reactions. The reversibility of material is characterized by potential interval ΔE_p. The smaller this value and larger peak current density reveal much less polarization and the more facile electrochemical reaction of the material (Triwibowo et al., 2016). From Figure 4.9, it is noticed that the increase in sintering temperature caused anodic/cathodic peak changes. Table 4.5 summarizes the value of potential anodic/cathodic peaks, E_p, potential interval, ΔE_p and current peak, I_p for peaks marked as a/c and a'/c'. The sample sintered at 1000 °C has the lowest potential interval which is ΔE_p =1.26 for the first anodic/cathodic pair and $\Delta E_{p'}$ = 0.35 for the second anodic/cathodic, a'/c'. For a reversible redox process, the ratio of cathodic peak current to anodic peak current equal to unity ($I_{pC}/I_{pA} = 1$). This value shows that the amount of current stored and delivered during intercalation and deintercalation process. Among all three samples, the value of cathodic to anodic peak current ratio for materials sintered at 900°C is close to unity $I_{pC} / I_{pA} = 0.4$ and $I_{pC'} / I_{pA'} = 1.0$. However, the sample sintered at 1000°C did not show the highest current intensity. Highest current intensity for sample sintered at 1000°C is about I_{pA} = 6.90 mA which is considered small compared to other samples. Sample sintered at 1100°C has a reasonable potential interval (ΔE_p = 1.62 V and $\Delta E_{p'}$ = 0.50 V), I_{pC} / I_{pA} = 0.21 and $I_{pC'}$ / $I_{pA'}$ = 0.80) and performs the highest current peak, I_{pA} = 8.7 mA. Thus, it can be concluded that this sample is the most reversible. This result shows that sintering temperature contributed in the electrochemical performance of materials.

Table 4.5: Potential interval and redox peak currents of Mg_2SiO_4

Parameter	**Sample Mg_2SiO_4**		
	900°C	**1000°C**	**1100 °C**
I_{pA} (mA)	2.80	6.90	8.70
I_{pC} (mA)	0.40	1.70	1.80
I_{pC} / I_{pA}	0.4	0.25	0.21
E_{pA} (V)	1.30	1.36	1.92
E_{pC} (V)	-0.24	0.10	0.30
ΔE_p (V)	1.54	1.26	1.62
$I_{pA'}$ (mA)	0.20	0.90	0.40
$I_{pC'}$ (mA)	0.20	1.50	0.50
$I_{pC'}$ / $I_{pA'}$	1.00	0.60	0.80
$E_{pA'}$ (V)	2.05	2.40	2.60
$E_{pC'}$ (V)	1.60	2.05	2.10
$\Delta E_{p'}$ (V)	0.45	0.35	0.50

CHAPTER 5: $Mg_{2-x}Mn_xSiO_4$

5.1 Introduction

This chapter focuses on the $Mg_{2-x}Mn_xSiO_4$ (x = 0.2, 0.4 and 0.6) which was the second system investigated in this work. The investigation was done to study the effects of Mn (ionic radius 0.83 Å) (Zhang et al., 2010) partial substitution on Mg^{2+} (ionic radius 0.65 Å) (Wang et al., 2014) into Mg_2SiO_4 compound. The choice of manganese was made for two reasons; its size and charge are comparable to those of Mg^{2+} ions which is hope to facilitate doping process. Initially, $Mg_{2-x}Mn_xSiO_4$ (x = 0.2 – 1.0) samples were prepared using water based sol-gel followed by sintering process at temperature 1100°C for 4 hours. The prepared samples were characterized using XRD, FTIR, SEM, EDX, particle size and impedance spectroscopy in order to investigate structural, morphological and electrical properties. Transference number measurement was conducted to identify the actual type of charge carrier in the sample while the CV test was conducted to study their electrochemical properties.

5.2 X-Ray Diffraction

The structure and crystallinity of the synthesized materials were characterized with XRD. XRD patterns of $Mg_{2-x}Mn_xSiO_4$ system with $0.0 \leq x \leq 1.0$ are shown in Figure 5.1. As shown in Figure 5.1, $Mg_{2-x}Mn_xSiO_4$ materials prepared by the sol-gel technique for $x \leq 0.6$ were well crystallized and indexed to orthorhombic forsterite based on ICSD 98-000-9688. However, as the dopant amount increased to ≥ 0.6, most peaks indexed to orthorhombic forsterite disappeared and new peak ascribed to MgO appeared at $2\theta = 41.75^{\circ}$. The presence of the impurity peak suggests that Mn doping can be doped to the forsterite structure up to a certain ratio. Therefore, $Mg_{1.2}Mn_{0.8}SiO_4$ and $Mg_{1.0}Mn_{1.0}SiO_4$ samples were not used for the other characterizations.

The magnified patterns of $Mg_{2-x}Mn_xSiO_4$ ($0.0 \leq x \leq 0.6$) displayed in Figure 5.2 (a) and Figure 5.2 (b) reveal a continuous shift in the 2θ ranging from 31.5° – 34.5° and 35.0° – 38.0°. The peaks were shifted to the lower 2θ indicating that an increase in lattice parameters. Figure 5.2(a) shows the peak (031) for $x = 0.0$ located at $2\theta = 32.5^{\circ}$. When the value of x increases from 0.2 to 0.6, the peak is shifted to the lower 2θ ranging from 32.4° - 32.2°. Peaks which were originally at $2\theta = 35.8^{\circ}$ for (131) and $2\theta = 36.6^{\circ}$ for (211) are also shifted to lower 2θ as shown in Figure 5.2(b). Peak (131) is shifted to $2\theta = 35.5$ for $x = 0.2$ and to $2\theta = 35.$ for $x = 0.6$. The observed changes also confirmed the formation of $Mg_{2-x}Mn_xSiO_4$ materials and suggest that Mn entered the structure rather than forming impurities for $x \leq 0.6$.

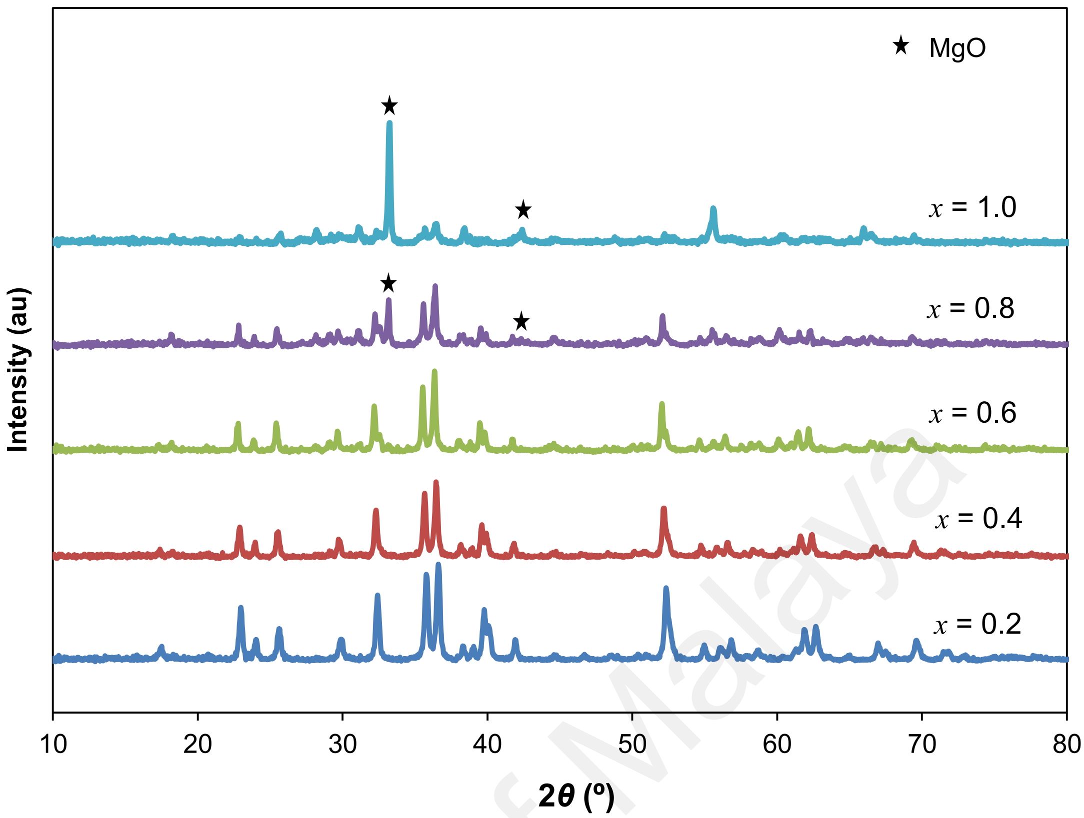

Figure 5.1: XRD spectra of $Mg_{2-x}Mn_xSiO_4$ (x = 0.0 – 1.0)

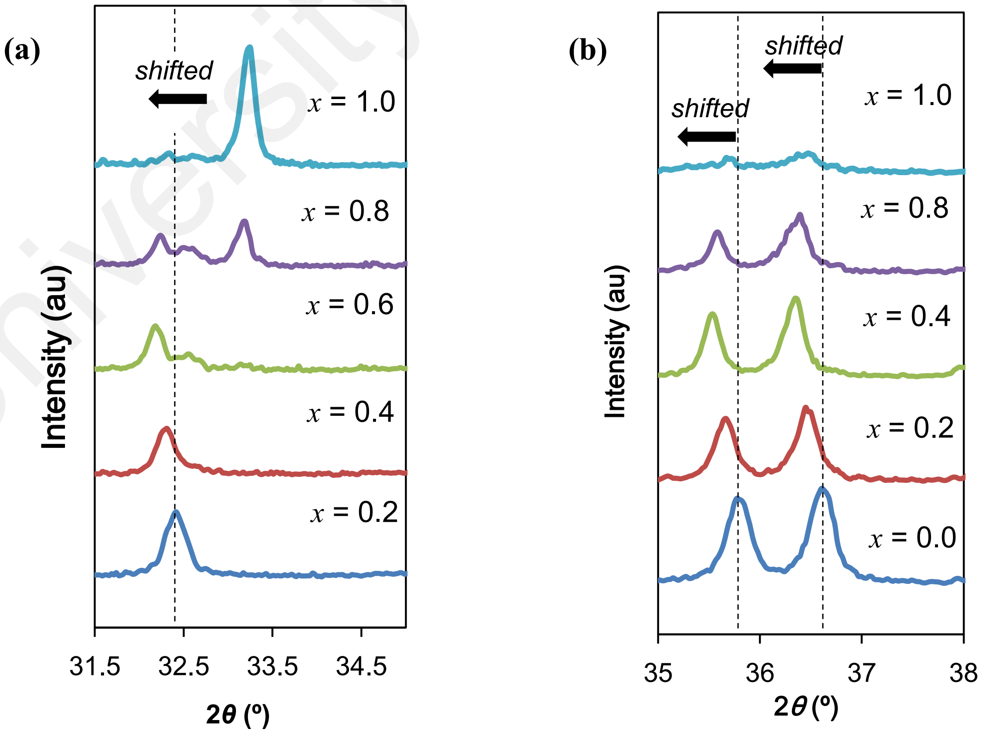

Figure 5.2: Extracted XRD spectra of $Mg_{2-x}Mn_xSiO_4$ (x = 0.0 – 1.0) system in the range of (a) 2θ = 31.5° – 35.0° and (b) 2θ = 35.0° – 38.0°

Using XRD data obtained, lattice parameters (*a*, *b* and *c*) and unit cell volume, *V* of the samples $Mg_{2-x}Mn_xSiO_4$ ($0.0 \leq x \leq 0.6$) were calculated according to the Bragg equation (Adnan et al., 2014). Results obtained are presented in Table 5.1 and compared with the parent $x = 0.0$. It can be seen that all lattice parameters significantly increase with the increase in doping amount. This corresponds to larger ionic radius of Mn compared to that of Mg (Kandhasamy et al., 2012). The increase in V of the doped samples not only proves the successful doping of Mn^{2+} in Mg_2SiO_4 crystal, but also favorable to enhance electrochemical properties due to larger diffusion pathways for Mg ion migration (Huang et al., 2007; Liu et al., 2008; Yang et al., 2010).

Table 5.1: Lattice parameters for $Mg_{2-x}Mn_xSiO_4$ ($x = 0.2 - 0.6$)

Sample	**Lattice parameter**			**Volume of unit cell, *V* [Å^3]**	**Crystallite Size [Å]**
	***a* [Å]**	***b* [Å]**	***c* [Å]**		
$Mg_{2.0}SiO_4$	10.1693	5.9685	4.6886	284.5759	39.57
$Mg_{1.8}Mn_{0.2}SiO_4$	10.0256	6.1249	4.7496	291.6539	25.59
$Mg_{1.6}Mn_{0.4}SiO_4$	10.0636	6.1432	4.7624	294.4258	25.86
$Mg_{1.4}Mn_{0.6}SiO_4$	10.0989	6.1548	4.7624	296.0189	29.90

5.3 Fourier Transform Infrared

FTIR spectra of $Mg_{2-x}Mn_xSiO_4$ ($0.0 \leq x \leq 0.6$) in the spectral region from 550 to 1350 cm^{-1} are illustrated in Figure 5.3.

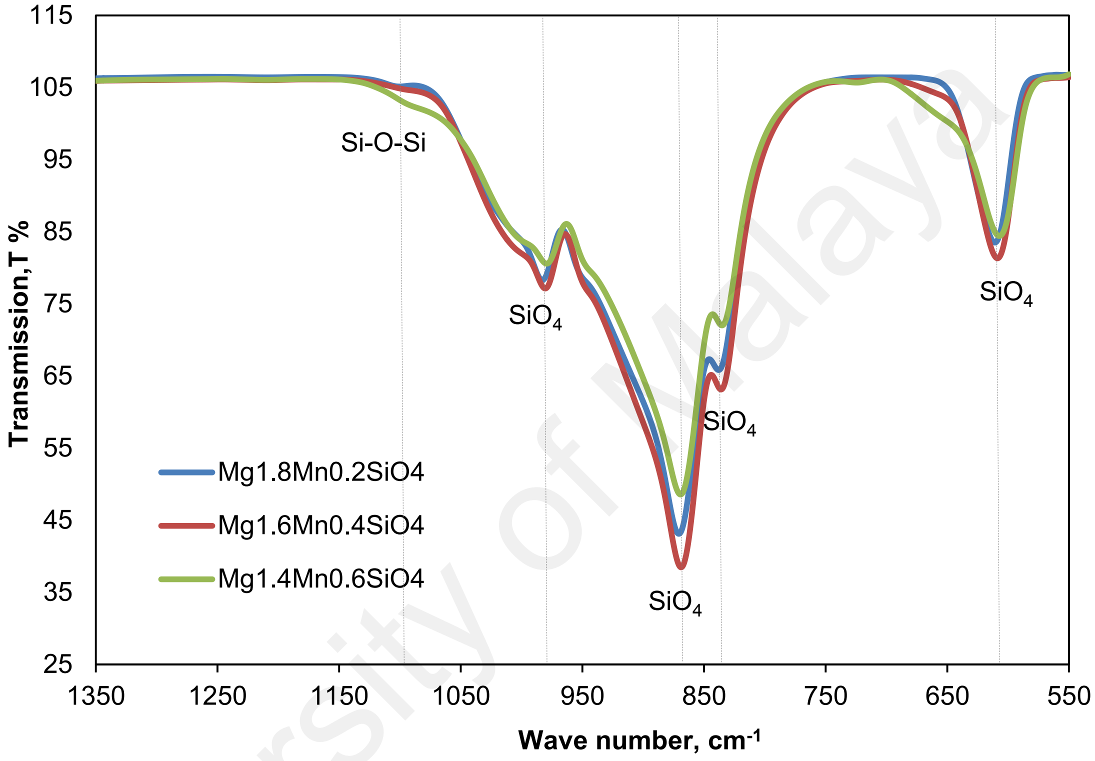

Figure 5.3: FTIR spectra of $Mg_{2-x}Mn_xSiO_4$ ($x = 0.2 – 0.6$)

It is notice that the entire region consists of characteristic bands correspond to the magnesium silicate. According to previous studies, the absorption bands observed at 610 cm^{-1} is mainly due to the bending vibration of SiO_4 (Paques-Ledent et al., 1973; Saberi et al., 2007). Meanwhile, absorption bands exist in the region from 800 cm^{-1} to 1090 cm^{-1} corresponds to the stretching vibration of SiO_4. Absorption bands observed at the wavelength of 840 cm^{-1}, 874 cm^{-1}, 959 cm^{-1} and 989 cm^{-1} belong to the asymmetric and symmetric stretching vibrations of SiO_4 which are consistent with previous works reported by other researchers (Mazza et al., 1993; Paques-Ledent et al., 1973; Saberi et al., 2007; Tsai, 2002). The shoulder appeared around 989 – 1072 cm^{-1} and bands observed in the range of 950 - 990 cm^{-1} are related to the characteristic of Si-O-Si asymmetric stretching (Tsai, 2002). Meanwhile the band centered at 1110 cm^{-1} corresponds to Si-O-Si vibration (Saberi et al., 2007) which appeared as a very weak band after heating at 1100 ºC. The existence of the magnesium silicate bands gives an additional proof of the formation of $Mg_{2-x}Mn_xSiO_4$ compound.

5.4 Scanning Electron Microscopy and Particle Sizer

Figure 5.4 shows SEM images and particle size distribution graphs of $Mg_{2-x}Mn_xSiO_4$ ($0.0 \leq x \leq 0.6$). The materials composed of agglomerated small primary particles with a broad particle size distribution. However, the particles agglomeration and the average particle size are relatively reduced by Mn doping. The particle size distribution in SEM image dispalyed in Figure 5.4 (c) is smaller and uniformly distributed compared to others. The reduction of particle size can shorten the diffusion path of ions as well as increase the electrochemical activation area (Shu et al., 2013). This observation is consistent with the particle size distribution displayed in Figure 5.4. Particle size distribution decreases with increase the ratio of Mn dopant content. The average particle size decreases from 36.7 µm in Mg_2SiO_4 sample to 13.70 µm in $Mg_{1.4}Mn_{0.6}SiO_4$ sample. Generally, smaller particle size and even homogenous distribution would provide better electrochemical performance as the smaller particle size facilitates ions insertion/deinsertion during electrochemical process (Shaju et al., 2002; Zou et al., 2004)

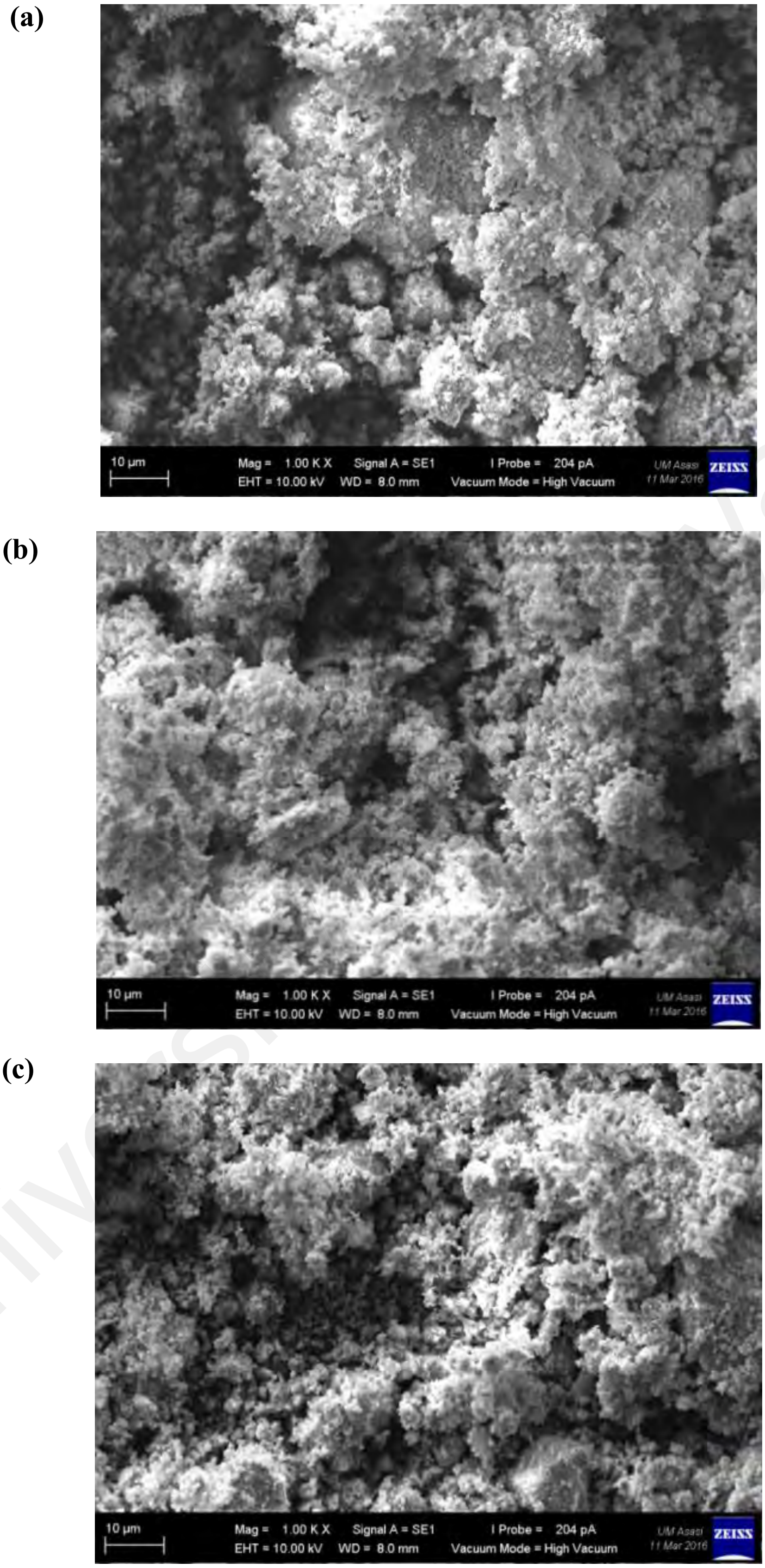

Figure 5.4: SEM images and particle size distributions of $Mg_{2-x}Mn_xSiO_4$ with x of (a) 0.2, (b) 0.4 and (c) 0.6 systems

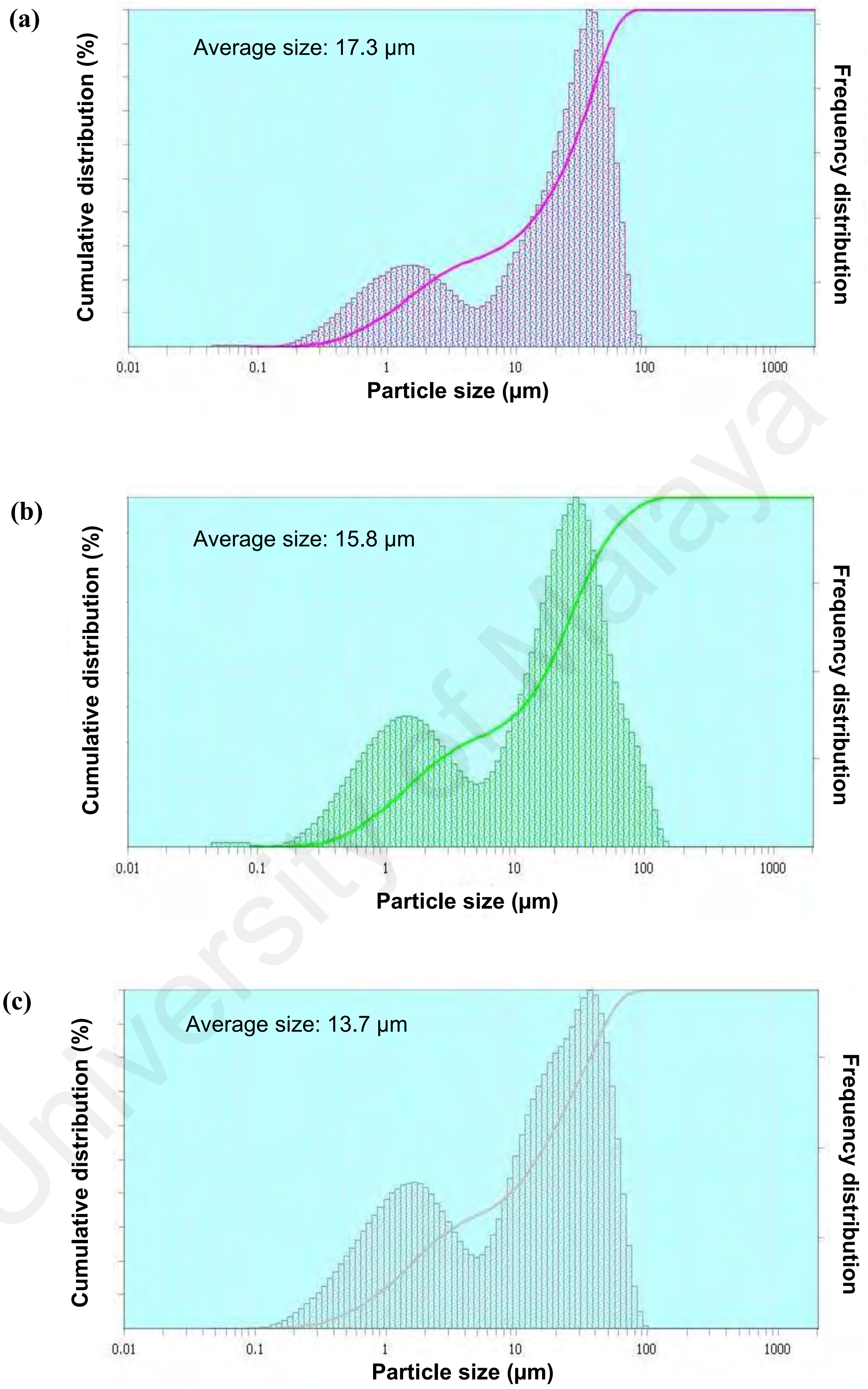

Figure 5.5: Particle size distributions of $Mg_{2-x}Mn_xSiO_4$ with *x* of (a) 0.2, (b) 0.4 and (c) 0.6 systems

5.5 Energy Dispersive X-Ray Analysis

Further analysis on the elemental composition was conducted using the EDX analysis on the doped system $Mg_{2-x}Mn_xSiO_4$ for $x = 0.2$, 0.4 and 0.6. The EDX spectra are presented in Figure 5.6. The average stoichiometric from three selected regions for each composition has been analyzed and data obtained are tabulated in Table 5.2. This analysis confirms that the compounds consisted of Mg, Mn, Si and O and followed the stoichiometric formula as designed in the preparation of samples.

Table 5.2: The EDX stoichiometric atomic ratios of $Mg_{2-x}Mn_xSiO_4$

Sample		**Average stoichiometric, atomic ratio**			
		Mg	**Mn**	**Si**	**O**
$Mg_{1.8}Mn_{0.2}SiO_4$	Calculated atomic ratio (%)	1.80	0.20	1.00	4.00
	EDX atomic ratio (%)	1.80	0.21	0.97	4.00
$Mg_{1.6}Mn_{0.4}SiO_4$	Calculated atomic ratio (%)	1.60	0.40	1.00	4.00
	EDX atomic ratio (%)	1.60	0.40	0.95	4.00
$Mg_{1.4}Mn_{0.6}SiO_4$	Calculated atomic ratio (%)	1.40	0.60	0.95	4.00
	EDX atomic ratio (%)	1.49	0.60	0.96	4.00

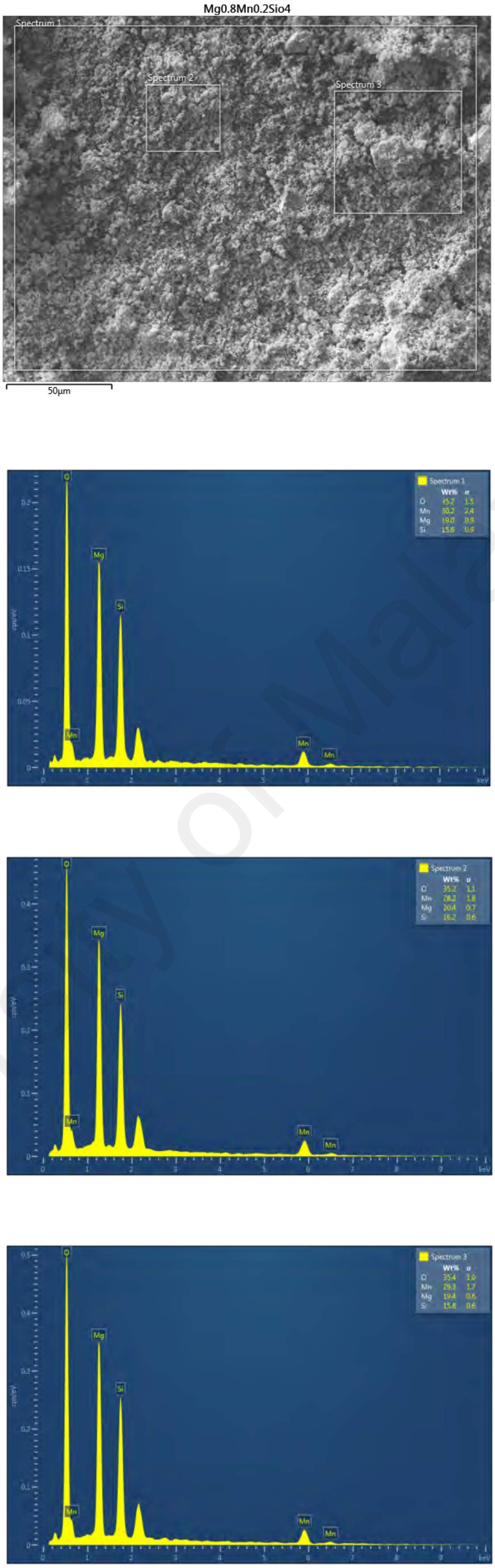

Figure 5.6 (a): EDX spectra of $Mg_{2-x}Mn_xSiO_4$ with x = 0.2

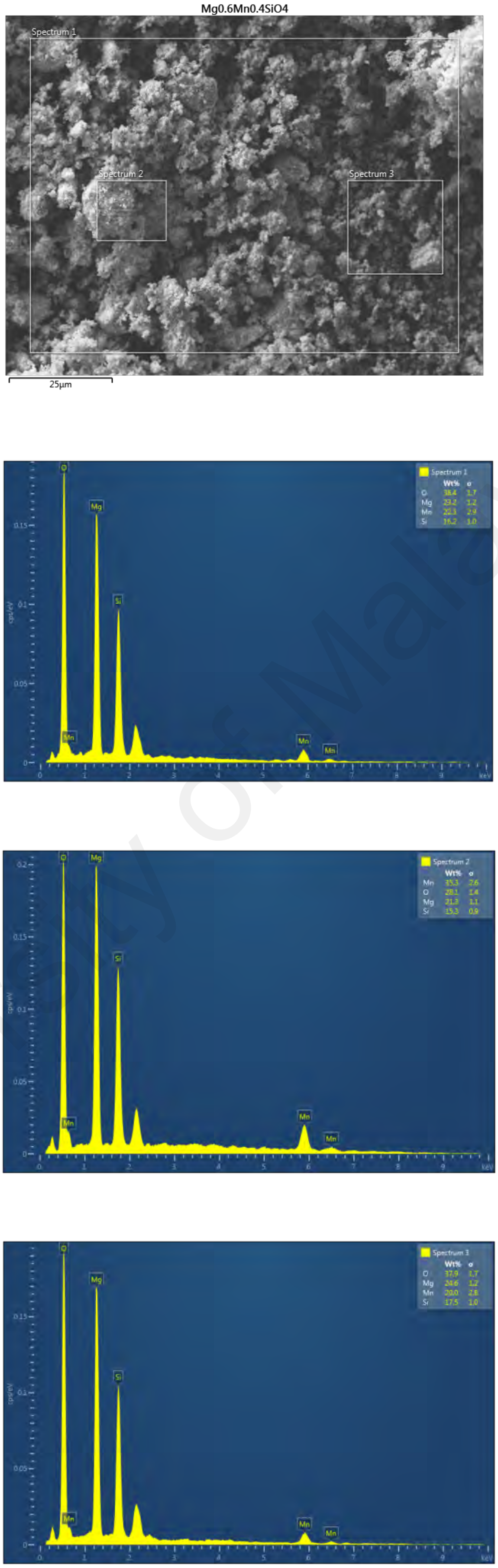

Spectrum 1

	Wt%	σ
O	38.4	1.7
Mg	23.2	1.2
Mn	22.3	2.9
Si	16.2	1.0

Spectrum 2

	Wt%	σ
Mn	35.3	2.6
O	28.1	1.4
Mg	21.3	1.1
Si	15.3	0.9

Spectrum 3

	Wt%	σ
O	37.9	1.7
Mg	24.6	1.2
Mn	20.0	2.8
Si	17.5	1.0

Figure 5.6 (b): EDX spectra of $Mg_{2-x}Mn_xSiO_4$ with x = 0.4

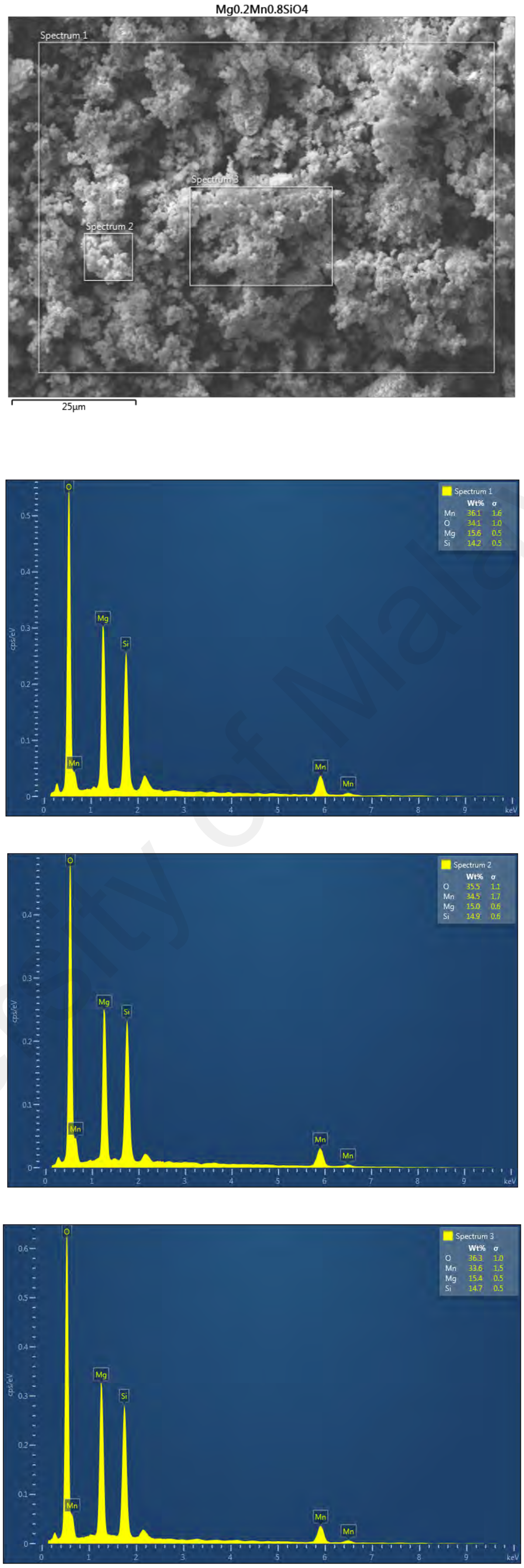

Figure 5.6 (c): EDX spectra of $Mg_{2-x}Mn_xSiO_4$ with $x = 0.6$

5.6 Electrochemical Impedance Spectroscopy

The complex impedance plots of $Mg_{2-x}Mn_xSiO_4$ (x = 0.2, 0.4 and 0.6) samples are presented in Figure 5.7 (a – c). As can be seen from the figure, all plots consist of a semicircle in the high frequency region which associated to the charge transfer process and a tilted spike at low frequency region which can be related to the ion diffusion in solid state phase (Shu et al., 2013). R_{ct} obtained in this system is much smaller compared to the R_{ct} of the undoped sample which is 7.01×10^8 Ω as revealed in Chapter 4. This significant decrease in the charge transfer resistance, R_{ct} value suggests that the doping reduced the charge transfer resistance hence improved the electrode charge transfer process. The R_{ct} values for $Mg_{2-x}Mn_xSiO_4$ ($x = 0.2 – 0.6$) are presented in Table 5.3. The table reveals that the charge transfer process was better in the doped samples compared to the undoped sample implying that doping gave favorable effect to the R_{ct} (Yang et al., 2010).

Table 5.3: Charge transfer resistance, R_{ct} of $Mg_{2-x}Mn_xSiO_4$ samples.

Name of sample	Charge transfer resistance R_{ct} (Ω)
$x = 0.2$	5.83×10^8
$x = 0.4$	3.68×10^8
$x = 0.6$	2.15×10^8

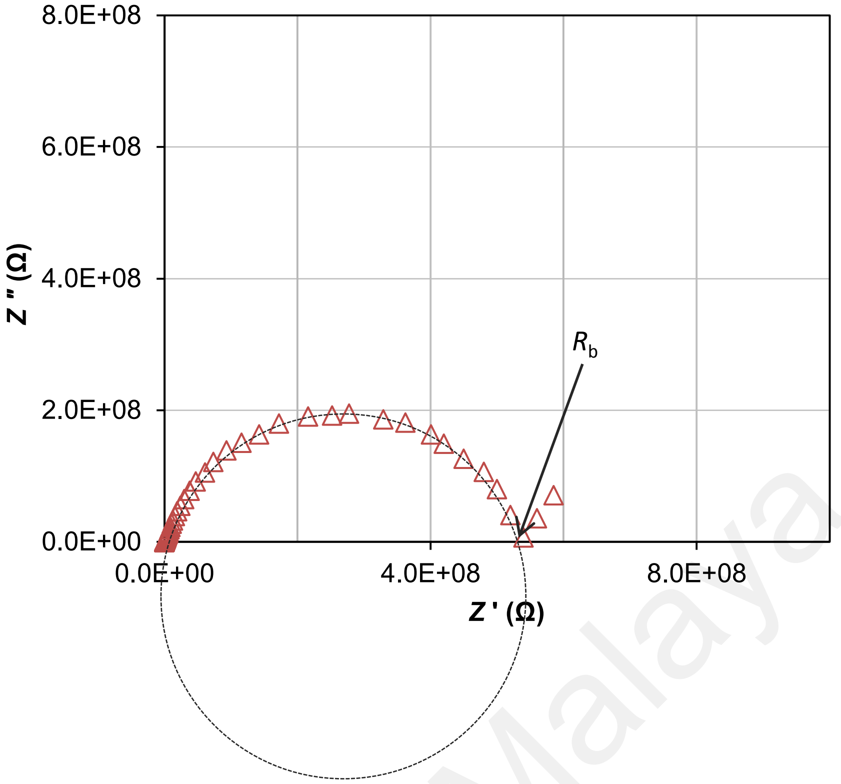

Figure 5.7(a): Impedance plot of $Mg_{2-x}Mn_xSiO_4$ (x = 0.2)

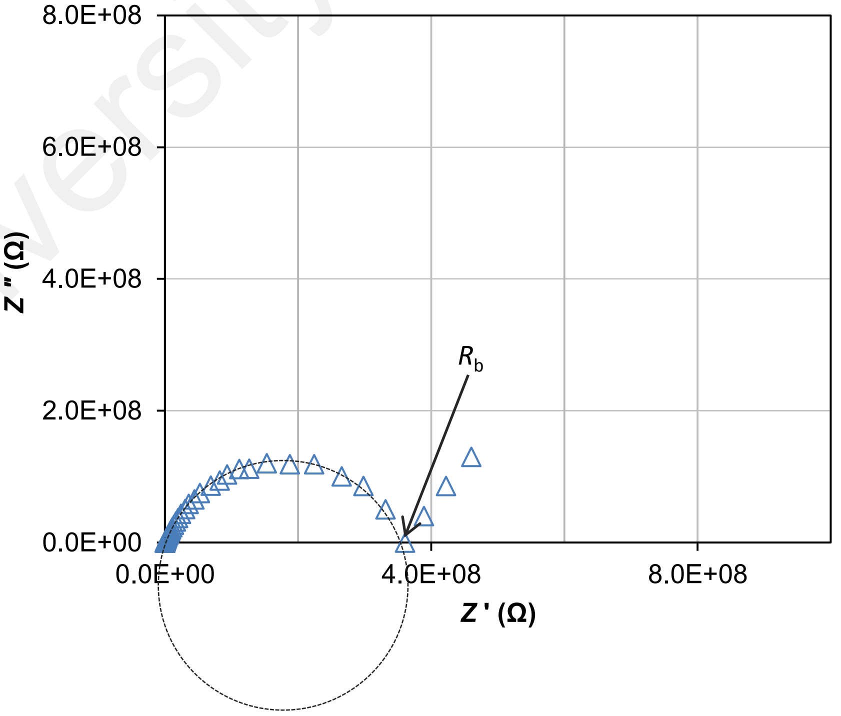

Figure 5.7(b): Impedance plot of $Mg_{2-x}Mn_xSiO_4$ (x = 0.4)

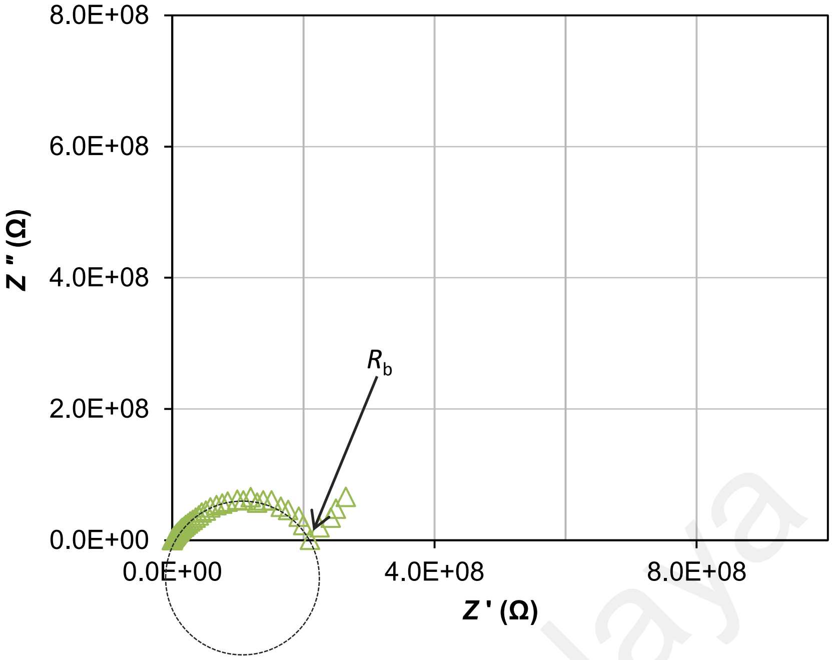

Figure 5.7(c): Impedance plot of $Mg_{2-x}Mn_xSiO_4$ ($x = 0.6$)

5.7 Transference number

Transference number measurement was done on the sample $Mg_{1.4}Mn_{0.2}SiO_4$ for x = 0.2, 0.4 and 0.6. Current time graph in Figure 5.8 discloses transference number for sample with the smallest R_{ct} value.

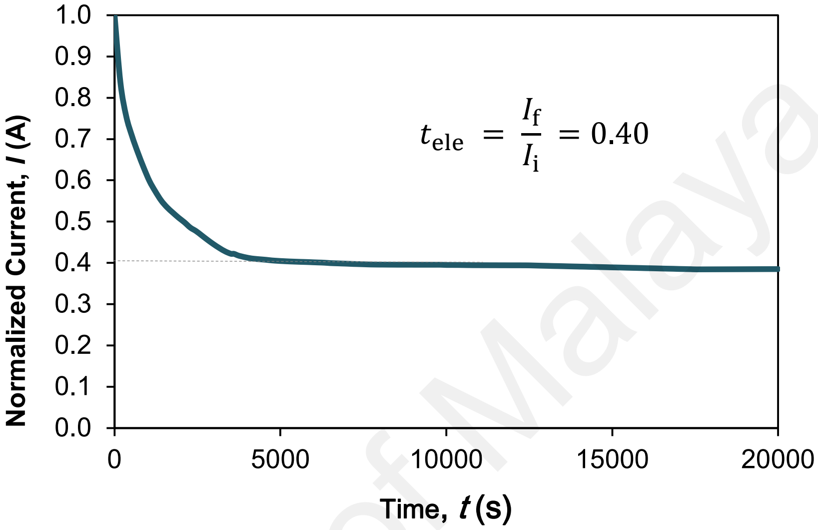

Figure 5.8: Current time curve of $Mg_{1.4}Mn_{0.6}SiO_4$ sample

Result of transference number value for $Mg_{2-x}Mn_xSiO_4$ (x = 0.2, 0.4 and 0.6) was listed in Table 5.4. Among all three sample, x = 0.6 with the smallest R_{ct} owned the highest transference number value, t_{ele} = 0.40. The smallest transference number for system II is 0.38 which owned by sample x = 0.2. This proved that the material was a mixed conductor making it suitable for use as cathode active material in electrochemical cells.

Table 5.4: Transference number value of $Mg_{2-x}Mn_xSiO_4$

Sample $Mg_{2-x}Mn_xSiO_4$	Transference number, t
$x = 0.2$	0.38
$x = 0.4$	0.38
$x = 0.6$	0.40

5.8 Cyclic voltammetry

The effect of Mn doping into $Mg_{2-x}Mn_xSiO_4$ on the electrochemical performance of the samples can be understood by cycliv voltammetry. Figure 5.9 show the CV curves of $Mg_{2-x}Mn_xSiO_4$ ($0.0 \leq x \leq 0.6$) samples between −1.0 V to 3.0 V at a scan rate of 0.5 mV s^{-1}. All samples show similar CV curves with 2 pairs of redox peaks respond (Yang et al., 2010). The first pair of anodic/cathodic was marked as a/c meanwhile the second pair of anodic/cathodic peak marked as a'/c'. The same trend is observed in the undoped Mg_2SiO_4 in Chapter 4. Table 5.4 summarizes the current intensity for anodic and cathodic (I_{pA}) and (I_{pC}), cathodic to anodic current ratio (I_{pC} / I_{pA}), cathodic and anodic peak potential and potential separation, ΔE for $Mg_{2-x}Mn_xSiO_4$ (x= 0.2 – 0.6) system. Table 5.4 shows the I_{pC} / I_{pA} ratio increases as the dopant amount increases.

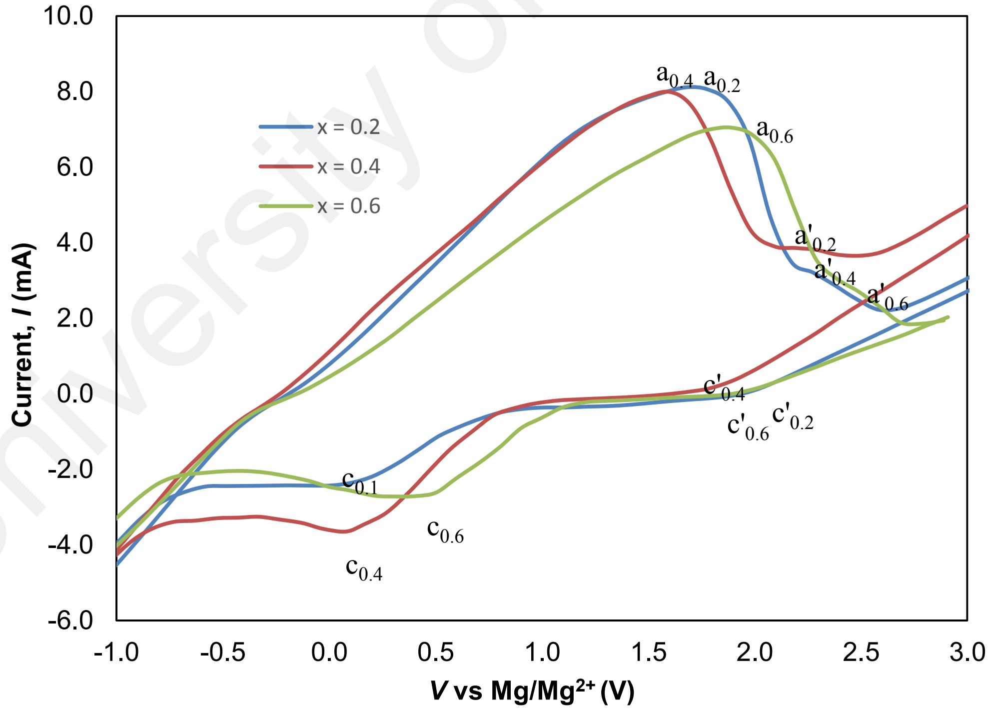

Figure 5.9: CV graph for $Mg_{2-x}Mn_xSiO_4$

For the first pair of redox peak, sample with $x = 0.6$ has the highest value of I_{pC} / I_{pA} which is 0.58. Even the anodic and cathodic peak currents are lower compared to the undoped samples in system 1, but the value is still acceptable. However, the value I_{pC} / I_{pA} ratios for this system is much better for Mn doped samples. In addition, the cathodic peak area of doped samples in Figure 5.13 is larger than that of undoped sample as shown in section 4.9. As such the Mn doped samples are expected to be able to intercalate and deintercalate more Mg ions (Yang et al., 2010). However, anodic (a') and cathodic (c') peak intensity for second pair of redox peak seem to be very low in the doped sample compared to the undoped sample. Similar to the undoped sample, this implies that occupation of Mg ions during intercalation and deintercalation process is dominant on Mg (1) site.

What is more, the peak separation of Mn doped sample reduced as dopant amount increases. From Table 5.5, for the first pair of redox peak, sample with less dopant amount (x = 0.2), had the largest ΔE_p meanwhile the smallest ΔE_p is owned by the sample with x = 0.6 which is 1.44 V. It implies that the polarization was alleviated by Mn doping, so that the performance of the samples was improved (Yang et al., 2010) which are shown in Figure 5.13. This observation is in line with the R_{ct} reported in section 5.6. Therefore, it can be understood that doping is one of beneficial techniques to enhance the performance of the Mg_2SiO_4 material.

Table 5.5: Potential interval and redox peak currents of $Mg_{2-x}Mn_xSiO_4$

Parameter	**Sample $Mg_{2-x}Mn_xSiO_4$**		
	***x* = 0.2**	***x* = 0.4**	***x* = 0.6**
I_{pA} (mA)	5.40	4.90	4.00
I_{pC} (mA)	1.10	2.20	2.30
I_{pC} / I_{pA}	0.20	0.45	0.58
E_{pA} (V)	1.72	1.60	1.88
E_{pC} (V)	0.08	0.08	0.44
ΔE_p (V)	1.64	1.52	1.44
$I_{pA'}$ (mA)	0.12	0.12	0.12
$I_{pC'}$ (mA)	0.10	0.09	0.10
$I_{pC'}$ / $I_{pA'}$	0.83	0.75	0.83
$E_{pA'}$ (V)	2.30	2.26	2.50
$E_{pC'}$ (V)	1.92	1.74	1.92
$\Delta E_{p'}$ (V)	0.38	0.52	0.58

CHAPTER 6: $Mg_{2-x}Mn_xSi_{1-y}O_4Zr_y$

6.1 Introduction

To further improve the forsterite material studied in this work, partial substitution at both Mg and Si sites have been done based on the stoichiometric formula ($Mg_{2-x}Mn_xZr_ySi_{1-y}O_4$). The work reported in this chapter was carried out to investigated the effects of Zr^{4+} doping on Si^{4+} site in $Mg_{2-x}Mn_xSiO_4$ system's properties especially the structural properties and the electrochemical properties. Larger size of Zr^{4+} (r_{Zr+} = 0.80 Å) compared to Si^{4+} (r_{Si+} = 0.41 Å) is expected to increase the lattice size of the parent compound's structure and improve the migration channel for Mg^{2+} ion which may enhance the electrochemical properties of $Mg_{2-x}Mn_xZr_ySi_{1-y}O_4$ samples. In this system, samples synthesized based on stoichiometric $Mg_{2-x}Mn_xSi_{1-y}O_4Zr_y$ for every x = 0.2, 0.4 and 0.6 with y varied from 0.1 - 0.3. The range of x were selected based on results obtained in system II and the sintering temperature used for this system is 1100 °C for 4 hours. Physical and electrochemical properties of the samples were investigated by using XRD, FTIR, SEM, particle size analysis, EDX, electrochemical impedance EIS and transference number measurement and CV.

6.2 X-Ray Diffraction

Based on the results obtained in chapter 5, a total of 9 samples have been prepared in this part initially and the structural information of the samples have been characterized by using XRD. Figure 6.1 shows the XRD spectra obtained for all 9 samples. From Figure 6.1, only 4 samples out of 9 were successfully synthesized. Impurity are detected in all samples with $x = 0.6$ and two samples with $x = 0.4$. Therefore, only three samples with $x = 0.2$ were used for further investigation and compared with the undoped sample.

Figure 6.2 compares the X-ray diffraction patterns of undoped $Mg_{1.8}Mn_{0.2}SiO_4$ and doped materials $Mg_{1.8}Mn_{0.2}Si_{1-y}O_4Zr_y$ ($0.1 \leq y \leq 0.3$). All the peaks for doped sample fit the peaks of undoped structure very well without any impurity detected. All materials can be indexed on the basis of olivine $MgMnSiO_4$ and the sharp peaks in the pattern give an indication that the powders possess high degree of crystallinity. The diffraction peaks of the samples correspond to a single phase and indexed based on Inorganic Chemistry Structure Database (ICSD) 98-008-8024 with orthorhombic crystal system of space group *Pmna* (62). Compared with the XRD pattern of undoped $Mg_{1.8}Mn_{0.2}SiO_4$, all Zr doped samples have no extra reflection peaks detected in the XRD patterns for $y \leq 0.3$. This indicates that Zr entered the structure of $Mg_{1.8}Mn_{0.2}SiO_4$ rather than forming impurities. However, the increase in the dopant Zr^{4+} amount to 0.4 into $Mg_{1.8}Mn_{0.2}Si_{1-y}O_4Zr_y$ resulted in the growth of impurity phase. Therefore, we decided not to do further characterizations on the $Mg_{1.8}Mn_{0.2}Si_{0.6}O_4Zr_{0.4}$ sample.

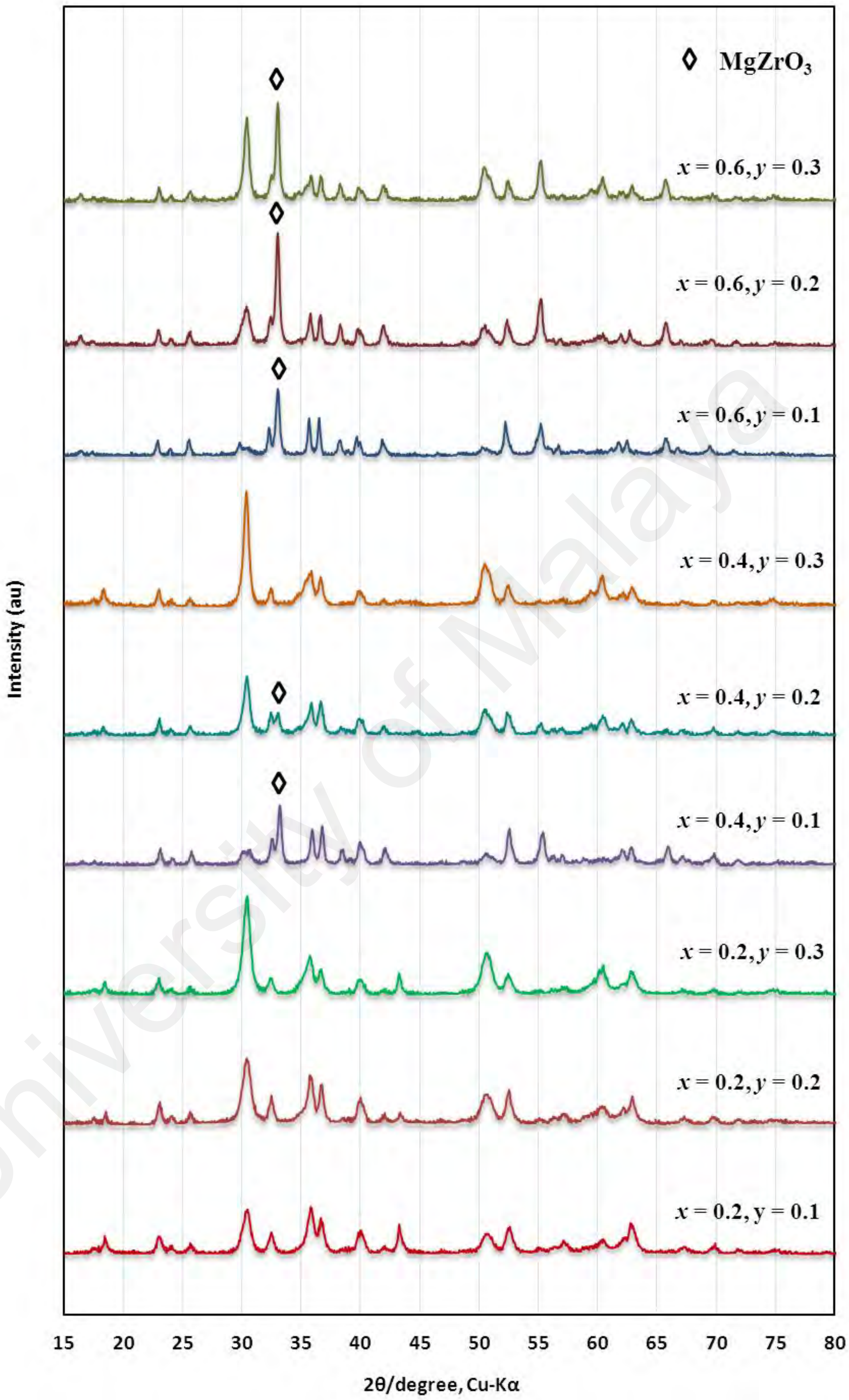

Figure 6.1: XRD spectra of $Mg_{2-x}Mn_xSi_{1-y}O_4Zr_y$ (x = 0.2, 0.4, 0.6 and y = 0.1, 0.2, 0.3) samples

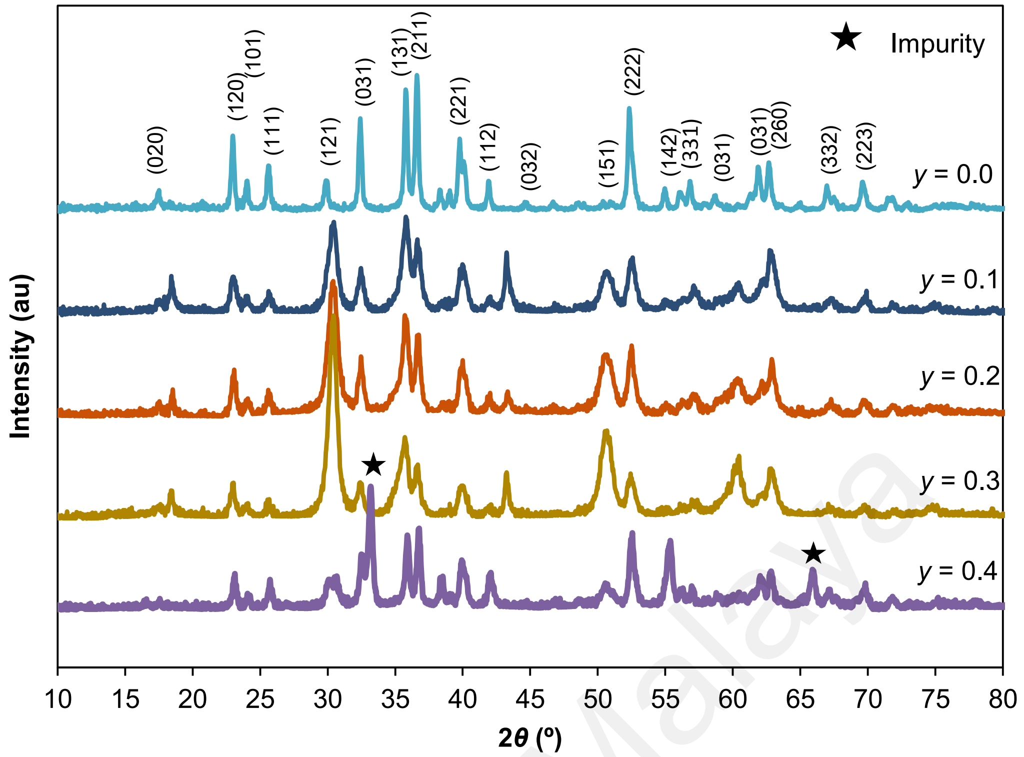

Figure 6.2: XRD spectra of $Mg_{1.8}Mn_{0.2}Si_{1-y}O_4Zr_y$ (y = 0.0 – 0.3)

The XRD spectra in the 29.0 ° ≤ 2θ ≤ 32.0 ° and 49.0 ° ≤ 2θ ≤ 52.0 ° spectral ranges were magnified and are illustrated in Figure 6.3(a) and Figure 6.3(b). As can be seen in Figure 6.3(a), varying the dopant ratio from 0.1, 0.2 and 0.3 leads to broadening of XRD peaks and a significant increase in their intensity. There is also a subtle but significant shift to the lower 2 theta angle of the diffraction peaks in Figure 6.3(b). These observations prove that zirconium was successfully incorporated into the $Mg_{1.8}Mn_{0.2}SiO_4$ lattice without altering its structure for $0.0 \leq y \leq 0.3$. The occupation of dopant in the undoped lattice can be expected to result in small changes in the lattice parameters of the crystal structure.

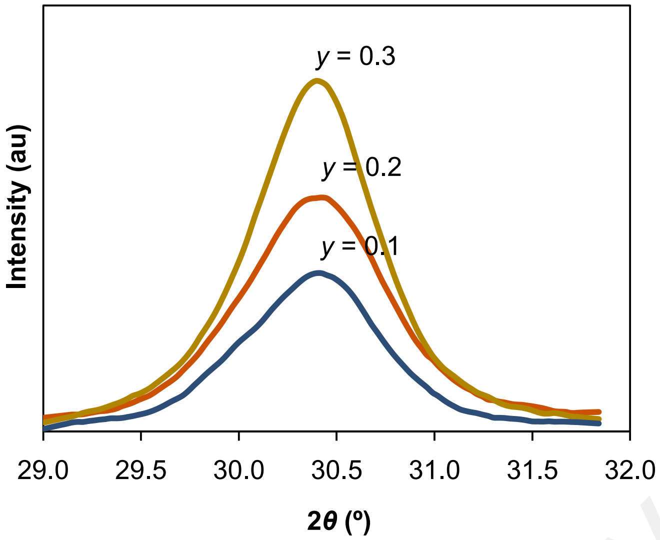

Figure 6.3 (a): Extracted XRD spectra of $Mg_{1.8}Mn_{0.2}Si_{1-y}O_4Zr_y$ ($y = 0.1 – 0.3$) system in the range of $2\theta = 29.0° – 32.0°$

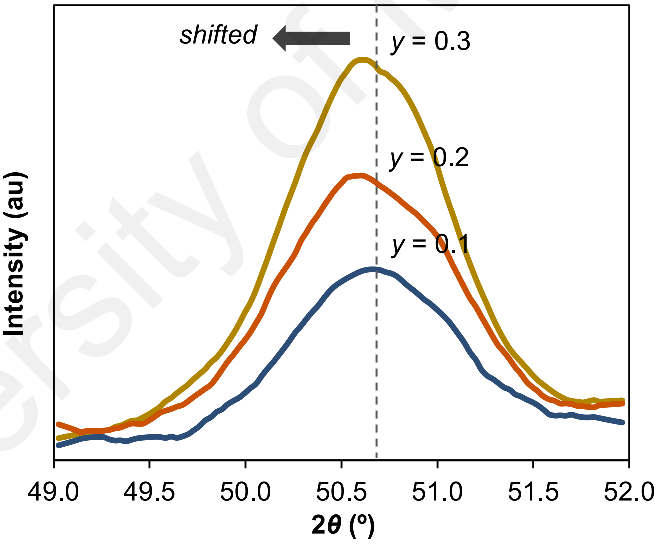

Figure 6.3 (b): Extracted XRD spectra of $Mg_{1.8}Mn_{0.2}Si_{1-y}O_4Zr_y$ ($y = 0.1 – 0.3$) system in the range of $2\theta = 49.0° – 52.0°$

The lattice parameters for $Mg_{1.8}Mn_{0.2}Si_{1-y}O_4Zr_y$ ($0.0 \leq y \leq 0.3$) samples were calculated using Bragg equation explained in (Adnan et al., 2014; West, 2007), and the results are listed in Table 6.1. Lattice parameters *a*, *b* and *c* for undoped sample are 10.0256 Å, 6.1249 Å and 4.7496 Å respectively. From Table 6.1, one can see that lattice parameter *a* increases with increasing Zr^{4+} dopant amount. However, the changes in lattice parameters *b* and *c* are not monotonous. Lattice parameter *b* is the largest for sample with y = 0.2 which is 6.1326 Å and the largest lattice parameter *c* is owned by the sample with y = 0.3 (c = 4.8351 Å). The unit cell volume expansion, caused by the increase in lattice parameters, may assist the intercalation and deintercalation of Mg ions during electrochemical processes. This increase in unit cell volume reveals the successful doping of Zr into the structure. The observed change is due to the replacement of the ionic radius or Zr^{4+} ion (0.72 Å) is larger than ionic radius of Si^{4+} ion (0.41 Å). A similar method has been employed in previous works. Zr doping has been used to stabilize and increase lattice parameter of olivine $LiFePO_4$ (Liu et al., 2008; Meethong et al., 2009; Wagemaker et al., 2008). According to Scherrer's equation (Equation 3.2), the crystallite size of the undoped sample was calculated to be 25.59 Å while the crystallite size of the Zr doped samples is in the range of 9.93 Å to 10.82 Å which is slightly smaller than that of the undoped $Mg_{1.8}Mn_{0.2}SiO_4$. This may be due to the small grain growth of Zr doped materials compared to the undoped materials (Mote et al., 2013).

Table 6.1: Lattice parameters, unit cell volume and crystallite size of $Mg_{1.8}Mn_{0.2}Si_{1-y}O_4Zr_y$ (y = 0.1 – 0.3)

Sample $Mg_{1.8}Mn_{0.2}Si_{1-y}O_4Zr_y$	**Lattice parameter**			**Volume of unit cell**	**Crystallite Size (Å)**
	***a* (Å)**	***b* (Å)**	***c* (Å)**	**V (Å^3)**	
y = 0.1	10.0190	6.1237	4.7499	291.6539	10.33
y = 0.2	10.0344	6.1324	4.7462	292.0528	10.82
y = 0.3	10.0417	6.1291	4.8351	297.5823	9.93

6.3 Fourier Transform Infrared (FTIR)

FTIR spectra of $Mg_{1.8}Mn_{0.2}Si_{1-y}O_4Zr_y$ ($0.0 \leq y \leq 0.3$) system in spectral region from 550 to 1350 cm^{-1} are shown in Figure 6.4.

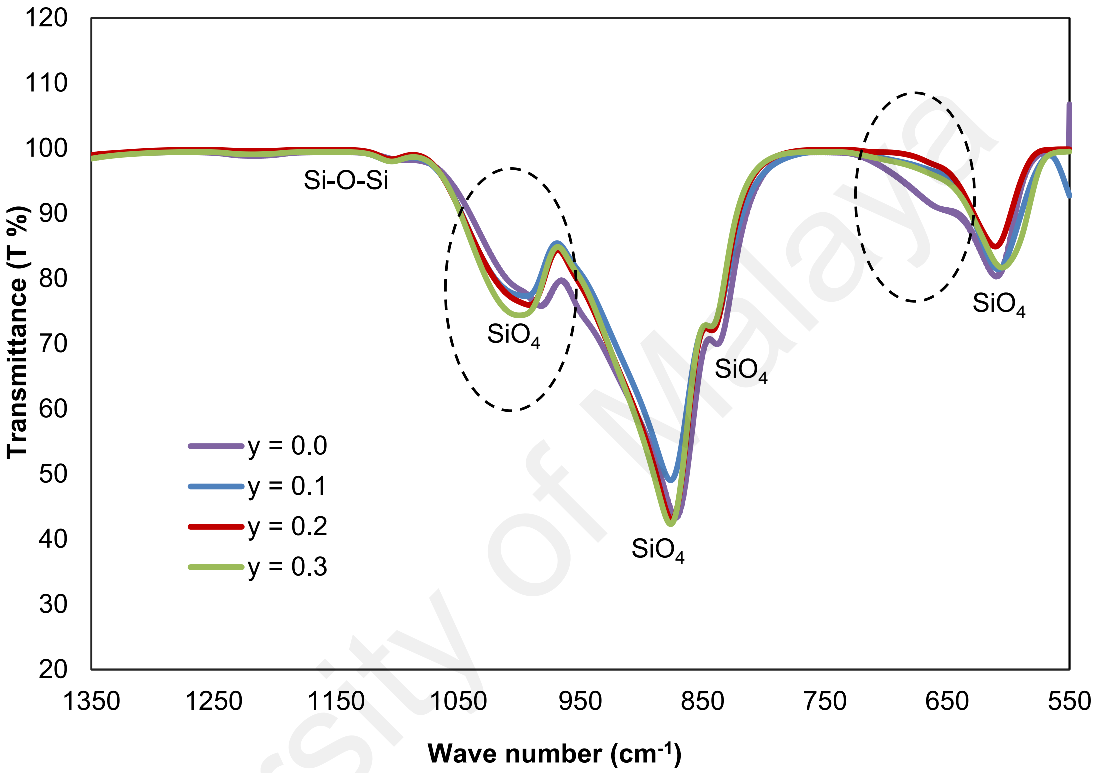

Figure 6.4: FTIR spectra of $Mg_{1.8}Mn_{0.2}Si_{1-y}O_4Zr_y$ ($y = 0.0 – 0.3$)

Figure 6.4 displays the FTIR spectra obtained for $Mg_{1.8}Mn_{0.2}Si_{1-y}O_4Zr_y$ ($y = 0.0 – 0.3$) system. The FTIR spectra for $Mg_{2-x}Mn_xZr_ySi_{1-y}O_4$ system are similar to that of magnesium silicate which contains five main characteristic peaks of $(SiO_4)^{4-}$ ion. There are peaks observed in the range of 550 - 650 cm^{-1} correspond to SiO_4 bending vibration modes (Saberi et al., 2007), peaks centered at 835 cm^{-1} and 874 cm^{-1} (Mazza et al., 1993; Tsai, 2002) are assigned to symmetric stretching vibrations of Si-O-Si. Meanwhile, the characteristic peaks associated to SiO_4 stretching vibration modes are located in the range from 950 cm^{-1} to 990 cm^{-1} (Saberi et al., 2007; Tsai, 2002). Lastly, the peaks appeared at 1105 cm^{-1} is attributed to Si-O-Si asymmetric stretching vibration mode of $Mg_{2-x}Mn_xZr_ySi_{1-y}O_4$ (Kharaziha et al., 2009; Saberi et al., 2007). Figure 6.5 clearly shows that SiO_4 stretching vibration peaks shifted to higher wavenumber. In addition, broadening of the shoulder peak at 600 cm^{-1} to 750 cm^{-1} is also observed. Adding Zr into the $Mg_{1.8}Mn_{0.2}SiO_4$ also gives a significant effect on the SiO_4 stretching vibration modes in the range of 950 cm^{-1} to 1050 cm^{-1}, Figure 6.5. The peaks for Zr doped materials are broader compared to the characteristics peaks for undoped material. The observed changes in the characteristic peaks prove that Zr has an inductive effect in lattice; this may introduce rearrangement of electric cloud in SiO_4^{4-} ion and is expected to enhance the electrochemical performance of the materials (Shu et al., 2013).

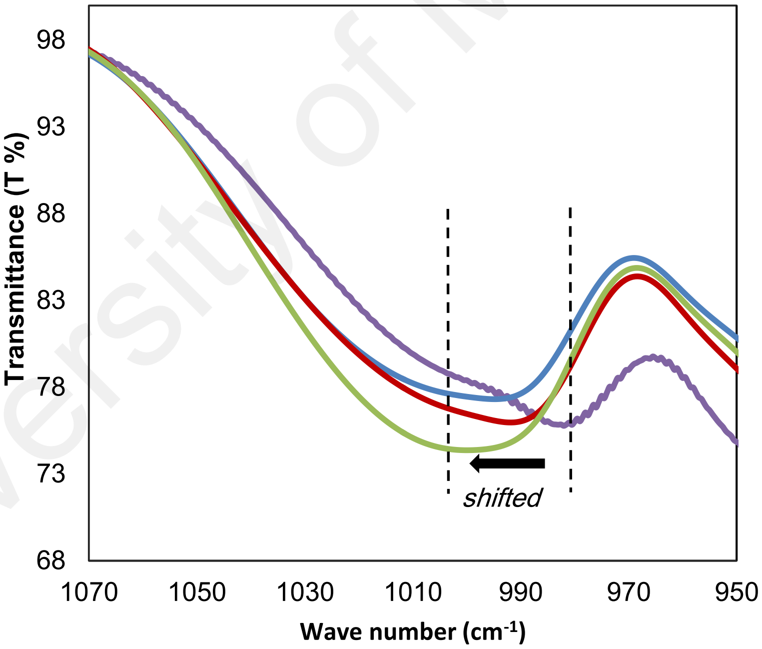

Figure 6.5: Extracted FTIR spectra of $Mg_{1.8}Mn_{0.2}Si_{1-y}O_4Zr_y$ ($y = 0.0 - 0.3$)

6.4 Scanning Electron Microscopy (SEM) and Particle size analysis

Scanning electron micrograph was performed to characterize the surface morphologies of the $Mg_{2-x}Mn_xZr_ySi_{1-y}O_4$ samples. Figure 6.6 presents the SEM micrographs of $Mg_{1.8}Mn_{0.2}Si_{1-y}O_4Zr_y$ ($0.0 \leq y \leq 0.3$). From SEM micrographs in Figure 6.6 (a), it can be seen that the $Mg_{1.8}Mn_{0.2}SiO_4$ powder is considered of uniform with small grains with sizes in micrometer range. The doped samples consist of agglomerated smaller particles that fused together creating a porous structure. The porous and loose structure is favorable for ion diffusion (Lin et al., 2008). The morphology of the samples is almost insensitive to the dopant amount. However, the particle size analysis (Figure 6.7) reveals that the average particle size increases with the increase of the dopant ratio.

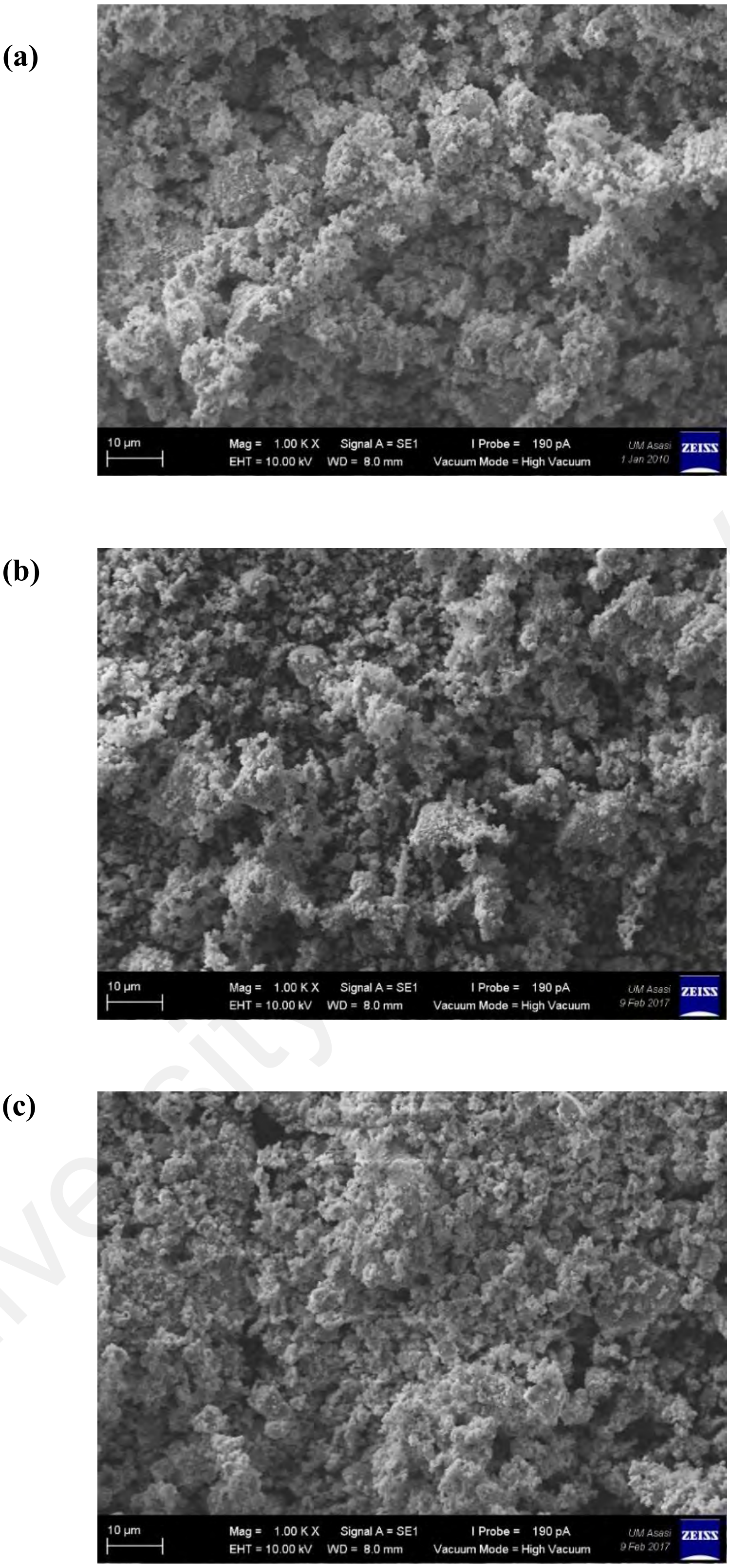

Figure 6.6: SEM micrographs of $Mg_{1.8}Mn_{0.2}Si_{1-y}O_4Zr_y$ with (a) $y = 0.1$, (b) $y = 0.2$ and (c) $y = 0.3$

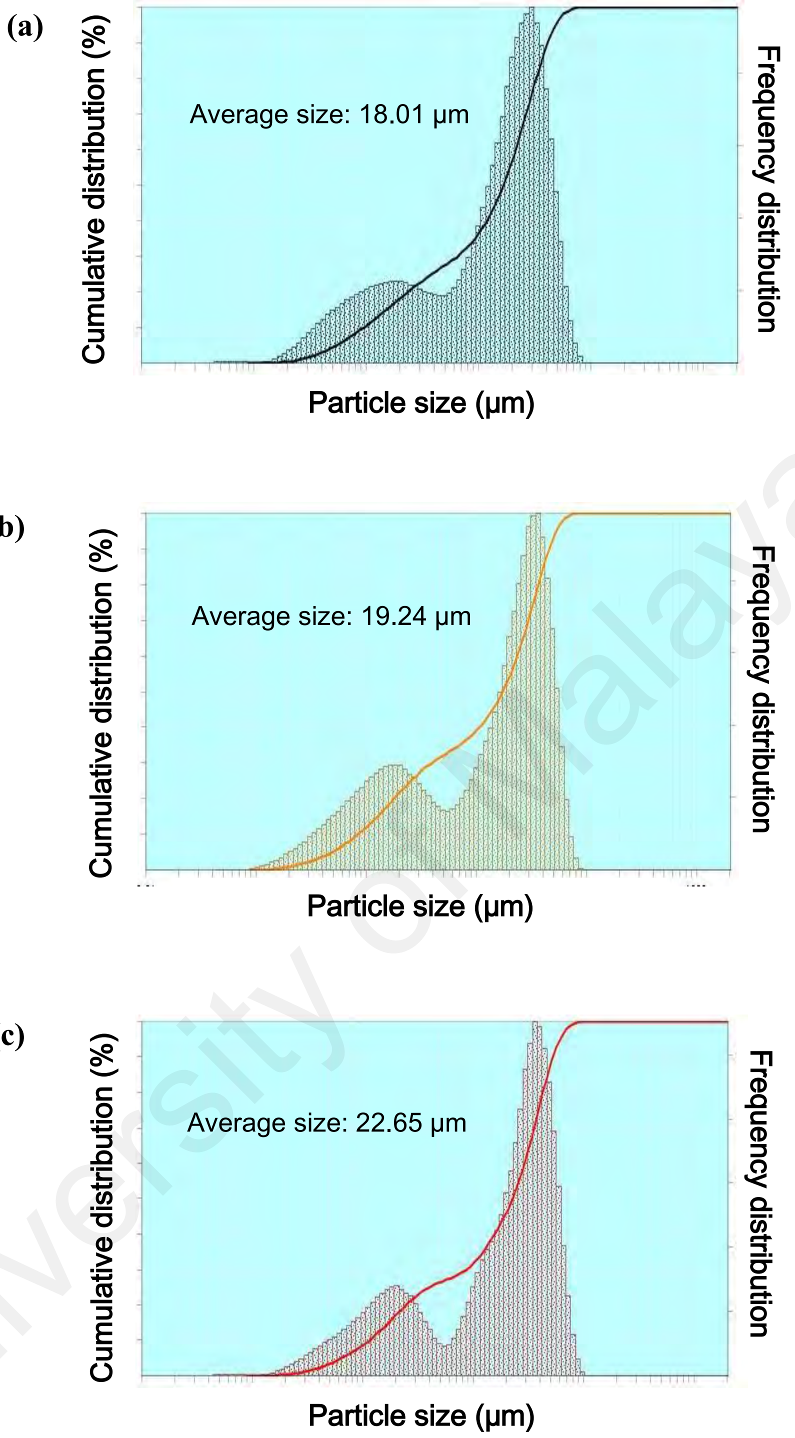

Figure 6.7: Particle size of $Mg_{1.8}Mn_{0.2}Si_{1-y}O_4Zr_y$ with (a) $y = 0.1$, (b) $y = 0.2$ and (c) $y = 0.3$

6.5 Energy Dispersive X-Ray Analysis (EDX)

EDX analysis was done on the samples and obtained spectra were displayed in Figure 6.8(a), Figure 6.8(b) and Figure 6.8(c). Data obtained from the EDX spectra are listed in Table 6.2. All samples consisted of magnesium (Mg), silicon (Si), oxygen (O), manganese (Mn) and Zirconium (Zr) elements. Elemental composition verification has been done by taking the average atomic ratios of three selected regions of each sample and compared with that of the theoretical atomic ratios. From the EDX results, it is found that the atomic ratio of Mg, Mn, Zr, Si and O are close to the designated composition as listed in Table 6.2. This suggests that the ratios of the elements in all samples are in a good agreement with the stoichiometric ratio of the starting materials confirming that the materials were successfully obtained.

Table 3.2: EDX stoichiometric atomic ratios of $Mg_{1.8}Mn_{0.2}Si_{1-y}O_4Zr_y$ ($y = 0.1 – 0.3$)

Sample	Composition	Mg	Mn	Zr	Si	O
$Mg_{1.8}Mn_{0.2}Zr_{0.1}Si_{0.9}O_{4.0}$	Calculated atomic ratio (%)	1.80	0.20	0.10	0.90	4.00
	EDX atomic ratio (%)	1.89	0.18	0.11	0.84	4.00
$Mg_{1.8}Mn_{0.2}Zr_{0.2}Si_{0.8}O_{4.0}$	Calculated atomic ratio (%)	1.80	0.20	0.20	0.8	4.00
	EDX atomic ratio (%)	1.74	0.21	0.20	0.79	4.00
$Mg_{1.8}Mn_{0.2}Zr_{0.3}Si_{0.7}O_{4.0}$	Calculated atomic ratio (%)	1.20	0.20	0.30	0.70	4.00
	EDX atomic ratio (%)	1.94	0.21	0.35	0.73	4.00

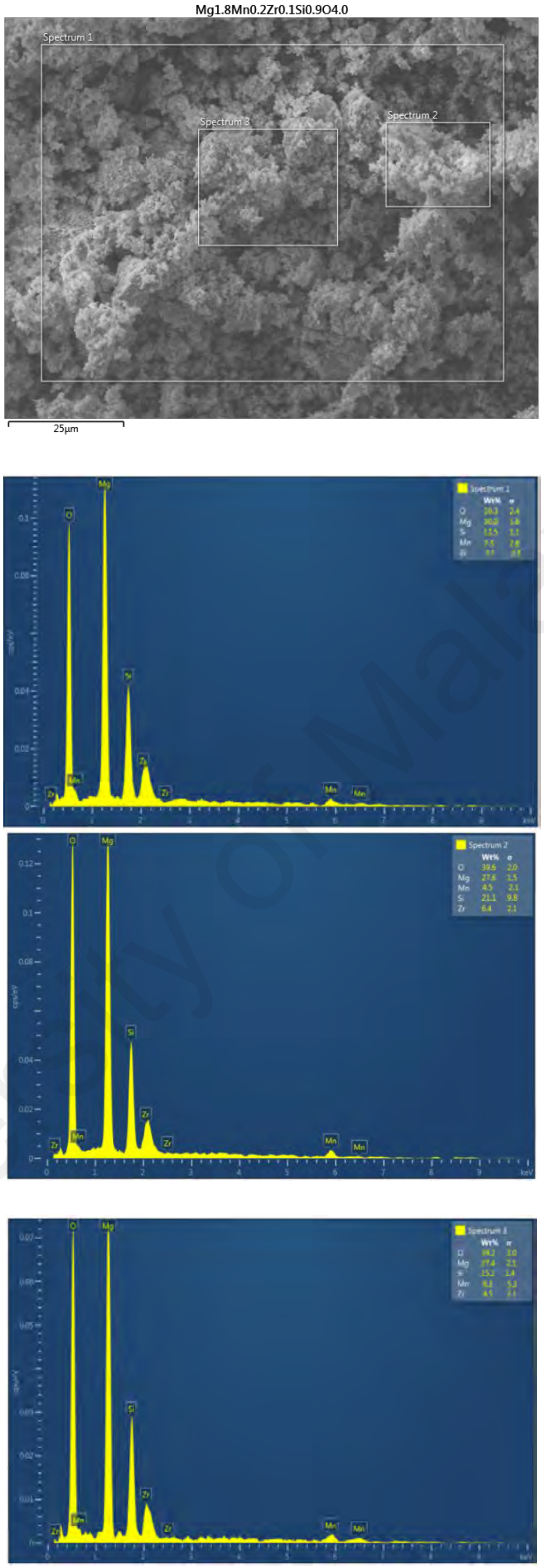

Figure 6.8 (a): EDX spectra of $Mg_{2-x}Mn_xSi_{1-y}O_4Zr_y$ sample with $x = 0.2$, $y = 0.1$

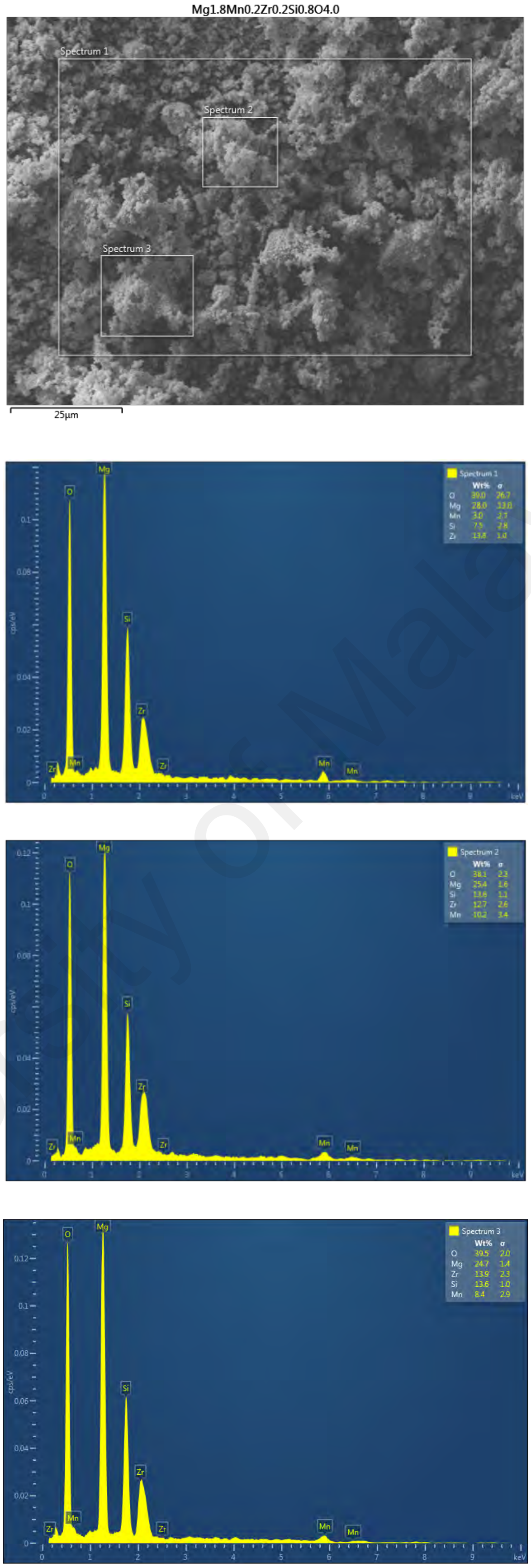

Spectrum 1	Wt%	σ
O	39.0	26.7
Mg	28.0	13.0
Mn	3.0	2.7
Si	7.5	2.8
Zr	13.8	1.0

Spectrum 2	Wt%	σ
O	38.1	2.3
Mg	25.4	1.6
Si	13.6	1.1
Zr	12.7	2.6
Mn	10.2	3.4

Spectrum 3	Wt%	σ
O	39.5	2.0
Mg	24.7	1.4
Zr	13.9	2.3
Si	13.6	1.0
Mn	8.4	2.9

Figure 6.8 (b): EDX spectra of $Mg_{2-x}Mn_xSi_{1-y}O_4Zr_y$ sample with $x = 0.2$, $y = 0.2$

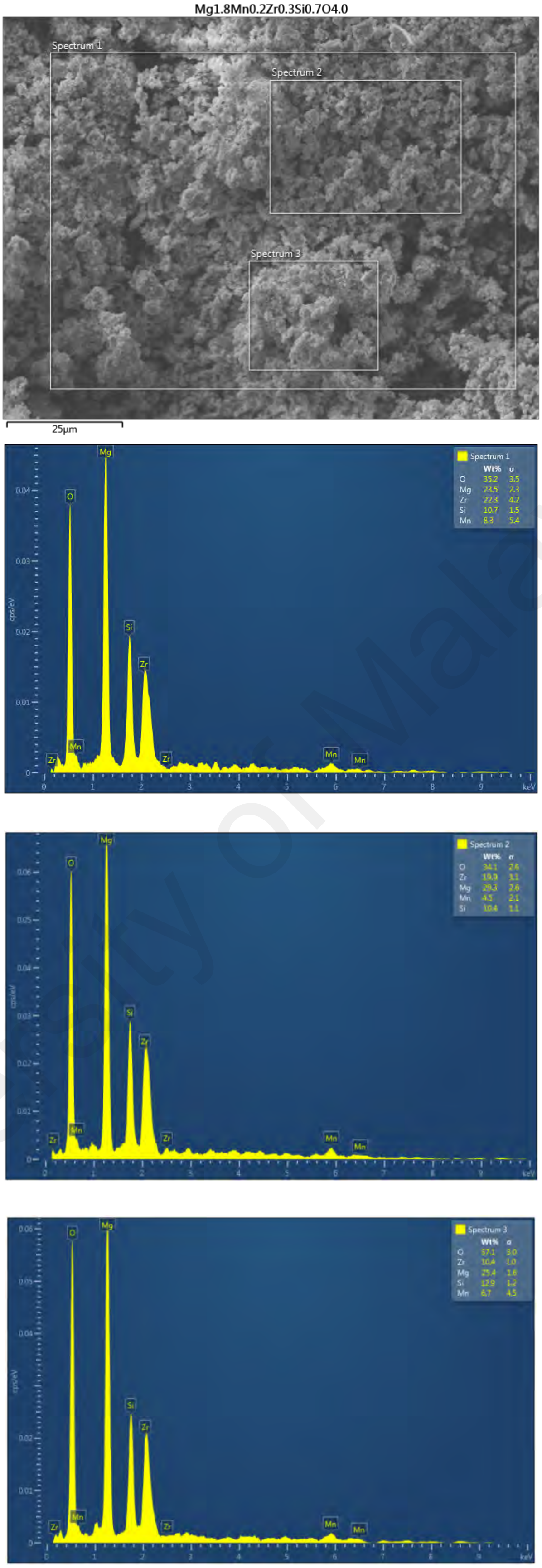

Figure 6.8 (c): EDX spectra of $Mg_{2-x}Mn_xSi_{1-y}O_4Zr_y$ sample with $x = 0.2$, $y = 0.3$

6.6 Electrochemical Impedance Spectroscopy (EIS)

The details of ion migration were investigated by impedance method. Typical Nyquist plots of $Mg_{1.8}Mn_{0.2}Si_{1-y}O_4Zr_y$ ($0.0 \leq y \leq 0.3$) electrode obtained are presented in Figure 6.9 (a - c). All plots exhibit a semicircle in the high frequency region and a tilted spike in the low frequency region. The sloping line at low frequency is associated with the ion diffusion (Deng et al., 2010). Significant depressed semicircle is observed for samples with higher dopant compared to those with lower dopant indicating a marked decrease in R_{ct}. Generally, the lower the R_{ct}, the easier charge transfer can occur (Yang et al., 2010). $Mg_{1.8}Mn_{0.2}Zr_{0.3}Si_{0.7}O_{4.0}$ sample exhibited the lowest R_{ct} value among the three samples which is 3.68×10^8 Ω. Meanwhile the $Mg_{1.8}Mn_{0.2}Zr_{0.2}Si_{0.8}O_{4.0}$ sample possessed the highest R_{ct} value. This result is in accordance with particle size result reported in section 6.4. Particle size distribution increased with the dopant amount increase. Larger particle size would provide smaller specific surface area and longer migration distance of Mg ion in solid phase resulting in higher concentration polarization on the electrode and thus reduces the performance of intercalation in materials (Örnek et al., 2015). Table 6.3 summarizes the R_{ct} values for each sample in this system.

Table 6.3: Charge transfer resistance, R_{ct} for $Mg_{1.8}Mn_{0.2}Si_{1-y}O_4Zr_y$ ($y = 0.1 - 0.3$) system

Sample $Mg_{1.8}Mn_{0.2}Si_{1-y}O_4Zr_y$	Charge transfer resistance R_{ct} (Ω)
$y = 0.1$	5.12×10^8
$y = 0.2$	5.34×10^8
$y = 0.3$	3.68×10^8

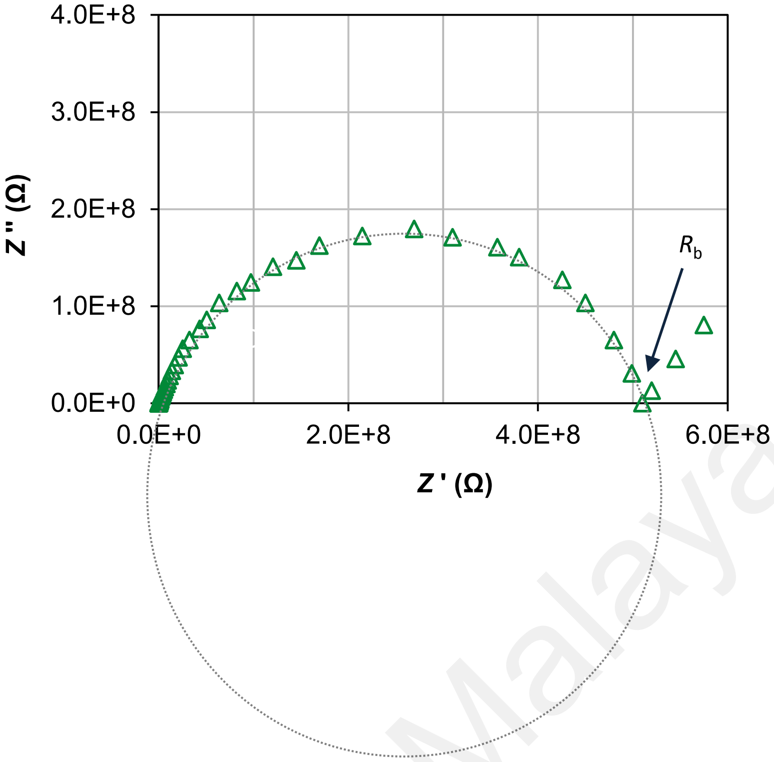

Figure 6.9(a): Impedance plot of $Mg_{1.8}Mn_{0.2}Si_{1-y}O_4Zr_y$ (y = 0.1)

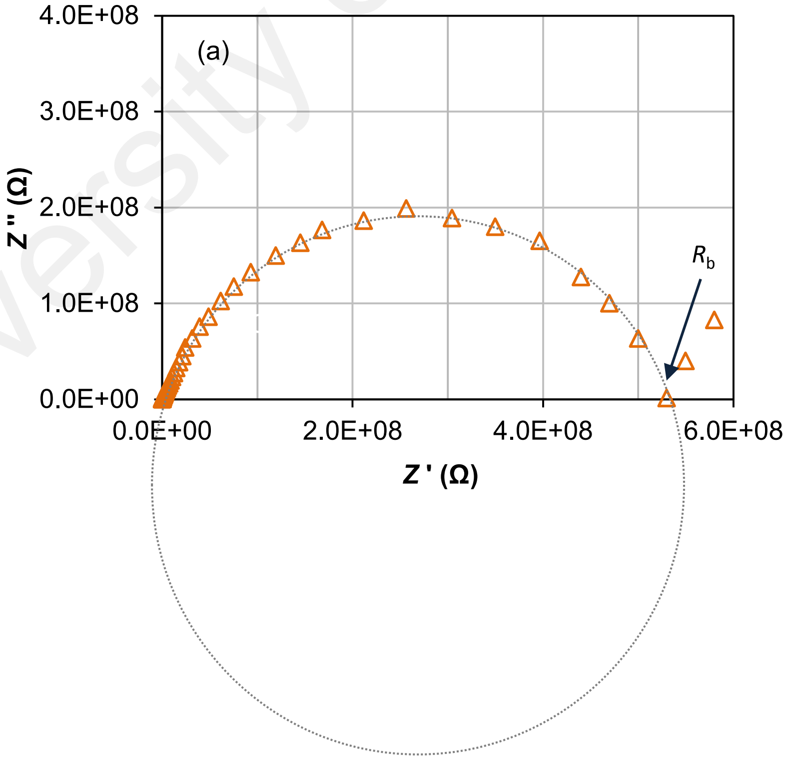

Figure 6.10(b): Impedance plot of $Mg_{1.8}Mn_{0.2}Si_{1-y}O_4Zr_y$ (y = 0.2)

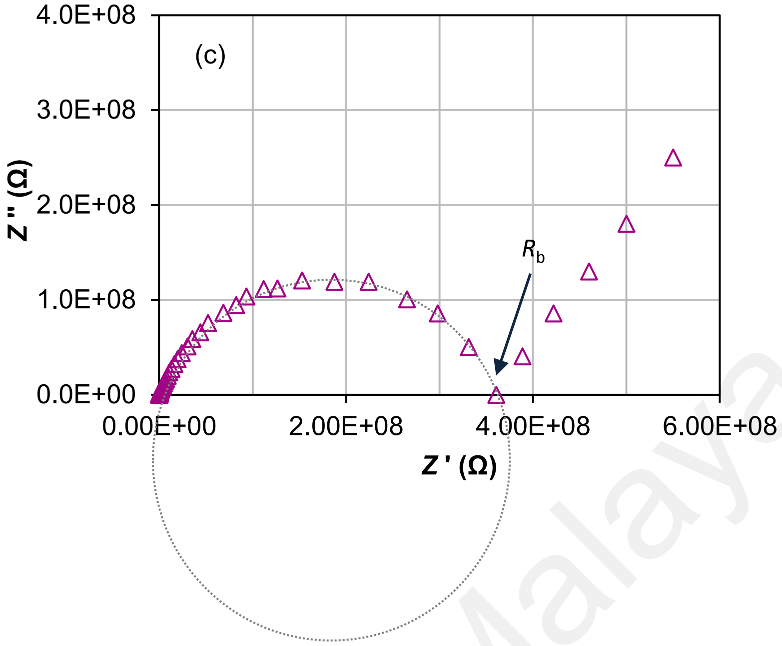

Figure 6.11: Impedance plot of $Mg_{1.8}Mn_{0.2}Si_{1-y}O_4Zr_y$ (y = 0.3)

6.7 Transference number

Sample with the smallest R_{ct} value was chosen for transference number measurement. Selected sample was evaluated using Wagner's polarization method. Direct current was monitored function of time of a fixed DC voltage across the sample. Figure 6.10 shows the plot of normalized current with respect to time for sample with the highest transference number $Mg_{1.8}Mn_{0.2}Si_{0.7}O_4Zr_{0.3}$. The transference, t_{ele} value for this sample is found to be 0.41. This value demonstrates that this type of materials is a mixed conductor indicating suitability for use as cathode active material in electrochemical cells.

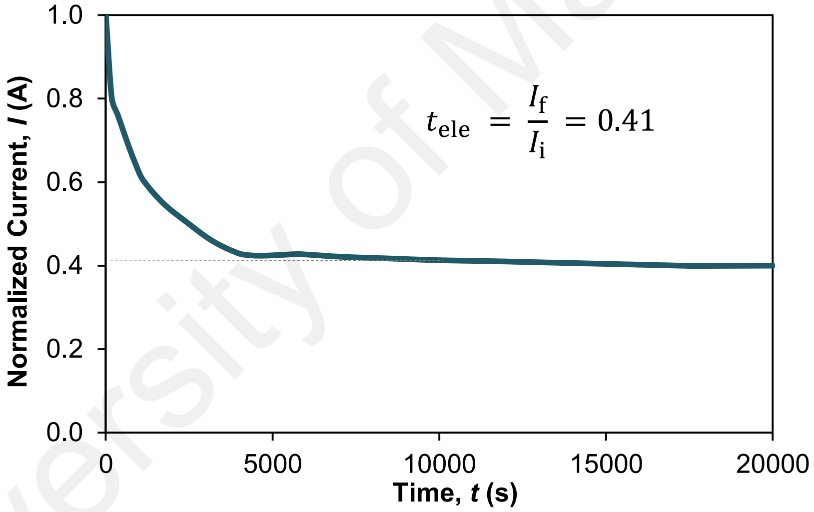

Figure 6.12: Current time curve of $Mg_{1.8}Mn_{0.2}Si_{1-y}O_4Zr_y$; $y = 0.3$

Listed in Table 6.4 is transference number for sample $Mg_{1.8}Mn_{0.2}Si_{1-y}O_4Zr_y$ ($y = 0.1 - 0.3$). Transference number increase as we increase the dopant amount. This results support the statement that doping approach is very useful to improve the performance of cathode materials.

Table 6.4: Transference number, *t* for $Mg_{1.8}Mn_{0.2}Si_{1-y}O_4Zr_y$ (y = 0.1 – 0.3) system

Sample $Mg_{1.8}Mn_{0.2}Si_{1-y}O_4Zr_y$	Transference number, *t*
$y = 0.1$	0.39
$y = 0.2$	0.40
$y = 0.3$	0.41

6.8 Cyclic voltammetry

CV was used to investigate the electrochemistry of the $Mg_{1.8}Mn_{0.2}Si_{1-y}O_4Zr_y$ materials as a function of Zr contents. Figure 6.11 depicts the CV curves of $Mg_{1.8}Mn_{0.2}Si_{1-y}O_4Zr_y$ (y = 0.0 – 0.3) system between –1.0 to 3.0 V at a scan rate 0.5 mVs^{-1}.

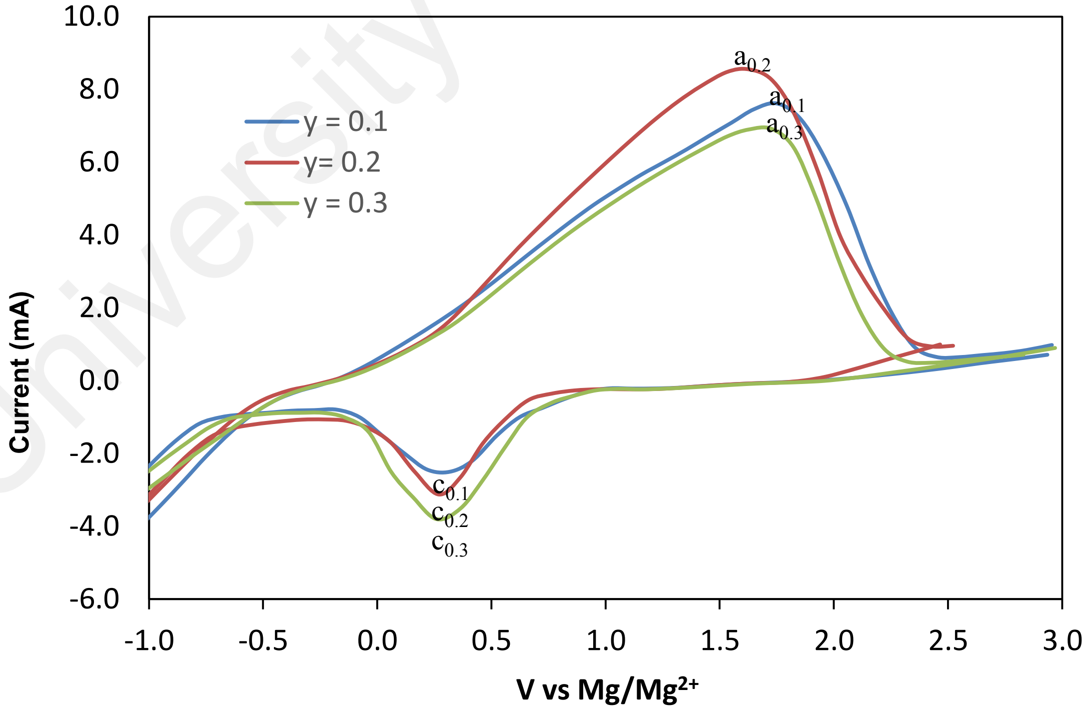

Figure 6.13: CV graph for $Mg_{2-x}Mn_xSi_{1-y}O_4Zr_y$

All samples reveal similar CV curves with one pair of redox peak responds. Cv curves obtained in this system are different from CV curves for systems 1 and 2. Only one pair of intercalation/deintercalation peak is observed for this system. Second pair of redox peaks completely disappeared in system 3. As mention earlier, there are two kinds of occupation sites for Mg atoms, Mg (1) and Mg (2) in the forsterite structure. However, Mg atoms prefer to occupy Mg(1) sites at first because the Mg(1)-O bonds can be formed more easily (NuLi et al., 2009). Based on the XRD result reported in section 6.2, adding Zr and Mn to the forsterite structure altered the lattice parameter values (especially lattice parameter *c*) as well as the unit cell volume of a structure. These changes contributed to a huge change in the electrochemical performance of the materials. Intercalation and deintercalation process only occur due to the migration of Mg ion in the first site Mg (1) with no contribution of the second site Mg (2) for this system. Adding Zr to the forsterite structure enlarged the migration channel for Mg ion.

Table 6.5 summarizes the current intensity for anodic and cathodic, I_{pA} and $I_{pC,}$ cathodic to anodic current ratio, I_{pC} / I_{pA} cathodic and anodic peak potential and potential separation, ΔE for $Mg_{1.8}Mn_{0.2}Si_{1-y}O_4Zr_y$ (y = 0.0 – 0.3) system. It can be observed that doped samples in this system possessed a higher current peak compare to the sample in system 2. Highest I_{pA} for system 2 owned by sample with x = 0.2 which is 5.40 mA. Meanwhile I_{pA} values for system 3 is in the range from 6.60 mA to 8.00 mA. This proves that, even adding Zr to the structure eliminated Mg (2) site. This helped in improving the migration channel hence the current intensity of the sample increased. Sample with y = 0.3 exhibited the highest I_{pC} / I_{pA} value of 0.5. For an electrochemical system, the potential separation between anodic and cathodic peaks reflects the reversibility of the electrochemical reaction. The potential separation between cathodic and anodic peak decreases as the dopant ratio increases. This is consistent with R_{ct} -y behavior reported in section 6.6. Therefore, it can be inferred that the potential separation in Figure 6.11 was improved by Zr doping (Yang et al., 2010). These suggest that performance of a forsterite system can be greatly improved upon Zr doping. $Mg_{1.8}Mn_{0.2}Si_{1-y}O_4Zr_y$ (y = 0.3) sample with cathodic-anodic peak located at 0.27/1.02 V exhibited the smallest potential separation and may contribute to a better electrochemical performance compared to other samples.

Table 6.5: Potential interval and redox peak currents of $Mg_{2-x}Mn_xSi_{1-y}O_4Zr_y$

Parameter	**Sample $Mg_{1.8}Mn_{0.2}Si_{1-y}O_4Zr_y$**		
	y = 0.1	**y = 0.2**	**y = 0.3**
I_{pA} (mA)	7.00	8.00	6.60
I_{pC} (mA)	2.00	2.40	3.30
I_{pC} / I_{pA}	0.29	0.30	0.50
E_{pA} (V)	1.74	1.60	1.69
E_{pC} (V)	0.28	0.27	0.27
ΔE_p (V)	1.46	1.33	1.02

CHAPTER 7: CONCLUSION AND SUGGESTIONS FOR FUTURE WORK

7.1 Conclusion

Pure Mg based compounds Mg_2SiO_4 (parent compound) have been successfully synthesized by using sol-gel method with selected final sintering temperature of 900, 1000 and 1100. Structural characteristics of the sample have been studied and found that Mg_2SiO_4 structure can be indexed to olivine crystal structure with the present of polyanion framework that makes them structurally stable. In addition to the structure information, TGA, DSC, FTIR, SEM, EDX and particle size analysis have been conducted to verify the thermal, structural and morphological analysis of the samples. Among three sample of Mg_2SiO_4, sample with sintering temperature of 1100 °C with lattice parameter of a = 10.1693 Å, b = 5.9685 Å and c = 4.6886 Å have the largest V = 284.5759 $Å^3$ and the lowest $R_{ct} = 7.01 \times 10^8\ \Omega$ suggesting that this sample possessed the easiest charge transfer process compared to the other samples. Cyclic voltammogram of Mg_2SiO_4 obtained from CV analysis disclosed typical feature of electrochemical magnesium deintercalation and intercalation reactions suggesting that these compounds have a great potential to be used as cathode material in Mg batteries. Mg_2SiO_4 sintered at 1100°C with the largest V and smallest Rct shows the best electrochemical performance among the other samples with a reasonable potential interval (ΔE_p = 1.62 V and $\Delta E_{p'}$ = 0.50 V), I_{pC} / I_{pA} = 0.21 and $I_{pC'}$ / $I_{pA'}$ = 0.80). Obtained Mg_2SiO_4 was further explored by performing elemental doping on the structure. Mn has been successfully doped into parent compound with stoichiometric of $Mg_{2-x}Mn_xSiO_4$ ($0.2 \le x \le 0.6$) by using sol gel method at sintering temperature of 1100°C. XRD analysis reveals that crystal structure of doped compound still same as the parent compound with improved structural properties. Lattice parameter of doped compound larger compared to the parent compound which was good and useful for intercalation and deintercalation of ions. $Mg_{1.4}Mn_{0.6}SiO_4$ compound with the smallest $R_{ct} = 2.15 \times 10^8\ \Omega$ owned by the sample with lattice parameters of a = a =10.0989 Å, b = 6.1548 Å and c = 4.7624 Å with the largest $V = 296.0189$ Å^3. CV analysis reveals that doped samples have similar trend of cyclic voltammogram with two pairs of redox reaction. $Mg_{2-x}Mn_xSiO_4$ sample with $x = 0.6$ has the highest value of I_{pC} / I_{pA} which is 0.58 and the smallest ΔE_p which is 1.44 V. Another system with stoichiometric of $Mg_{1.8}Mn_{0.2}Si_{1-y}O_4Zr_y$ $(0.1 \le y \le 0.3)$ have been synthesize by using sol gel method to observe the effect double doping of Mn and Zr to the parent compound. Introducing larger Zr ion into the compound effectively enlarged the unit cell volume of the compound. $Mg_{1.8}Mn_{0.2}Si_{0.7}O_4Zr_{0.3}$ compound with a = 10.0417 Å, b= 6.1291 Å and c = 4.8351 Å have the largest V among the other sample. On the other hand, it can be observed that the R_{ct} value for Mn and Zr doped sample $Mg_{1.8}Mn_{0.2}Si_{0.7}O_4Zr_{0.3}$ is $3.68 \times 10^8\ \Omega$ which much smaller compared to Mn doped sample. Elemental doping was proved able to reduce the R_{ct} value of a material. CV analysis reveals reveal similar CV curves with one pair of redox peak responds. Cv curves obtained for Mn Zr doped samples are different from CV curves for parent and Mn doped samples but improved in electrochemical properties. Sample with $y = 0.3$ with smallest R_{ct} exhibited the highest I_{pC} / I_{pA} value of 0.5 with ΔE_p =0.75 V. The electrochemical analysis results for parent and doped samples strengthen the fact that olivine type structure has a great potential to be applied in Mg electrochemical cell. Knowledge related to elemental doping reported here is also useful for Mg electrochemical cell. Table 7.1 summarized results for system I, system II and system III.

Table 7.1: Summary of results for system I, system II and system III

Results	System I	System II	System III
Best sample	1100 °C	$x = 0.6$	$y = 0.3$
Stoichiometric	Mg_2SiO_4	$Mg_{1.4}Mn_{0.6}SiO_4$	$Mg_{1.8}Mn_{0.2}Si_{0.7}O_4Zr_{0.3}$
Structural analysis (XRD)	a = 10.1693 Å b = 5.9685 Å c = 4.6886 Å V = 284.5759 Å^3 (*largest unit cell volume*)	a = 10.0989 Å b = 6.1548 Å c = 4.7624 Å V = 284.5759 Å^3 (*largest unit cell volume*)	a = 10.0417 Å b = 6.1291 Å c = 4.8351 Å V = 297.5823 Å^3 (*largest unit cell volume*)
Particle size	36.7 μm	13.7 μm	22.65 μm
Electrochemical Impedance Spectroscopy	$R_{ct} = 7.01 \times 10^8$ (*smallest* R_{ct})	$R_{ct} = 2.15 \times 10^8$ (*smallest* R_{ct})	$R_{ct} = 3.68 \times 10^8$ (*smallest* R_{ct})
Transference number	0.38 (*highest*)	0.40 (*highest*)	0.41(*highest*)
Cyclic voltammetry	$\Delta E = 0.5$ V (*reasonable potential separation*) $I_{pC} / I_{pA} = 0.80$ (*close to unity among all three samples in system I*)	$\Delta E = 0.58$ V (*Smallest potential separation*) $I_{pC} / I_{pA} = 0.83$ (*closest to unity among all samples in system II*)	$\Delta E = 1.02$ V (*Smallest potential separation*) $I_{pC} / I_{pA} = 0.5$ (*closest to unity among all samples in system III*)

7.2 Suggestions for Future Work

Further work should be carried out in order to enhance the performance of cathode materials based on Mg_2SiO_4 orthorhombic structured. This can be done by several possible approaches listed below

1) In cathode material, intercalation and deintercalation takes place along specific crystallographic planes and direction. From XRD data obtained in system I, it can be observed that upon increasing sintering temperature, the crystallinity of obtained materials improved. In addition, lattice parameters and unit cell volume also increase as we increase the sintering temperature. Elevate the sintering temperature could be a good idea to increase the lattice parameter, unit cell volume hence improve the electrochemical performance of material. However, in this work the choices of sintering temperature are very limited due to inadequate research equipment. Therefore, in future work, we suggest to extend the sintering temperature higher than 1100°C. For further discuss the structural properties of forsterite materials, Rietveld method should be employed. The Rietveld method creates a virtual separation of the overlapping peaks in XRD analysis thereby allowing an accurate determination of the structure.

2) In addition, the performance of cathode materials was greatly enhanced by doping approach. The interpretation of doping effects can be complicated by the intercalation between doping and microstructure and morphology since the microstructure formed can be affected by dopant addition. Doping with other potential transition metal such as Ruthenium and Titanium should be proposed for future exploration. Ruthenium has been added as dopant to orthorhombic structure $LiFePO_4$. The improvement of $LiFePO_4$ performance was reported due

to the present of Ru^{4+}/Ru^{5+} redox couple (Wang et al., 2009). Besides that, Titanium has been used to stabilizing the crystal structure of $LiFePO_4$ (Wu et al., 2009) and $LiMnPO_4$ (Shiratsuchi et al., 2009), hence improved the electrochemical performance of the materials. Since studied materials in this work, have similar structure as $LiFePO_4$, therefore, introduction Ruthenium and Titanium into studied materials is expected will enhance the electrochemical properties of the studied materials.

REFERENCES

Adnan, S. B. R. S., & Mohamed, N. S. (2014). Characterization of novel $Li_4Zr_{0.06}Si_{0.94}O_4$ and $LI_{3.94}Cr_{0.02}Zr_{0.06}Si_{0.94}O_4$ ceramic electrolytes for lithium cells. *Ceramics International, 40*(4), 6373-6379.

Amatucci, G. G., Badway, F., Singhal, A., Beaudoin, B., Skandan, G., Bowmer, T., … Jaworski, R. (2001). Investigation of yttrium and polyvalent ion intercalation into nanocrystalline vanadium oxide. *Journal of the Electrochemical Society, 148*(8), A940-A950.

Aurbach, D., Gizbar, H., Schechter, A., Chusid, O., Gottlieb, H. E., Gofer, Y., & Goldberg, I. (2002). Electrolyte solutions for rechargeable magnesium batteries based on organomagnesium chloroaluminate complexes. *Journal of The Electrochemical Society, 149*(2), A115-A121.

Aurbach, D., Gofer, Y., Lu, Z., Schechter, A., Chusid, O., Gizbar, H., … Turgeman, R. (2001). A short review on the comparison between Li battery systems and rechargeable magnesium battery technology. *Journal of Power Sources, 97*, 28-32.

Aurbach, D., Levi, M. D., Levi, E., Teller, H., Markovsky, B., Salitra, G., … Heider, L. (1998). Common electroanalytical behavior of Li intercalation processes into graphite and transition metal oxides. *Journal of the Electrochemical Society, 145*(9), 3024-3034.

Aurbach, D., Lu, Z., Schechter, A., Gofer, Y., Gizbar, H., Turgeman, R., … Levi, E. (2000). Prototype systems for rechargeable magnesium batteries. *Nature, 407*(6805), 724-727.

Aurbach, D., Schechter, A., Moshkovich, M., & Cohen, Y. (2001). On the mechanisms of reversible magnesium deposition processes. *Journal of The Electrochemical Society, 148*(9), A1004-A1014.

Barak, M. (1980). *Electrochemical power sources: Primary and secondary batteries*. London, England: The Institution of Electrical Engineerings.

Bard, A. J., & Faulkner, L. R. (1980). *Electrochemical Methods: Fundamentals and Applications*. New York, NY: Wiley.

Behera, S., Barpanda, P., Pratihar, S., & Bhattacharyya, S. (2004). Synthesis of magnesium–aluminium spinel from autoignition of citrate–nitrate gel. *Materials letters, 58*(9), 1451-1455.

Bragg, W. L. (1929). The diffraction of short electromagnetic waves by a crystal. *Proceedings of the Cambridge Philosophical Society 17*, 43–57.

Brenner, A. (1971). Note on the Electrodeposition of Magnesium from an Organic Solution of a Magnesium-Boron Complex. *Journal of The Electrochemical Society, 118*(1), 99-100.

Brown, O., & Mcintyre, R. (1985). The magnesium and magnesium amalgam electrodes in aprotic organic solvents a kinetic study. *Electrochimica Acta, 30*(5), 627-633.

Burney, H., & Talbot, J. B. (1991). Report of the electrolytic industries for the year 1990. *Journal of The Electrochemical Society, 138*(10), 3140-3172.

Chen, C. C., Shen, C. H., Liu, R. S., Lin, J. G., & Huang, C. Y. (2002). Synthesis and characterization of the colossal magnetoresistance manganite $La_{1.2}(Sr_{1.4}Ca_{0.4})Mn_2O_7$ by citrate gel. *Materials Research Bulletin, 37*(2), 235-246.

Chen, Z., & Dahn, J. R. (2002). Reducing carbon in $LiFePO_4$/C composite electrodes to maximize specific energy, volumetric energy, and tap density. *Journal of The Electrochemical Society, 149*(9), A1184-A1189.

Colin, A. V. (1984). Theoritical background. In M. Lazzari & B. Scrosati (Eds.), *Modern batteries: An introduction to electrochemical power sources* (pp. 18-55). Edward, England: Arnold.

Dell, R. (2000). Batteries: fifty years of materials development. *Solid State Ionics, 134*(1), 139-158.

Dell, R. (2001). Rechargeable batteries. In D. A. J. Rand & R. Dell (Eds.), *Understanding batteries* (pp. 97-214). Cambridge, England: Royal Society of Chemistry.

Deng, C., Zhang, S., Fu, B. L., Yang, S. Y., & Ma, L. (2010). Characterization of Li_2MnSiO_4 and Li_2FeSiO_4 cathode materials synthesized via a citric acid assisted sol–gel method. *Materials Chemistry and Physics, 120*(1), 14-17.

Dibner, B. (1964). *Alessandro Volta and the electric battery*. New York, NY: Franklin Watts.

Di Stefano, C., Ferro, V., & Mirabile, S. (2010). Comparison between grain-size analyses using laser diffraction and sedimentation methods. *Biosystems Engineering, 106*(2), 205-215.

Dominko, R., Gaberscek, M., Drofenik, J., Bele, M., Pejovnik, S., & Jamnik, J. (2003). The role of carbon black distribution in cathodes for Li ion batteries. *Journal of Power Sources, 119-121*, 770-773.

Dyer, C. K. (2002). Fuel cells for portable applications. *Journal of Power Sources, 106*(1), 31-34.

Edison, T. A. (1907). *Primary and secondary battery.* Retrieved from https://patents.google.com/patent/US858862A/en.

Feng, Z., Yang, J., NuLi, Y., Wang, J., Wang, X., & Wang, Z. (2008). Preparation and electrochemical study of a new magnesium intercalation material $Mg_{1.03}Mn_{0.97}SiO_4$. *Electrochemistry Communications, 10*(9), 1291-1294.

Fergus, J. W. (2010). Recent developments in cathode materials for lithium ion batteries. *Journal of Power Sources, 195*(4), 939-954.

Fey, G. T. K., Chen, Y. G., & Kao, H. M. (2009). Electrochemical properties of $LiFePO_4$ prepared via ball-milling. *Journal of Power Sources, 189*(1), 169-178.

Frackowiak, E. (2007). Carbon materials for supercapacitor application. *Physical Chemistry Chemical Physics, 9*(15), 1774-1785.

Fritts, S. D., & Gopal, R. (1993). Report of the Electrolytic Industries for the Year 1992. *Journal of The Electrochemical Society, 140*(11), 3337-3363.

Genders, J. D., & Pletcher, D. (1986). Studies using microelectrodes of the Mg (II)/Mg couple in tetrahydrofuran and propylene carbonate. *Journal of Electroanalytical Chemistry and Interfacial Electrochemistry, 199*(1), 93-100.

Gershinsky, G., Yoo, H. D., Gofer, Y., & Aurbach, D. (2013). Electrochemical and spectroscopic analysis of Mg^{2+} intercalation into thin film electrodes of layered oxides: V_2O_5 and MoO_3. *Langmuir, 29*(34), 10964-10972.

Gofer, Y., Chusid, O., Gizbar, H., Viestfrid, Y., Gottlieb, H. E., Marks, V., & Aurbach, D. (2006). Improved electrolyte solutions for rechargeable magnesium batteries. *Electrochemical and Solid-State Letters, 9*(5), A257-A260.

Goodenough, J. B., & Kim, Y. (2009). Challenges for rechargeable Li batteries. *Chemistry of Materials, 22*(3), 587-603.

Gregory, T. D., Hoffman, R. J., & Winterton, R. C. (1990). Nonaqueous electrochemistry of magnesium applications to energy storage. *Journal of The Electrochemical Society, 137*(3), 775-780.

Gummow, R. J., & He, Y. (2010). Morphology and preferred orientation of pulse electrodeposited magnesium. *Journal of The Electrochemical Society, 157*(4), E45-E49.

Haynes, W. M. (2014). *CRC Handbook of Chemistry and Physics* (98th ed.). Boca Raton, Florida: CRC press.

Hossain, S., & Linden, D. (1995). Selection and application batteries. In D. Linden & T. B. Reddy (Eds.), *Handbook of Batteries* (pp. 101-115). New York, NY: McGraw-Hill.

Huang, Y. J., Gao, D. S., Lei, G. T., Li, Z. H., & Su, G. Y. (2007). Synthesis and characterization of Li $(Ni_{1/3}Co_{1/3}Mn_{1/3})_{0.96}Si_{0.04}O_{1.96}$ $F_{0.04}$ as a cathode material for lithium-ion battery. *Materials Chemistry and Physics, 106*(2), 354-359.

Huggins, R. (2008). *Advanced batteries: Materials science aspects*. New York, NY: Springer Science & Business Media.

Huheey, J. E., Keiter, E. A., Keiter, R. L., & Medhi, O. K. (2006). *Inorganic chemistry: Principles of structure and reactivity*. Delhi, India: Pearson Education India.

Jiao, L., Yuan, H., Wang, Y., Cao, J., & Wang, Y. (2005). Mg intercalation properties into open-ended vanadium oxide nanotubes. *Electrochemistry Communications, 7*(4), 431-436.

Kakihana, M. (1996). Invited review “sol-gel” preparation of high temperature superconducting oxides. *Journal of Sol-Gel Science and Technology, 6*(1), 7-55.

Kandhasamy, S., Nallathamby, K., & Minakshi, M. (2012). Role of structural defects in olivine cathodes. *Progress in Solid State Chemistry, 40*(1), 1-5.

Kazakos, A., Komarneni, S., & Roy, R. (1990). Preparation and densification of forsterite (Mg_2SiO_4) by nanocomposite sol-gel processing. *Materials Letters, 9*(10), 405-409.

Kharaziha, M., & Fathi, M. (2009). Synthesis and characterization of bioactive forsterite nanopowder. *Ceramics International, 35*(6), 2449-2454.

Kim, B. H., Chang, I. S., & Gadd, G. M. (2007). Challenges in microbial fuel cell development and operation. *Applied Microbiology and Biotechnology, 76*(3), 485.

Kim, C., Phillips, P. J., Key, B., Yi, T., Nordlund, D., Yu, Y. S., … Zhang, Z. (2015). Direct observation of reversible magnesium ion intercalation into a spinel oxide host. *Advanced Materials, 27*(22), 3377-3384.

Kim, H. S., Arthur, T. S., Allred, G. D., Zajicek, J., Newman, J. G., Rodnyansky, … Muldoon, J. (2011). Structure and compatibility of a magnesium electrolyte with a sulphur cathode. *Nature Communications, 2*, 427.

Kim, J. S., Chang, W. S., Kim, R. H., Kim, D. Y., Han, D. W., Lee, K. H., … Doo, S. G. (2015). High-capacity nanostructured manganese dioxide cathode for rechargeable magnesium ion batteries. *Journal of Power Sources, 273*, 210-215.

Kissinger, P. T., & Heineman, W. R. (1983). Cyclic voltammetry. *Journal of Chemical Education, 60*(9), 702.

Kolar, D. (2000). Chemical research needed to improve high-temperature processing of advanced ceramic materials. *Pure and Applied Chemistry, 72*(8), 1425-1448.

Konert, M., & Vandenberghe, J. (1997). Comparison of laser grain size analysis with pipette and sieve analysis: A solution for the underestimation of the clay fraction. *Sedimentology, 44*(3), 523-535.

Koteswara Rao, K., Banu, T., Vithal, M., Swamy, G. Y. S. K., & Ravi Kumar, K. (2002). Preparation and characterization of bulk and nano particles of $La_2Zr_2O_7$ and $Nd_2Zr_2O_7$ by sol–gel method. *Materials Letters, 54*(2), 205-210.

Lee, J. S., Tai, S., Cao, R., Choi, N. S., Liu, M., Lee, K. T., & Cho, J. (2011). Metal–air batteries with high energy density: Li–air versus Zn–air. *Advanced Energy Materials, 1*(1), 34-50.

Lee, S. K., Tan, C., Lai, S. K., Tolouei, R., Amiriyan, M., Yap, B., & Ramesh, S. (2011, Sep). Sintering behaviour of forsterite bioceramics. Proceeding of *National Postgraduate Conference 2011,* 1-3. doi: 10.1109/NatPC.2011.6136415

Lee, W. E., & Rainforth, M. (1994). *Ceramic microstructures: Property control by processing*. New York, NY: Springer Science & Business Media.

Levi, E., Gershinsky, G., Aurbach, D., Isnard, O., & Ceder, G. (2009). New insight on the unusually high ionic mobility in chevrel phases. *Chemistry of Materials, 21*(7), 1390-1399.

Levi, E., Gofer, Y., & Aurbach, D. (2009). On the Way to Rechargeable Mg Batteries: The Challenge of New Cathode Materials. *Chemistry of Materials, 22*(3), 860-868.

Levi, E., Lancry, E., Mitelman, A., Aurbach, D., Ceder, G., Morgan, D., & Isnard, O. (2006). Phase Diagram of Mg Insertion into Chevrel Phases, Mg x Mo_6T_8 (T= S, Se). *Chemistry of Materials, 18*(23), 5492-5503.

Levi, E., Levi, M., Chasid, O., & Aurbach, D. (2009). A review on the problems of the solid state ions diffusion in cathodes for rechargeable Mg batteries. *Journal of Electroceramics, 22*(1-3), 13-19.

Li, Y., Nuli, Y., Yang, J., Yilinuer, T., & Wang, J. (2011). $MgFeSiO_4$ prepared via a molten salt method as a new cathode material for rechargeable magnesium batteries. *Chinese Science Bulletin, 56*(4-5), 386-390.

Liang, Y., Feng, R., Yang, S., Ma, H., Liang, J., & Chen, J. (2011). Rechargeable Mg Batteries with Graphene-like MoS_2 Cathode and Ultrasmall Mg Nanoparticle Anode. *Advanced Materials, 23*(5), 640-643.

Liao, X. Z., He, Y. S., Ma, Z. F., Zhang, X. M., & Wang, L. (2007). Effects of fluorine-substitution on the electrochemical behavior of $LiFePO_4/C$ cathode materials. *Journal of Power Sources, 174*(2), 720-725.

Liebenow, C. (1997). Reversibility of electrochemical magnesium deposition from Grignard solutions. *Journal of Applied Electrochemistry, 27*(2), 221-225.

Liebenow, C., Yang, Z., & Lobitz, P. (2000). The electrodeposition of magnesium using solutions of organomagnesium halides, amidomagnesium halides and magnesium organoborates. *Electrochemistry Communications, 2*(9), 641-645.

Lin, B., Wen, Z., Gu, Z., & Huang, S. (2008). Morphology and electrochemical performance of $Li(Ni_{1/3}Co_{1/3}Mn_{1/3})O_2$ cathode material by a slurry spray drying method. *Journal of Power Sources, 175*(1), 564-569.

Linden, D. (1984). Principles of operation. In T. B. Reddy & D. Linden (Eds.), *Handbook of Batteries and Fuel Cells* (pp. 1075-1081). New York, NY: McGraw-Hill.

Liu, B., Luo, T., Mu, G., Wang, X., Chen, D., & Shen, G. (2013). Rechargeable Mg-ion batteries based on WSe_2 nanowire cathodes. *American Chemical Society, 7*(9), 8051-8058.

Liu, H., Li, C., Cao, Q., Wu, Y., & Holze, R. (2008). Effects of heteroatoms on doped $LiFePO_4/C$ composites. *Journal of Solid State Electrochemistry, 12*(7-8), 1017-1020.

Lu, Z., Schechter, A., Moshkovich, M., & Aurbach, D. (1999). On the electrochemical behavior of magnesium electrodes in polar aprotic electrolyte solutions. *Journal of Electroanalytical Chemistry, 466*(2), 203-217.

Lv, D., Xu, T., Saha, P., Datta, M. K., Gordin, M. L., Manivannan, A., … Wang, D. (2013). A scientific study of current collectors for Mg batteries in $Mg(AlCl_2EtBu)_2$/THF electrolyte. *Journal of The Electrochemical Society, 160*(2), A351-A355.

Makino, K., Katayama, Y., Miura, T., & Kishi, T. (2001). Electrochemical insertion of magnesium to $Mg_{0.5}Ti_2(PO_4)_3$. *Journal of Power Sources, 99*(1), 66-69.

Makino, K., Katayama, Y., Miura, T., & Kishi, T. (2001). Magnesium insertion into $Mg_{0.5+y}(Fe_yTi_{1-y})_2(PO_4)_3$. *Journal of Power Sources, 97*, 512-514.

Makino, K., Katayama, Y., Miura, T., & Kishi, T. (2002). Preparation and electrochemical magnesium insertion behaviors of $Mg_{0.5+y}(Me_y\,Ti_{1-y})2(PO_4)3$ (Me = Cr, Fe). *Journal of Power Sources, 112*(1), 85-89.

Mazza, D., Lucco-Borlera, M., Busca, G., & Delmastro, A. (1993). High-quartz Solid-solution Phases from Xerogels with Composition $2MgO.2Al_2O_3.5SiO_2$ (μ-Cordierite) and $Li_2O.Al_2O_3.nSiO_2$ (n =2 to 4) (β-Eucryptite): Characterization by XRD, FTIR and Surface Measurements. *Journal of the European Ceramic Society, 11*(4), 299-308.

Meethong, N., Kao, Y. H., Speakman, S. A., & Chiang, Y. M. (2009). Aliovalent substitutions in olivine lithium iron phosphate and impact on structure and properties. *Advanced Functional Materials, 19*(7), 1060-1070.

Mitchell, M. B., Jackson, D., & James, P. F. (1999). Preparation of forsterite (Mg_2SiO_4) powders via an aqueous route using magnesium salts and silicon tetrachloride ($SiCl_4$). *Journal of Sol-gel Science and Technology, 15*(3), 211-219.

Moore, E. (2016). *Fourier Transform Infrared Spectroscopy (FTIR): Methods, Analysis and research insights*. Washington, DC: Nova Science Publishers.

Mote, V., Dargad, J., & Dole, B. (2013). Effect of Mn doping concentration on structural, morphological and optical studies of ZnO nano-particles. *Nanoscience and Nanoengineering, 1*(2), 116-122.

Muldoon, J., Bucur, C. B., Oliver, A. G., Sugimoto, T., Matsui, M., Kim, H. S., … Kotani, Y. (2012). Electrolyte roadblocks to a magnesium rechargeable battery. *Energy & Environmental Science, 5*(3), 5941-5950.

Nakayama, Y., Kudo, Y., Oki, H., Yamamoto, K., Kitajima, Y., & Noda, K. (2008). Complex structures and electrochemical properties of magnesium electrolytes. *Journal of the Electrochemical Society, 155*(10), A754-A759.

Ni, S., Chou, L., & Chang, J. (2007). Preparation and characterization of forsterite (Mg_2SiO_4) bioceramics. *Ceramics International, 33*(1), 83-88.

Nishi, Y. (2001). Lithium ion secondary batteries; past 10 years and the future. *Journal of Power Sources, 100*(1), 101-106.

Novak, P., & Desilvestro, J. (1993). Electrochemical insertion of magnesium in metal oxides and sulfides from aprotic electrolytes. *Journal of The Electrochemical Society, 140*(1), 140-144.

Novak, P., Imhof, R., & Haas, O. (1999). Magnesium insertion electrodes for rechargeable nonaqueous batteries: A competitive alternative to lithium?. *Electrochimica Acta, 45*(1), 351-367.

NuLi, Y., Jun Yang, Yongsheng Li, and Jiulin Wang. (2010). Mesoporous magnesium manganese silicate as cathode materials for rechargeable magnesium batteries. *Chemical Communications, 46*(21), 3794-3796.

NuLi, Y., Yang, J., Li, Y., Feng, Z., & Wang, J. (2008). Molten salt synthesis of $MgMnSiO_4$ for rechargeable magnesium battery cathode. *The Electrichemical Society Meeting Abstracts 4,* 450. doi: 10.1007/s11434-010-4247-4

NuLi, Y., Yang, J., Li, Y., & Wang, J. (2010). Mesoporous magnesium manganese silicate as cathode materials for rechargeable magnesium batteries. *Chemical Communications, 46*(21), 3794-3796.

NuLi, Y., Yang, J., Wang, J., & Li, Y. (2009). Electrochemical intercalation of Mg^{2+} in magnesium manganese silicate and its application as high-energy rechargeable magnesium battery cathode. *The Journal of Physical Chemistry C, 113*(28), 12594-12597.

NuLi, Y., Zheng, Y., Wang, F., Yang, J., Minett, A. I., Wang, J., & Chen, J. (2011). $MWNT/C/Mg_{1.03}Mn_{0.97}SiO_4$ hierarchical nanostructure for superior reversible magnesium ion storage. *Electrochemistry Communications, 13*(10), 1143-1146.

NuLi, Y., Zheng, Y., Wang, Y., Yang, J., & Wang, J. (2011). Electrochemical intercalation of Mg^{2+} in 3D hierarchically porous magnesium cobalt silicate and its application as an advanced cathode material in rechargeable magnesium batteries. *Journal of Materials Chemistry, 21*(33), 12437-12443.

Ornek, A., & Efe, O. (2015). Doping Qualifications of $LiFe_{1-x}Mg_xPO_4$-C Nano-scale Composite Cathode Materials. *Electrochimica Acta, 166*, 338-349.

Padhi, A. K., Nanjundaswamy, K., & Goodenough, J. B. (1997). Phospho-olivines as positive-electrode materials for rechargeable lithium batteries. *Journal of The Electrochemical Society, 144*(4), 1188-1194.

Palacin, M. R. (2009). Recent advances in rechargeable battery materials: a chemist’s perspective. *Chemical Society Reviews, 38*(9), 2565-2575.

Paladini, V., Donateo, T., De Risi, A., & Laforgia, D. (2007). Super-capacitors fuel-cell hybrid electric vehicle optimization and control strategy development. *Energy Conversion and Management, 48*(11), 3001-3008.

Paques-Ledent, M. T., & Tarte, P. (1973). Vibrational studies of olivine-type compounds - I. The i.r. and Raman spectra of the isotopic species of Mg_2SiO_4. *Spectrochimica Acta Part A: Molecular Spectroscopy, 29*(6), 1007-1016.

Peled, E., & Straze, H. (1977). The kinetics of the magnesium electrode in thionyl chloride solutions. *Journal of the Electrochemical Society, 124*(7), 1030-1035.

Pereira-Ramos, J., Messina, R., & Perichon, J. (1987). Electrochemical formation of a magnesium vanadium bronze $Mg_x V_2O_5$ in sulfone-based electrolytes at 150 C. *Journal of Electroanalytical Chemistry and Interfacial Electrochemistry, 218*(1), 241-249.

Pletcher, D. (1991). *A first course in electrode processes*. Cambridge, UK: The Royal Society of Chemistry.

Press, C. (2003). *CRC handbook of chemistry and physics* (84th ed.). New York, NY, CRC Press.

Rasul, S., Suzuki, S., Yamaguchi, S., & Miyayama, M. (2012). High capacity positive electrodes for secondary Mg-ion batteries. *Electrochimica Acta, 82*, 243-249.

Reddy, T. B. (2001). An introduction to secondary batteries. In D. Linden & T. B. Reddy (Eds.), *Handbook of Batteries* (pp. 131-152). New York, NY: McGraw-Hill.

Roberts, M. R., Vitins, G., & Owen, J. R. (2008). High-throughput studies of $Li_{1-x}Mg_{x}/2FePO_4$ and $LiFe_{1-y}Mg_{y}PO_4$ and the effect of carbon coating. *Journal of Power Sources, 179*(2), 754-762.

Ross, D. (2006). Hydrogen storage: the major technological barrier to the development of hydrogen fuel cell cars. *Vacuum, 80*(10), 1084-1089.

Saberi, A., Alinejad, B., Negahdari, Z., Kazemi, F., & Almasi, A. (2007). A novel method to low temperature synthesis of nanocrystalline forsterite. *Materials Research Bulletin, 42*(4), 666-673.

Saberi, A., Negahdari, Z., Alinejad, B., & Golestani-Fard, F. (2009). Synthesis and characterization of nanocrystalline forsterite through citrate–nitrate route. *Ceramics International, 35*(4), 1705-1708.

Saha, P., Datta, M. K., Velikokhatnyi, O. I., Manivannan, A., Alman, D., & Kumta, P. N. (2014). Rechargeable magnesium battery: Current status and key challenges for the future. *Progress in Materials Science, 66*, 1-86.

Scrosati, B. (1992). Lithium rocking chair batteries: An old concept? *Journal of The Electrochemical Society, 139*(10), 2776-2781.

Shaju, K. M., Subba Rao, G. V., & Chowdari, B. V. R. (2002). Performance of layered $Li(Ni_{1/3}Co_{1/3}Mn_{1/3})O_2$ as cathode for Li-ion batteries. *Electrochimica Acta, 48*(2), 145-151.

Shao, Y., Gu, M., Li, X., Nie, Z., Zuo, P., Li, G., … Liu, J. (2014). Highly Reversible Mg Insertion in Nanostructured Bi for Mg Ion Batteries. *Nano Letters, 14*(1), 255-260.

Shiga, T., Hase, Y., Kato, Y., Inoue, M., & Takechi, K. (2013). A rechargeable non-aqueous $Mg–O_2$ battery. *Chemical Communications, 49*(80), 9152-9154.

Shin, H. C., Park, S. B., Jang, H., Chung, K. Y., Cho, W. I., Kim, C. S., & Cho, B. W. (2008). Rate performance and structural change of Cr-doped $LiFePO_4/C$ during cycling. *Electrochimica Acta, 53*(27), 7946-7951.

Shiratsuchi, T., Okada, S., Doi, T., & Yamaki, J. I. (2009). Cathodic performance of $LiMn_{1-x}M_{x}PO_4$(M= Ti, Mg and Zr) annealed in an inert atmosphere. *Electrochimica Acta, 54*(11), 3145-3151.

Shklover, V., Haibach, T., Ried, F., Nesper, R., & Novak, P. (1996). Crystal structure of the product of Mg^{2+} insertion into V_2O_5 single crystals. *Journal of Solid State Chemistry, 123*(2), 317-323.

Shu, H., Wang, X., Wu, Q., Hu, B., Yang, X., Wei, Q., … Wu, C. (2013). Improved electrochemical performance of $LiFePO_4$/C cathode via Ni and Mn co-doping for lithium-ion batteries. *Journal of Power Sources, 237*, 149-155.

Sian, T. S., & Reddy, G. B. (2004). Infrared and electrochemical studies on Mg intercalated a-MoO_3 thin films. *Solid State Ionics, 167*(3), 399-405.

Sides, C. R., Croce, F., Young, V. Y., Martin, C. R., & Scrosati, B. (2005). A high-rate, nanocomposite $LiFePO_4$/carbon cathode. *Electrochemical and Solid-State Letters, 8*(9), A484-A487.

Simon, P., & Gogotsi, Y. (2008). Materials for electrochemical capacitors. *Nature Materials, 7*(11), 845-854.

Smith, B. C. (1995). *Fundamentals of Fourier Transform Infrared Spectroscopy*. London, England: Taylor & Francis.

Sun, C. S., Zhou, Z., Xu, Z. G., Wang, D. G., Wei, J. P., Bian, X. K., & Yan, J. (2009). Improved high-rate charge/discharge performances of $LiFePO_4$/C via V-doping. *Journal of Power Sources, 193*(2), 841-845.

Sun, J. Z. (2013). Study of a Novel Cathode Material for Magnesium Secondary Battery. *Journal of New Materials for Electrochemical Systems, 16*(4), 253-256.

Sutto, T. E., & Duncan, T. T. (2012). Electrochemical and structural characterization of Mg ion intercalation into RuO_2 using an ionic liquid electrolyte. *Electrochimica Acta, 79*, 170-174.

Takeda, Y., Kanno, R., Noda, M., & Yamamoto, O. (1985). Lithium organic electrolyte cells using the copper chevrel phase as cathode. *Materials Research Bulletin, 20*(1), 71-77.

Tao, Z. L., Xu, L. N., Gou, X. L., Chen, J., & Yuan, H. T. (2004). TiS_2 nanotubes as the cathode materials of Mg-ion batteries. *Chemical Communications, 18*, 2080-2081.

Tarascon, J. M., & Armand, M. (2001). Issues and challenges facing rechargeable lithium batteries. *Nature, 414*(6861), 359-367.

Triwibowo, J., Priyono, S., Purawiardi, I., Lestariningsih, T., & Ratri, C. R. (2016). Study on electrochemical performance of carbon-coated $LiFePO_4$ as cathode material for lithium ion batteries. *Proceedings of American Institute of Physics Conference 1755,* 150009-1–150009-7. doi: 10.1063/1.4958582

Tsai, M. (2002). Hydrolysis and condensation of forsterite precursor alkoxides: modification of the molecular gel structure by acetic acid. *Journal of Non-crystalline Solids, 298*(2), 116-130.

Van Mierlo, J., Maggetto, G., & Lataire, P. (2006). Which energy source for road transport in the future? A comparison of battery, hybrid and fuel cell vehicles. *Energy Conversion and Management, 47*(17), 2748-2760.

Wagemaker, M., Ellis, B. L., Lützenkirchen-Hecht, D., Mulder, F. M., & Nazar, L. F. (2008). Proof of supervalent doping in olivine $LiFePO_4$. *Chemistry of Materials, 20*(20), 6313-6315.

Wakihara, M., Uchida, T., Suzuki, K., & Taniguchi, M. (1989). A rechargeable lithium battery employing iron Chevrel phase compound $Fe_{1.25}Mo_6S_{7.8}$ as the cathode. *Electrochimica Acta, 34*(6), 867-869.

Wang, B., Xu, B., Liu, T., Liu, P., Guo, C., Wang, S., … Zhao, X. S. (2014). Mesoporous carbon-coated $LiFePO_4$ nanocrystals co-modified with graphene and Mg^{2+} doping as superior cathode materials for lithium ion batteries. *Nanoscale, 6*(2), 986-995.

Wang, R. Y., Wessells, C. D., Huggins, R. A., & Cui, Y. (2013). Highly reversible open framework nanoscale electrodes for divalent ion batteries. *Nano Letters, 13*(11), 5748-5752.

Wang, X., Rao, T. S., Batchelor, K., Ben-Zvi, I., & Fischer, J. (1995). Measurements on photoelectrons from a magnesium cathode in a microwave electron gun. *Nuclear Instruments and Methods in Physics Research Section A: Accelerators, Spectrometers, Detectors and Associated Equipment, 356*(2-3), 159-166.

Wang, Y., Yang, Y., Hu, X., Yang, Y., & Shao, H. (2009). Electrochemical performance of Ru-doped $LiFePO_4/C$ cathode material for lithium-ion batteries. *Journal of Alloys and Compounds, 481*(1), 590-594.

Wen, Y., Zeng, L., Tong, Z., Nong, L., & Wei, W. (2006). Structure and properties of $LiFe_{0.9}V_{0.1}PO_4$. *Journal of Alloys and Compounds, 416*(1-2), 206-208.

West, A. R. (2007). *Solid state chemistry and its applications*. New York, NY. Wiley.

Winter, M., & Brodd, R. J. (2004). What are batteries, fuel cells, and supercapacitors?. *Chemical Reviews, 104*(10), 4245-4270.

Wu, S. H., Chen, M. S., Chien, C. J., & Fu, Y. P. (2009). Preparation and characterization of Ti^{4+}-doped $LiFePO_4$ cathode materials for lithium-ion batteries. *Journal of Power Sources, 189*(1), 440-444.

Yang, L., Jiao, L., Miao, Y., & Yuan, H. (2010). Synthesis and characterization of $LiFe_{0.99}Mn_{0.01}(PO_4)_{2.99/3}F_{0.01}/C$ as a cathode material for lithium-ion battery. *Journal of Solid State Electrochemistry, 14*(6), 1001-1005.

Yang, S., Li, D., Zhang, T., Tao, Z., & Chen, J. (2011). First-principles study of zigzag MoS_2 nanoribbon as a promising cathode material for rechargeable Mg batteries. *The Journal of Physical Chemistry C, 116*(1), 1307-1312.

Ying, J., Lei, M., Jiang, C., Wan, C., He, X., Li, J., … Ren, J. (2006). Preparation and characterization of high-density spherical $Li_{0.97}Cr_{0.01}FePO_4/C$ cathode material for lithium ion batteries. *Journal of Power Sources, 158*(1), 543-549.

Yoo, H. D., Shterenberg, I., Gofer, Y., Gershinsky, G., Pour, N., & Aurbach, D. (2013). Mg rechargeable batteries: An on-going challenge. *Energy & Environmental Science, 6*(8), 2265-2279.

Zhang, M., Jiao, L. F., Yuan, H. T., Wang, Y. M., Guo, J., Zhao, M., … Zhou, X. D. (2006). The preparation and characterization of olivine $LiFePO_4/C$ doped with MoO_3 by a solution method. *Solid State Ionics, 177*(37-38), 3309-3314.

Zhang, R., Yu, X., Nam, K. W., Ling, C., Arthur, T. S., Song, W., … Matsui, M. (2012). α-MnO_2 as a cathode material for rechargeable Mg batteries. *Electrochemistry Communications, 23*, 110-113.

Zhang, S., Huang, Y., Kai, W., Shi, L., & Seo, H. J. (2010). Tunable red luminescence of Mn^{2+}-doped $NaCaPO_4$ phosphors. *Electrochemical and Solid-state Letters, 13*(2), J11-J14.

Zhang, W. J. (2010). Comparison of the rate capacities of $LiFePO_4$ cathode materials. *Journal of the Electrochemical Society, 157*(10), A1040-A1046.

Zhang, X. J., Ding, J., Zhu, H. X., Deng, C. J., & Yuan, W. J. (2014). Effect of particle size on properties of novel thermal insulation materials synthesized by molten salt method. *Key Engineering Materials, 602*, 644-647.

Zheng, Y., Yanna, N., Qiang, C., Wang, Y., Yang, J., & Jiulin, W. (2012). Magnesium cobalt silicate materials for reversible magnesium ion storage. *Electrochimica Acta, 66*, 75-81.

Zou, M., Yoshio, M., Gopukumar, S., & Yamaki, J. I. (2004). Synthesis and electrochemical performance of high voltage cycling $LiM_{0.05}Co_{0.95}O_2$ as cathode material for lithium rechargeable cells. *Electrochemical and Solid-state Letters, 7*(7), A176-A179.

LIST OF PUBLICATIONS, CONFERENCES ATTENDED AND AWARDS

Publications

1. S.H. Tamin, S.B.R.S Adnan,M.H. Jaafar, N.S. Mohamed, (2017) Effects of sintering temperature on the structure and electrochemical performance of Mg_2SiO_4 cathode materials, *Ionics,* 1-7
2. S. H. Tamin, S.B.R.S. Adnan, M.H. Jaafar, N. S. Mohamed, (2018) Powder of $Mg_2SiO_4:Mn^{2+}$ Obtained via a Sol-gel Method and Their structural, morphological and electrochemical properties. *Journal of Sol-Gel Science and Technology*, 86:24-33
3. S. H. Tamin, S.B.R.S. Adnan, M.H. Jaafar, N. S. Mohamed, Doping effects of zirconium on the structural, morphological, electrical and electrochemical properties of $Mg_{1.8}Mn_{0.2}SiO_4$. (*under review*)

Conference and workshop attended:

1. 4th International Conference on Nano and Materials Engineering (ICNME 2016) 7-8 April 2016, Kuta Central Park Hotel, Bali Indonesia (Oral Presenter)
2. 4th ASEAN Synchrotron Science Camp, which held on 10-14 November 2015 at Synchrotron Light Research Institute (SLRI), Nakhon Ratchasima, Thailand.

Award:

1. Bronze medal: Invention, Innovation & Design Exposition (IIDEX) 2015, 27-30 April 2015, UiTM Shah Alam.